ERT in Vacuum Chambers. 3D simulations of the most interesting features*

Presented at the 31th International Electric Propulsion Conference, USA

IEPC-2009-142

September 20 –24, 2009

Grigory Toropov

Russia, Kaliningrad, Rimskaya 29,79

grigory.toropov@gmail.com

Sergey Khartov

Moscow Aviation Institute (State Technical University) MAI

Electric Propulsion and Space Power Plants Department

4, Volokolamskoe sh., Moscow, 125971, Russia

Abstract: In space technology comes increased use as a traction modules plasma accelerators, especially one of their varieties - stationary plasma engine (SPT). Most important issue of development and improvement of the SPT is the problem of ground tests. The main drawback is the inability of ground tests to fully simulate the environmental conditions of the engine environment, typical of his work in outer space. When circulating in the vacuum chamber, a jet of accelerated ions interact with neutral particles moving chaotically residual atmosphere, forming reload ions. As a result, the phenomenon of value is measured in current jet in the nucleus are reduced, and at the periphery (in the corners above 30 degrees from the axis) is significantly increased. The authors are currently developing a methodology for modeling of the jet SPT in a vacuum chamber, which can be used to estimate the proportion of ions formed by the exchange on neutral atoms, in the measurement of electric propulsion jets. This article describes a model of jet SPT and the results of the calculations on the dynamics of neutral particles and estimate the proportion of ions that have not flown to the sensor probe from interaction with residual gas in a vacuum chamber. Interaction of jet engine with a wall of vacuum chamber formed fused backwash. Sputtering return flows depend on the geometry and size, so the upper limit defines the requirements for the minimum size of vacuum chambers for a given engine. Contamination of the sputtered particles can have an impact on the insulators, the electrodes (anode, cathode, neutralizer), and surface properties of the discharge chamber in the Hall engines. Recently, in connection with promotion of the SPT on the world market for numerical simulation of the engine in a vacuum chamber exercise group of foreign scientists – I.Boyd of Micheganskogo University, Alta Group in Italy, and others - who have managed to achieve in some cases, the qualitative consistency of model results with experimental data. Given the above, as the goals of the selected development methodology in the simulation of three-dimensional spread of the accelerated ions from the engine, an analysis of their interaction with residual gas analysis fused with the walls of the vacuum chamber of particles and their influence on the accelerator, the analysis of the distribution of neutral particles in a vacuum chamber at an engine for designing an appropriate geometry of the camera, or upgrading an existing camera, given the parameters of the tested engine.

To achieve the goal of the following tasks:

1. Development of three-dimensional mathematical models of the plasma jet engine in a vacuum chamber.

**** Text is a google translation from Russian (sorry for inconvenience)***

2. Experimental study of laboratory model of SPD in a vacuum chamber to measure probe characteristics, describing a jet engine, as well as the backward flow. Experimental measurement of pressure in a vacuum chamber using vacuum gauges. With the removal of cross-linked probes energospektra along the angle of spread of the jet.

3. The development of mathematical surface analyzer (SMA), to compare the absolute value of the parameter

(pressure, current density) from experimentally measured, and modeled energospektra at a given point.
4. Development of modules for the analysis of the elastic interaction of particles, as well as the interaction of particles in recharging.
5. Creating a module for calculating the distribution of sputtered particles.
6. Verification of calculation results with the experiment and the results of studies of other developers.
Scientific novelty of the work is that for the first time developed a three-dimensional engineering model based on a triangular grid, which allows to work with the real geometry of any complexity, and numerically implemented the stationary model of plasma jet engine in a vacuum chamber. The model allows to study the impact on the dynamics of "heavy" particles such factors as the impact of the wall cells, the distribution of neutral gas, as well as to determine the characteristics of the flow of ions and neutral atoms inside a vacuum chamber. The first was the method of hard spheres for the analysis of the distribution of velocity field in the interaction of particles in the simulation of electric propulsion. The first was developed by an auxiliary numerical essence - Mathematics surface analyzer (PMA), to measure the integral characteristics (thrust, the total ion current), as well as local values of the parameters (pressure, ion current density, distribution of particle velocity) in that situation or girder .

The practical significance of the paper is as follows:

- The method of modeling the spread of the jet plasma accelerator, taking into account the impact of its neutral gas in the chamber as well as interaction with the walls of vacuum chamber;

- Developed a method of determining the dynamic distribution of neutral particles in the chamber when the engine;

- The method for measuring parameters at fixed points by numerical simulation of probe for removal of various characteristics of simulated gas;

- The method reload particle tracking of the camera;

- The method of calculating the distribution of dispersal and perepyleniya

- The method to calculate the integral parameters of the engine (thrust, the total ion current).

1. Review of the issue.....5

1.2. Survey carried out experiments in a vacuum chamber to assess the impact of cameras on the functioning of ETD.....6

2. A mathematical model of the spread of the plasma jet engine in a vacuum chamber.....12

2.3. The methods in this system 13

2.3.1. Simulation of the dynamic vacuum.....13

2.3.2. Modeling the distribution of primary ions.....15

2.3.3. Modeling the concentration of ions, formed by the exchange of primary ions to neutral atoms....15
2.3.4. Sputtering / deposition....16
2.3.4.1. Model of ion sputtering of surface....16
2.3.4.2. Model deposition sprayed material....19
2.3.5. The problem of definition of electric field....21
Electric field....23
2.3.6. The problem of the layer lying next to the wall Numerical simulation of nonequilibrium plasma parameters for the Faraday probe....23
2.4 Modeling of the magnetic field in the SPT....26
2.4.1. Analysis of the trajectory of an electron off from the cathode-compensator in the vicinity of the outlet SPD....27
3. The implementation of the mathematical model....31
3.1. Project Description....31
3.2 Determination of initial and boundary conditions....32
3.2.1. The initial and boundary conditions for calculating the distribution of neutral particles....32
Engine № 1.1....32
Engine № 1.2....33
The engine number 2....34
The engine number 3....35
The engine number 4....35
The engine number 5....36
3.2.2. The initial and boundary conditions for calculating the distribution of primary ions....37
3.2.3. The initial and boundary conditions for calculating the distribution of recharge of ions formed by the interaction of the jet with the gas in the vacuum chamber....45
3.2.4. The initial and boundary conditions for calculating the distribution of sputtered particles with the walls of the vacuum chamber....46
3.3 The method for determining surface characteristics using mathematical analysis (SMA)....48
3.1. Determination of pressure on a given surface of SMA....48
3.2. Determination of traction....48
3.3. Determination of current density of primary ions....49
3.4. Determination of current density ion recharging....49
3.4 Visualization of results....49
3.4.1. The trajectories of particles....50
3.4.2. Distribution of parameters in a selected plane....50

3.4.3. The distribution of the parameter along the parametric curve....50
3.4.4. Distribution of parameters on surfaces phone....51
3.5 Analysis of cross sections of elastic interaction between atoms of xenon....51
3.6 Analysis of the probability distribution of the direction and speed of xenon atoms after collision with an atom of xenon environment with an average temperature of 300 K using solid spheres....56
3.7. Calculation of the coefficients Klauzinga for tubes of different cross section....67
3.8. Testing models deposition on the hemispherical....68
4. Simulation results in different cells....71
4.1. The calculation of dynamic pressure....71
4.1.1. Stand MAI....71
4.1.2. Stand in the center of Keldysh....73
4.1.4. Comparison with the calculation of Alta....77
4.1.5. Comparison with simulations carried out by [8]....80
4.1.6. Calculation of the area near the engine....81
4.2. The calculation of the distribution of primary ions....82
4.2.1. Stand in the MAI....82
4.2.2. Stand in the center of Keldysh....86
4.2.3. Stand 71-3-90 in KB «Torch»....94
4.2.4. Comparison with the calculation of ISP....95
4.2.5. Comparison with simulations carried out by [8]....96
4.2.6. The calculation for the area around the accelerator....97
4.3. Calculation of sputtering and deposition....98
4.3.1. Stand MAI....98
4.3.1.1. Calculation ISP....98
4.3.1.2. Calculation EPCLab....102
4.3.2. Stand in the center of Keldysh....104
4.4. Application of magnetohydrodynamic models and calculation of ions generated by the exchange of neutral gas atoms with ions off of the accelerator....105
4.4.1. Stand MAI....105
4.4.2. Stand 71-3-90 in KB «Torch»....106
4.4.3. Comparison with simulations carried out by [8]....110
Conclusions....116
References....118

1. Review of the issue

If tests of plasma engines should be the parameters of their environment, close to the actual parameters of operation. To simulate the plasma of the engine in the space required to create a vacuum 10^{-4} ... 10^{-6} Pa. In fact maintaining a level of vacuum in the test plasma engine is technically unnecessary, and he usually rises to 10^{-2} ... 10^{-3} Pa. Pre-vacuum in the vacuum chamber (before the motor) is ~ 6 * 10^{-4} Pa, and as a result of the camera is always a residual atmosphere, consisting of gas molecules of air and vacuum pumps working phone. The concentration of these gases reaches ~ 10^{15} - 10^{18} 1/m3 and he maintained almost constant due to the proceeds of molecules through the sealing elements of the vacuum chamber, as well as the means of pumping. The percentage of residual atmosphere depends on the chosen method of creating a vacuum. So when using the diffusion pump in the composition of the residual atmosphere will prevail molecules of gas pumps, while funds Cryogenic pumping - not condensing gases, including hydrogen. The interaction of high-energy ions generated by plasma accelerator, with atoms of residual atmosphere leads to the formation of ion exchange and radicals, the probability of loss which the elements of design and their getting into the working volume of the accelerator is large enough. The presence of active residual gases in the atmosphere and their interaction with the design of the engine leads to the need to take into account changes in the physic-chemical properties of working surfaces of the device with its long-term work. By submitting a working body of the motor (now mainly gas) in the vacuum chamber is installed a dynamic vacuum, the level which defines the processes of a revenue (from the volume of the chamber) of neutral particles of gas in the area of localization of the main processes of ionization and acceleration. This process helps to restructure the level in the engine and overstates the level of its integral characteristics. This may be the heterogeneity in spatial distribution of reverse flow caused by the configuration of the inner surface of the vacuum chamber. A local increase of concentration of neutral atoms can lead to a change in the conditions of transport of particles in selected areas of the accelerator level.

1.1. Specificity

For each new engine is required to pass a series of ground tests to show its properties and shelf life in the working environment, with design solutions to various devices in the transportation, storage, assembly and launch.

Although mechanical testing and testing in different environments ETD have small specific difference in comparison with other tests for space equipment, the test to identify the characteristics and resources have many characteristics in comparison with conventional (chemical) systems accelerate. Specificity is determined by some specific aspects of accelerators and electrical systems:

low-and very low levels of traction control (on 1mN up to 10 N)

-high and very high level of vacuum required for proper operation (for

comparison, the pressure around the spacecraft after the release at less than 10^{-6} mm Hg GEO)
- A long time (up to 18000 hours for the mission in deep space);
- Especially related to the jet accelerator, which is composed of high-speed (up to 100 km / s), high energy plasma.
EPT tests require the use of special equipment, tools and measuring devices. Most of them are not available as industrial products, and certified, especially if we are referring to the device for measuring low-thrust, some parameters of the plasma pencil: such devices are rarely designed and constructed, providing a poor comparative performance.
Another important point in testing EPT is a need for the installation requirements for a vacuum test. Ideally, these conditions must repeat the actual environment in space in the surrounding gas environment (chemical composition, temperature, density, etc.) Unfortunately, these ideal conditions are almost always impossible to achieve. Therefore, less restricted interpretation of the requirements above mentioned «ideal», depending on the type of information or evidence that is expected with the help of special tests: the «real» requirements are based on the experience of producers and consumers with previous engines, or other space technologies.

1.2. Survey carried out experiments in a vacuum chamber to assess the impact of cameras on the functioning of ETD

The problem of the suitability of the conditions that create experimental stands with those who want to satisfactory testing, ETD was initially. Several works on evaluating the effect of pressure in the vacuum chamber on the characteristics of a jet engine, and [2,3,4], as well as implemented a series of measurements in space [5,6]. In this section, I will give a brief overview of what has been done in these papers.
[2] - Askhabov (80 years)
In the early 80's were carried out on the measurement of spray parameters, mainly the density of ion current in desyatimetrovoy cell [2].
[3] - Fakel thesis Pridannikova
In [3] studied the influence of test conditions on the parameters of the engine and its stability during the test. Special attention in this work was given to the impact of spraying on the walls of the camera to work the accelerator. The following are major provisions:
In the long engine pollution occurs the outer surfaces. In doing so, the greatest significance is the pollution of the surfaces,

which are involved in the work process and the status and properties of which depended the parameters of working process. These surfaces are the walls of the discharge chamber and the anode-gazoraspredelitelya that contact with the discharge. When pollution they formed dark film, the electrical conductivity which is different from the properties of the core material. As a consequence, in the long-term testing of declining traction and increase the amplitude of voltage fluctuations bit.
In the film of dirt on the detention facility and the anode were found: Si, B, Cr, Ni, Fe, which are part of the insulator material, the anode and the walls of the vacuum chamber. The thickness of the film to lock-in increases over the durability of up to a certain critical thickness at which the peeling of its fragments. Under the influence of gravity particles fall and form clusters at the bottom of the outer and upper part of the internal insulator discharge chamber. Release of fragments in the plasma jet is a short-term reduction of resistance to bit interval and «throw» Description of the current value is determined by load characteristics of the transformation (SPU). In this visually observed «spark», departing from the discharge chamber.
As the sources of pollution are the following:
- A pair of vacuum oil of the vacuum chamber (products of their thermal decomposition);
- The allocation of pollution of the elements of the engine design;
- Dispersion of structural materials of vacuum chamber of plasma jet;
- Spraying of insulators bit cells.
In a vacuum chamber with cryogenic pumping sources are products of sputtering of insulators and the walls of the vacuum chamber. In a vacuum chamber with pumping paromaslyanoy of contamination is complemented by the products of thermal decomposition of vapors of the vacuum oil. Effect of spraying the walls of the vacuum chamber is reflected in the lengthy trials, when the conductivity formed conductive film becomes comparable to the conductivity of the plasma.
(4) NASA Glen Center
In the 90 years of work have been made on measuring the parameters of the plasma jet engine at various pressures in a vacuum chamber, the test results are shown in Figure 1, published in [4]. From the data shows that, in order to remove a fairly reliable data especially at the corners more than 30 degrees from the axis, you need a little pressure, or require

special probes [7], filtering low-energy ions, which are mostly the ions formed by re - , neutral atoms in a cell, and are not part of the jet ETD.

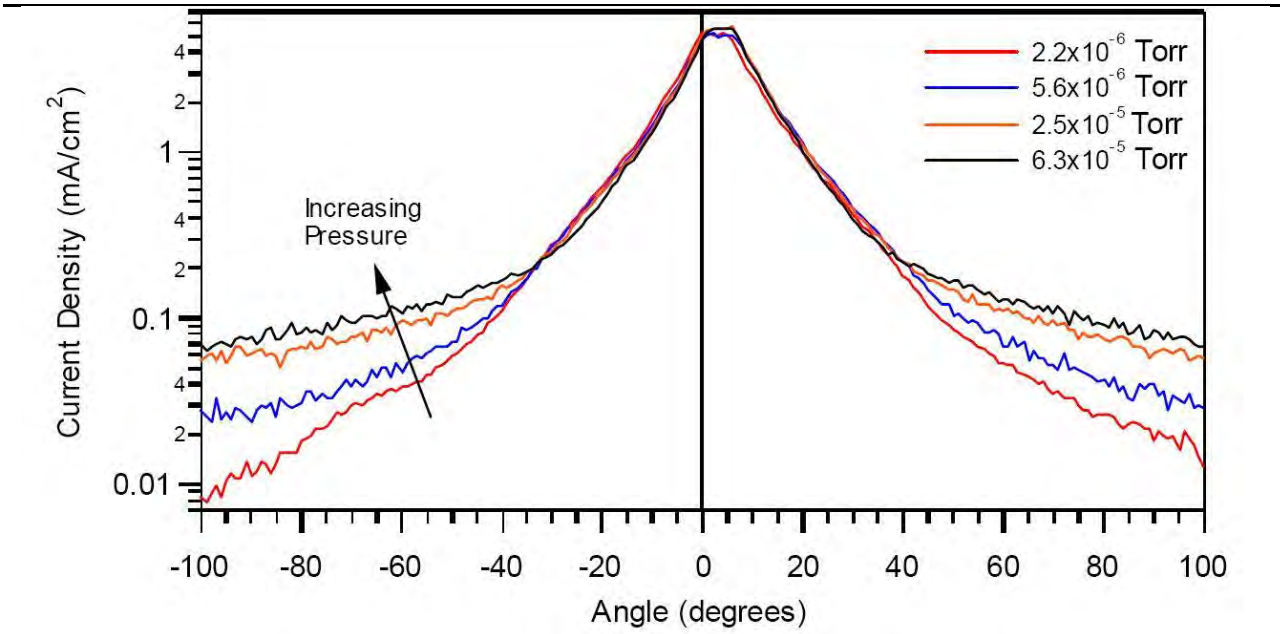

Fig.1.1. The data published in [4]. Angular distribution of SAP-100 at different pressure

The measurement of almost all the main parameters of the jet has been done NIIPME MAI [11]. A density distribution of accelerated ions at a distance of 0.5 m from the engine, the allocation of capacity, measured using the probe Langmyura, the distribution of ions formed as a result of overcharging in the back of the plane engine. Also, an analysis of these parameters and their influence on the characteristics of the engine.
The article [12] examined various characteristics of the jet SPD-100, and also lifted the distribution of energies of ions in the jet, depending on the angle to the axis of the engine.
[5] - Meteor
One of the first studies in space has been working on satellite Meteor [5], where the xenon ions were recorded in the rear hemisphere satellite, which can be attributed to exchange effects.
[6] - Express
In this study performed a comparison between the SPT-100 jet characteristic measured in a vacuum chamber, and data from on board the spacecraft polchennymi «Express». Especially, it shows that the jet EPT growing more intense in terms of space than in the ground. This gives a smaller flow of particles, momentum and energy at the periphery of the plasma flow.

1.4. Review of existing models for simulation of EPT in the vacuum chamber

There are several approaches to assess the conditions for simulating the operation of EPT in a vacuum chamber. Besides the different parameters are modeled in different ways, even more to simulate the same setting, you can use a variety of methods. In addition to selecting the optimal method, you must also choose initial conditions, boundary conditions, the properties of the materials used, tabular data (such as a cross-section of collisions, etc.). It should also reflect on methods of simplifying the problem, to calculate the parameter, so that there is no loss in accuracy (for example, although some processes are taking place in the dynamics can be considered fixed and do not take into account the iteration time, in some cases, you can ignore the fluctuations in the plasma, etc. .). All this will increase the accuracy of the calculation of savings of machine time, and using a larger number of simulated particles or increase the parameters of the grid.

This model is not the first in the modeling of plasma engines, were conducted in 2 organizations attempt to model PD in a vacuum chamber.

A group of Micheganskogo the University under the direction of Boyd [8] implemented a hybrid simulation methods. Mixed fluid-particle method is applied to the plasma jet from the ERT. The model uses a statistical method for the direct simulation Monte Carlo method and the «particle in cell», to simulate the dynamics of atoms and ions. Liquid model based on the Boltzmann equation is applied to the parameters of electronic components. The effects of exchange and electrostatic fields are investigated.

In the process of designing a new installation of the Italian group conducted a simulation methods Alta PIC and DSMC concentration of neutral gas in a vacuum chamber in two-dimensional, symmetric approximation [9,10].

In terms of describing the processes, methods used in these models, not bad, but because of their two-dimensional setting, the use of algorithms used in these techniques, besides evaluation of the impact of spraying on the plasma engine was not implemented because of the complexity of the writing of three-dimensional models . In addition the use of three-dimensional modeling reveals details of which do not show two-dimensional approximation.

Problem

Known work on modeling the dynamics of a jet engine in the plasma [1], as well as calculations of the neutral gas in a

vacuum chamber [2,3].
In [1] presents a model very similar to the used by us, but we use a significant simplification: we consider a stationary problem, and we have no iteration in time. This simplification does not allow us to simulate and evaluate the fluctuation of plasma jet, but gives us a significant advantage in cost of machine time. And in some calculations, such as the algorithm for calculating the distribution of neutral gas by volume of the vacuum chamber iteration in time have little meaning. In the models discussed in [1] the simulated space of 2-dimensional axisymmetric, the model used here is written for three-dimensional space. The main drawback of our models to the real devices is that the size of the estimated volumetric grid more Debayevskogo radius shielding, which does not allow us to take into account the influence of fields generated by charged particles in the range of the Coulomb force generated by them. The model described in [2,3] describes 2D calculation of the distribution dynamics of the neutral gas in the vacuum chamber. The essential difference patterns as shown in the description below is in [2,3] there is no local increase in concentration of particles at the edges of the chamber.

In connection with the shortcomings of models, we were offered an engineering design model, which neglects some physical phenomena, but is applicable to obtain good results of modeling of engine operation in the vacuum chamber. Production targets for the model is given below:
1. Development of three-dimensional mathematical models of the plasma jet engine in a vacuum chamber.
2. Experimental study of laboratory model of SPD in a vacuum chamber to measure probe characteristics, describing a jet engine, as well as the backward flow. Experimental measurement of pressure in a vacuum chamber using vacuum gauges. With the removal of cross-linked probes energospektra along the angle of spread of the jet.
3. The development of mathematical surface analyzer (PMA), to compare the absolute value of the parameter (pressure, current density) from experimentally measured, and modeled energospektra at a given point.
4. Development of modules for the analysis of the elastic interaction of particles, as well as the interaction of particles in recharging.
5. Creating a module for calculating the distribution of sputtered particles.

6. Verification of calculation results with the experiment and the results of studies of other developers.

2. A mathematical model of the spread of the plasma jet engine in a vacuum chamber

2.1 Description of the environment and the processes occurring in a vacuum chamber at work ERT

Before proceeding to the choice of a mathematical model, I would like to outline a few conditions that arise when the plasma engine in a vacuum chamber.
Inside the vacuum chamber is a mixture of gases, which can be roughly evaluated by analyzing the spectrum [13]. Basically, it consists of elements that are present in the composition of the air. In cells with turbomolekulyarnymi pumps are a pair of components of oil, but with cryogenic pumps - hydrogen, which is difficult to evacuate these types of pumps. In general, this mixture is in a neutral state, a mixture of atoms and molecules move freely within the chamber (the free run of the atoms and molecules of the mixture is commensurate with the characteristic size of the camera). Temperature of the mixture can be taken equal to the wall surface temperature of approximately 300K.

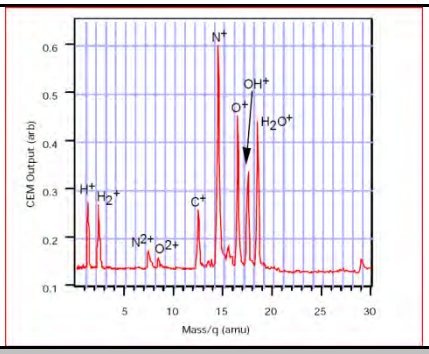

Fig. 2.1. Mass spectrometry data

When the engine picture is changing dramatically: the engine has become a source of accelerated ions (~ 95% mass flow rate) and neutral atoms (~ 5% mass flow rate). In addition, the area around the engine is the source of a strong external magnetic field. In addition, the composition of the gas mixture chamber appear knock plasma jet engine atoms wall of vacuum chamber. The predominant gas in the vacuum chamber becomes the working body of the engine, in this case xenon ions which interact with the end of the chamber, become neutrally charged.

The state of gas in the chamber when the engine can be described as low-temperature, nonequilibrium, partially ionized plasma. The degree of ionization of the plasma varies in volume and falls with the distance from the engine. Condition kvanzineytralnosti, in general, complied with, except for small zones near the walls of the vacuum chamber.

The degree of ionization of the plasma in different parts of the camera changes: 1) because of the spatial distribution of a jet engine (reducing the extent of ionization with distance from the engine), 2) are affected by interactions of various components of plasma:
A) Because of the resonant exchange of atoms of gas mixtures of ionic blow. Although changes in the charge does not occur in the interaction of fast ions with the atom gas mixture (Xe + + Xe-> Xe + Xe +), because of differences in velocity (by several orders of magnitude), the number of charged atoms is also increased.
B) Electron impact ionization of atoms is negligible, as measured experimentally [14] values for the temperature of electrons is an order of magnitude less than the ionization energy of atoms of Xe (12.1 eV).

The system of the engine - vacuum chamber is located in the dynamic-stationary state, ie while the engine is running, the system of plasma parameters are stable over time, in the approximation, which averaged the effects of fluctuations in the emission of ions from the engine and the plasma oscillations.
Another characteristic of the plasma is its electrical conductivity. When motion of particles in the volume of the chamber led self-consistent field E and B, which defines the motion of charged particles. These fields affect the movement and speed of reload particles.

Collisions of particles with each other and with the wall leads to Maksvelovskomu distribution of velocities. However, electric fields have a different impact on the speed of the particles, so the problem is also a topic for consideration.
Based on the briefly outlined the conditions of the process, consider the methods for the simulation of plasma and gas. Various methods can be used in the simulation of different processes, as well as to find the same setting can be applied numerically and fundamentally different modeling techniques. In the next section describes the approaches to mathematical modeling of plasma.

2.3. The methods in this system

2.3.1. Simulation of the dynamic vacuum

The concentration of neutral particles generated in the vacuum chamber, with the equality of the particle flux and particle accelerator, went into a means of pumping, will form a dynamic vacuum in the system. The distribution of these particles is crucial for the analysis of the other processes taking place in a vacuum chamber, as well as other parameters: the concentration of ions, formed as a result of CEX exchange, building space, the distribution of primary ions in the stream, etc.

The most effective method for estimating the concentration of neutral particles, is a simulation using particles (ions build paths, analysis of the intersection of these trajectories with the vacuum chamber walls and track the movement of particles relative to the volume of the chamber until it does not happen with the touch input section of pump means). In doing so, the following assumptions. When you hit a wall of gas ion rekombiniruet and goes to the wall in the form of neutral atoms at a rate determined by taking into account the Maxwell distribution for the temperature of the wall. Since walls of the chamber has a surface roughness, then hit it a particle is not known exactly in which direction it will affect. Therefore, the calculation algorithm used random reflection on the «law of Cosine» about the normal to the point of tangency. The atoms move in a strictly linear path, to take account of collisions, as described in Equation (2.3.2), we introduce factor weakening the beam of atoms. Reflections occur until the particle will not be in the entrance section of the pump. In order to record the output of the atomic volume of the chamber, set «collecting» surface pumps. When you touch the surface of the particles is considered that it took off from the volume of the chamber. After a transition to the calculation of the trajectory of the next particle. During the computation is filled with an array of the time, which had a particle of certain cells in this area. With this array is the actual concentration of particles in the chamber.

For the approximation to the real picture of the process of modeling the interaction of particles from the sides of the chamber is modeled by taking into account the Maxwell distribution with an average temperature of the wall:

$$f(V) = 4\pi\left(\frac{m}{2\pi kT}\right)V^2 \exp\left(-\frac{mV^2}{2kT}\right), \qquad (2.3.1)$$

For correct use of Maxwell distribution in these models need to pick up his degree of freedom «Chi-distribution» [20]. In this paper, we used the method of least squares (sm.ris.2.5).

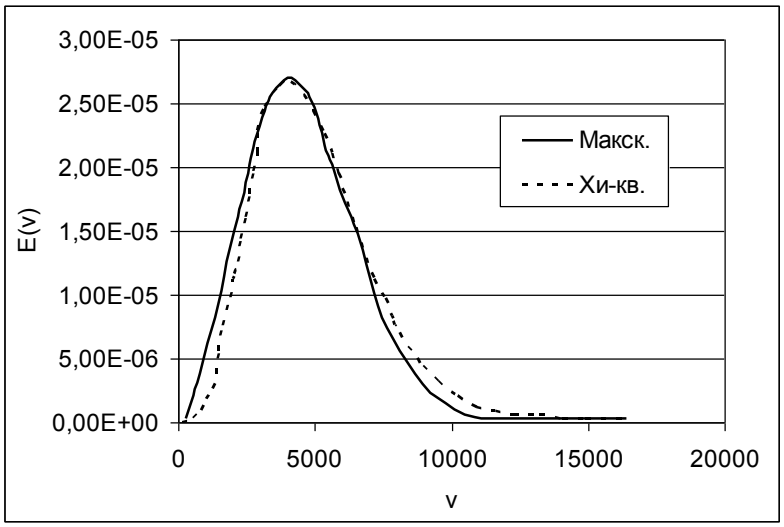

Fig.2.5. The result of selection Chi-distribution to the Maxwellian

«Weight particles» (the number of real particles in one modeled) are determined from the equation of motion:

$$m\frac{dV}{dt} = \frac{\nabla p_н}{n_н} + \frac{\nabla p_u}{n_u}, \qquad (2.3.2)$$

The first and last member of the right takes into account the influence of collisions with neutral atoms and ions. This influence can be assessed using the DSMC method. We used the «method of hard spheres», described in [21].

2.3.2. Modeling the distribution of primary ions

Under the «primary ions», we will understand the particle, ionized and accelerated in the plasma accelerator. The equation of motion of these ions in a vacuum chamber is as follows:

$$m_u\frac{dV_u}{dt} = -eE - \frac{\nabla p_н}{n_н} - \frac{\nabla p_u}{n_u} - e\left[\bar{V}_u \times \bar{B}\right], \qquad (2.3.3)$$

The first and last member of the right side of relation (2.3.3) take into account the influence of electromagnetic field, second and third - take into account the influence of collisions with neutral atoms and ions. The process of collisions with neutral atoms and ions, we also evaluated using the DSMC «method of hard spheres» [21].

2.3.3. Modeling the concentration of ions, formed by the exchange of primary ions to neutral atoms

Number of atoms in a rechargeable cell is determined by the estimated primary ions pass through it. Knowing the precise

trajectory of the ion cell and the value of the resonance cross section for the energy of ion exchange, we can determine the probability of re-gas of neutral atoms in the ion. Thus, tracking the number of primary ions, we obtain the number of particles in each rechargeable cell.

After gathering information on the number of ion rechargeable cells, each cell in the algorithm is a source of ion rechargeable. Sufficient ion rechargeable emitted by a given distribution lines, and speeds. Their trajectories are constructed, taking into account the equations of motion (2.3.3).

As a result of this algorithm we obtain the distribution of ion rechargeable in this area.

2.3.4. Sputtering / deposition

2.3.4.1. Model of ion sputtering of surface

In order to describe the surface ion sputtering in the energy range 100 ... 600 eV, there are several models that use one of two mechanisms of this process [22]. The first mechanism, dispersion of atoms occurs as a result of strong local heating of the surface material in place of the ion strike. The second mechanism, the transfer of energy and momentum of incident ions in atoms of the wall material produces a cascade of elastic interactions of atoms, which take them from the stable position. The result is a dispersal.

The thermal model, in some cases, allows to explain the dispersion of high-organic components, such as Teflon. But for most materials, the theory of dispersion, based on the mechanism of momentum, gives the best result. One of the best theories that describe the details of the ion sputtering of poly crystalline and amorphous materials m the energy range from threshold U_B ~ 10eV to 100 keV is the theory of Sigmund [22]. According to this theory, the coefficient of dispersion of S directly proportional to the deceleration section of elastic S (ε) incident ions. U_B-threshold energy dissipation of the material surface.

$$S = 0.042 \frac{\alpha_S S(\varepsilon)}{U_B} \qquad (2.3.4.)$$

where α_S - dimensionless coefficient characterizing the efficiency of energy transfer, which depends on the mass ratio of ions and atoms, as well as the incidence angle.

With increasing angle of incidence of ions on the surface normal with almost all materials there is an increase rate of dispersal. Quantitative analysis within the theory of Zygmunt shows:

$$S(\theta) = S(0)\cos(h\theta) \qquad (2.3.5.)$$

where S (0) - coefficient of dispersion at θ = 0 (ions fall on the normal to the surface), as h - setting the relationship of mass ion (m1) and the atom (m2).

Studied above theoretical presentation of the observed behavior corresponds to quantify ion sputtering. But its practical use is limited by the fact that it can not explain all the common effects of certain experimental sputtering. For this reason, developed counting model [23] use the approximation of experimentally measured data. Thus, the dispersion of the values recorded in the table with a fixed value of energy of ions, and to determine the coefficient of dispersion of random value, energy and angle of incidence, interpolation equation is used, based on the presentation above.

For example, to determine the coefficient of dispersion of S (ε) at θ = 0sleduyuschee interpolation equation is used:

$$S(\varepsilon) = S_1 + \frac{(S_2 - S_1)}{(\varepsilon_2 - \varepsilon_1)}(\varepsilon_2 - \varepsilon_1) \qquad (2.3.7.)$$

where S_2, S_1 - tabulated values of the coefficient of dispersion for the energy of ions ε_2, ε_1, so that ε_1 <ε <ε_2. The dependence of the coefficient of dispersion of the incidence angle θ, is approximated by using spline functions: Set the longitudinal and transverse distribution of spray particles on the corner of departure:

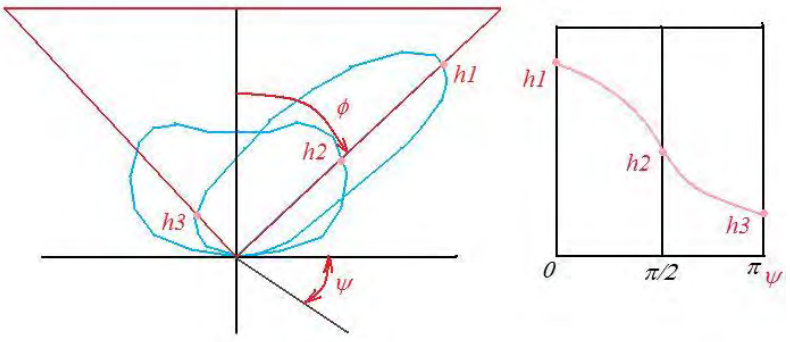

Fig. 2.6. Schematic drawing describing the spline model approximation

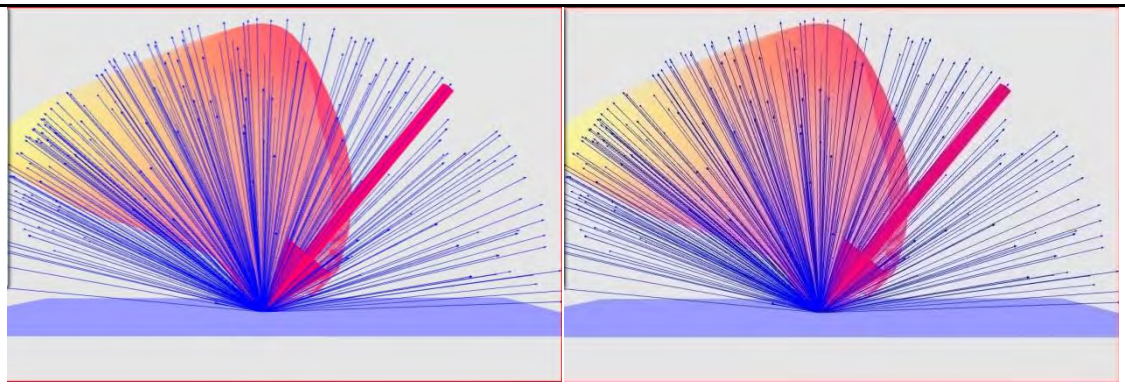

Fig. 2.7. Three-dimensional visualization of model

The main problem is the realization giperbolyatsii (nV) for intermediate azimuth angle of departure ψ particles. The proposed solution to the spline approximation to a cone that is built on the points of intersection of longitudinal and transverse distributions.

Basic conditions:

$$\varphi = 0 \ldots \frac{\pi}{2}; \psi = \pm 0 \ldots \pi; nV(\psi) = nv(-\psi) \tag{2.3.8}$$

Using the boundary conditions of 1-st kind for spline:

$$S'(0) = S'(\pi) = 0 \tag{2.3.9.}$$

Spline based on 3-m pixels, which allows an analytic solution for the spline. [24]

$$S(\psi) = -S_{i-1}^2 \frac{(\psi-\psi_i)^3}{6h} + S_i^2 \frac{(\psi-\psi_{i-1})^3}{6h} + \left(\frac{y_i}{h} - \frac{hS_i^2}{6}\right)(\psi - \psi_{i-1}) - \left(\frac{y_{i-1}}{h} - \frac{hS_{i-1}}{6}\right)(\psi - \psi_i) \tag{2.3.10}$$

As the number of segments is equal to 2 then h = π / 2

System:

$$S_0^2 \frac{h}{3} + S_1^2 \frac{h}{6} + S_2^2 \cdot 0 = C_0 = \frac{y_1 - y_0}{h} - y_0'$$

$$S_0^2 \frac{h}{6} + S_1^2 \frac{2h}{3} + S_2^2 \cdot \frac{h}{6} = C_1 = C_2 - C_0$$

$$S_0^2 \cdot 0 + S_1^2 \frac{h}{6} + S_2^2 \cdot \frac{h}{3} = C_2 = -\frac{y_2 - y_1}{h} + y_2' \tag{2.3.11}$$

S_0^2, S_1^2, S_2^2--spline unknown constants

$$D = \begin{bmatrix} 2h & h & 0 \\ h & 4h & h \\ 0 & h & 2h \end{bmatrix} = 12h^3; D_0 = \begin{bmatrix} C_0 & h & 0 \\ C_1 & 4h & h \\ C_2 & h & 2h \end{bmatrix} = h^2(9C_0 + 3C_2);$$

$$D_1 = \begin{bmatrix} 2h & C_0 & 0 \\ h & C_1 & h \\ 0 & C_2 & 2h \end{bmatrix} = h^2(-6C_0 - 6C_2); D_2 = \begin{bmatrix} 2h & h & C_0 \\ h & 4h & C_1 \\ 0 & h & C_2 \end{bmatrix} = h^2(3C_0 + 9C_2)$$

(2.3.12.)

Ie for the spline coefficients are:

$$S_0^2 = \frac{9C_0+3C_2}{12h}; S_1^2 = \frac{-6C_0-6C_2}{12h}; S_2^2 = \frac{3C_0+9C_2}{12h} \qquad (2.3.14)$$

Now for the calculation of the flow, you can use the formula:

A) for angles ψ = 0 ... π / 2:

$$\frac{(\psi-\psi_1)^3}{6h} + S_1^2\frac{(\psi-\psi_0)^3}{6h} + \left(\frac{y_1}{h} - \frac{hS_1^2}{6}\right)(\psi-\psi_0) - \left(\frac{y_0}{h} - \frac{hS_0^2}{6}\right)(\psi-\psi_1) \qquad (2.3.15.)$$

A) for the angles ψ> π / 2:

$$+\left(\frac{y_2}{h} - \frac{hS_2^2}{6}\right)(\psi-\psi_1) - \left(\frac{y_1}{h} - \frac{hS_1^2}{6}\right)(\psi-\psi_2) \qquad (2.3.16.)$$

The degradation of the surface is not taken into account.

2.3.4.2. Model deposition sprayed material

When sputtering chamber wall surface under the influence of the plasma jet engine atomized material may defer to the surface and working details of the engine, thereby altering its properties. The situation described above is shown in fig.2.8.

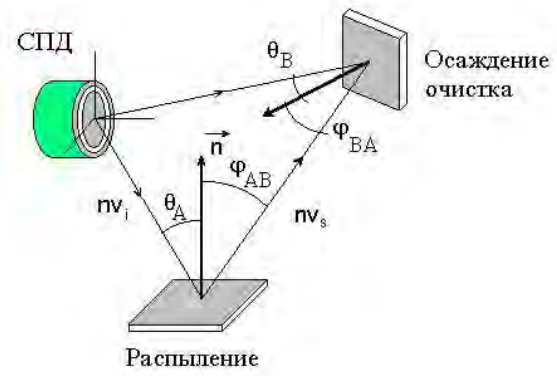

Fig. 2.8. The scheme of spraying the surface of the wall of the camera under the influence of the plasma jet engine

The distribution of sputtered atoms at an angle of emission of ω for amorphous and polycrystalline material scorer ions fall along the normal to the surface, as a first approximation, in conformity with the law:

$$f_{sf}(\omega) = KJ_{sf}cos\beta(\omega) \quad (2.3.17.)$$

where the normalizing factor K = (β +1) / 2π, Jsf = nfuf. At energies of ions scorer 0.1 ... 1 keV, is usually used subcosine distribution with the parameter β <1. The parameter β, which normally characterizes the spatial distribution of sputtered atoms with energies 0.1 ... 1 keV, is close to 1.
The flow of particles in an element of the spatial angle dΩB θAB in the direction of the element A, where the dispersion of the material, the following:

$$f_s(\theta_{AB})\Delta S_A d\Omega_B \quad (2.3.18.)$$

where f_s (θ_AB) - function of the angular dispersion of the material, as defined above (1). Potomdlya flux density of particles on the surface ΔS_B, coming from the surface ΔS_A following dependence:

$$nu_{BA} = f_s(\theta_{AB})\frac{\cos(\theta_{AB})}{d_{AB}^2}\Delta S_A \quad (2.3.19.)$$

Summing up the mass comes to point B with all elements of the camera, which is sputtering, and being in direct line of sight from point B, the total flux density ⟦nu⟧ _B, may be represented as follows:

$$nu_{BA} = \sum_i f_s(\theta_{A_iB})\frac{\cos(\theta_{AB_i})}{d_{A_iB}^2}\Delta S_{A_i} \quad (2.3.20.)$$

Assuming the full deposition of material on the surface (in most cases, this assumption seems true) for the coefficient of mass perepyleniya might write:

$$m_d = nu_B m_S \quad (2.3.21.)$$

where m_S-atomic weight of the sprayed material.
To allow for cleaning the surface, the proportion of recently sprayed material to be found. This value:

$$\vartheta = \sum_i \frac{nu_{B_i}\cos(\theta_{B_i})S(\varepsilon_i,\theta_B)}{nu_B} \quad (2.3.22.)$$

where ⟦nu⟧ _ (B_i) ion flux at point B, S (ε_i, θ_B) - this ratio spread film (the same as the original material).
Then, the rate of mass perepyleniya:

$$m_d = nu_B(1-\vartheta)m_B \quad (2.3.23.)$$

Thus, the coefficient of dispersion of material from the surface of an accelerated beam of ions (number of ions in the beam is equal to N), with energy E, lean over the surface at an angle and will be equal to Y = Y (E) * Y (a). A number of atoms knocked out of the wall of Nw = N * Y; whereas the mass of broken walls of the material to the beam will be equal to m ˙ = N_w / (M · N_a); where M - molecular mass of atoms of the wall, as Na - Avogadro constant.

Then, using the spline approximation described in the previous section, find distribution volume sputtered particles.

2.3.5. The problem of definition of electric field

To determine the capacity of plasma has several differential equations that are used on different occasions. The main are: 1) the Poisson equation, 2) Boltzmann equation 3) The system of MHD equations, which includes the equation for the continuity of the electron gas, the equation of conservation of momentum, the equation of energy conservation, 4) Using the method of "thermilized potential" proposed by A. Morozov et al [28]. The modeling capabilities in the jet considered in [25], which provides a comparison of simulations using the Boltzmann formula, and solution of equations of MHD. Great accuracy is observed in the second case. In [26] examined the use of the ""thermilized potential", to the calculation of channel capacity in the SPT.

The main difficulty of modeling is the correct definition of the distribution capacity of the vacuum chamber.
The main area of the camera, we believe the state of the plasma quasi-neutrality, and to describe the relation of its parameters, we use three basic magnetohydrodynamic equations (equation for the continuity of the electron gas, the equation of conservation of momentum, the equation of conservation of energy) which we solve using the method of finite differences. The initial conditions of the problem are as follows: an initial potential of space and temperature of electrons at a certain point. To do this, to use experimental measurements to a fixed point of the vacuum chamber.

1. The equation of continuity of:

$$\frac{\partial}{\partial t} n_e + \nabla(n_e \cdot V_e) = n_e n_н \cdot <\sigma_i \cdot V_e> \qquad (2.3.24)$$

2. The equation of conservation of momentum:

$$\frac{\partial}{\partial t}(m_e n_e V_e) + m_e n_e (V_e \nabla) V_e = -e n_e E - \nabla p_e + R_c, \quad (2.3.25)$$

where

$$p_e = n_e k T_e \quad (2.3.26.)$$

$$R_c = \frac{e n_e j}{\sigma} \quad (2.3.27.)$$

$$\sigma = \frac{e^2 n_e}{m_e \nu_e} \quad (2.3.28.)$$

$$\nu_e = <\sigma_y V_e> \quad (2.3.29.)$$

Assuming steady state and neglecting the inertial member of the left equation 2.3.25, typing - $\nabla \varphi = E$, we get a generalized Ohm law:

$$j = \sigma\left[-\nabla\varphi + \frac{1}{e n_e}\nabla(n_e k T_e)\right] \quad (2.3.30.)$$

For given ne, Ve and the write down the equation of continuity of charge:

$$\nabla j = 0 \quad (2.3.31.)$$

Substituting equation (2.3.30.) In (2.3.31.) Compute the distribution of the capacity of plasma, using the finite-difference scheme for calculating the gradient and Laplacian, calculating the parameters for the new iteration (layer) using the values at the previous iteration (layer).

3. The equation of conservation of energy:

$$\frac{\partial}{\partial t}\left(\frac{3}{2} n_e k T_e\right) + \frac{3}{2} n_e (V_e \nabla) k T_e + p_e \nabla V_e =$$

$$= \nabla \lambda_e \nabla T_e + jE - 3\frac{m_e}{m_i}\nu_e n_e k (T_e - T_H) - n_e n_H <\sigma_i V_e> \varepsilon_i$$

(2.3.32.)

$$\text{where } \lambda_e = \frac{2.4}{1+\frac{\nu_{ei}}{\sqrt{2}\nu_e}} \cdot \frac{k^2 n_e T_e}{m_e \nu_e} \qquad (2.3.33.)$$

As modeled in this way the field of plasma quasi-neutrality condition is maintained:

$$n_e = n_u \qquad (2.3.34.)$$

Electric field

Now, knowing the distribution of the capacity distribution of fields will find the tension:

$$E = grad(\varphi) \qquad (2.3.35.)$$

Tension affects the trajectory of particles as follows:

$$F_x = qE_x; F_x = ma_x; S_x = V_{0x}t + \frac{a_x t^2}{2} \qquad (2.3.36.)$$

The same could be sign for the axes y and z.

This field can significantly affect the motion of particles of rechargeable, as well as their speed. In calculating the trajectory of motion of particles, we inserted the rechargeable account the influence of the field, so we need to convert the algorithm to find the concentration of particles rechargeable.

2.3.6. The problem of the layer lying next to the wall Numerical simulation of nonequilibrium plasma parameters for the Faraday probe.

In addition to a wall area of the camera there is a rapid drop in capacity, the concentration of electrons and ions (ris.2.9.), As well as the quasi-neutrality condition is violated, we must also take into account the nonequilibrium plasma.

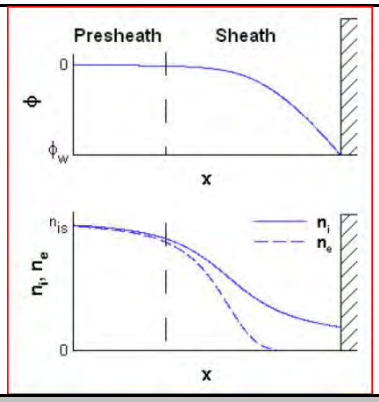

Fig.2.9. Schematic view of the fall capacity of plasma, and

For these areas, we used the model described in [29]. Its essence is as follows.

For a boundary layer with the «cold» ions, and the inseparability of the equation of energy conservation for the ions can be written for the parameters of the concentration of ions and their velocity:

$$n_u(x)V_u(x) = n_{uc}V_{uc} \tag{2.3.37}$$

$$\frac{1}{2}m_u V_u{}^2(x) + e\varphi(x) = \frac{1}{2}m_u V_{uc}{}^2, \tag{2.3.38}$$

Index «c» refers to the setting on the boundary of computational domain, where we assume the plasma becomes the equilibrium.

The concentration of electrons is dependent on local capacity and is determined by using the Boltzmann equation:

$$n_e(x) = n_{uc}\exp\left(\frac{e\varphi(x)}{kT_e}\right) \tag{2.3.39}$$

Poisson's equation is complementary to the system of equations:

$$\frac{d^2\varphi}{dx^2} = -\frac{e}{\varepsilon_0}\left(n_u(x) - n_e(x)\right) \tag{2.3.40}$$

The solution of course is using the difference method for solving differential equations. In [29] for 2D axisymmetrical model of a nonequilibrium plasma parameters are calculated from the plasma near the wall Faraday probe, and their comparison with analytical solution Bom. We are interested in this work to create a 3D model calculated the distribution of plasma parameters in the cells of the boundary wall. Experimental data were taken, put in the article [29]. We have used finite-difference scheme for solving differential equations in space. Figures 2.11-2.14 present the results of the model.

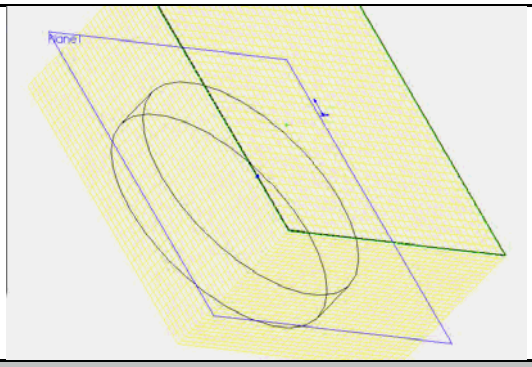

Figure 2.10. Calculated area

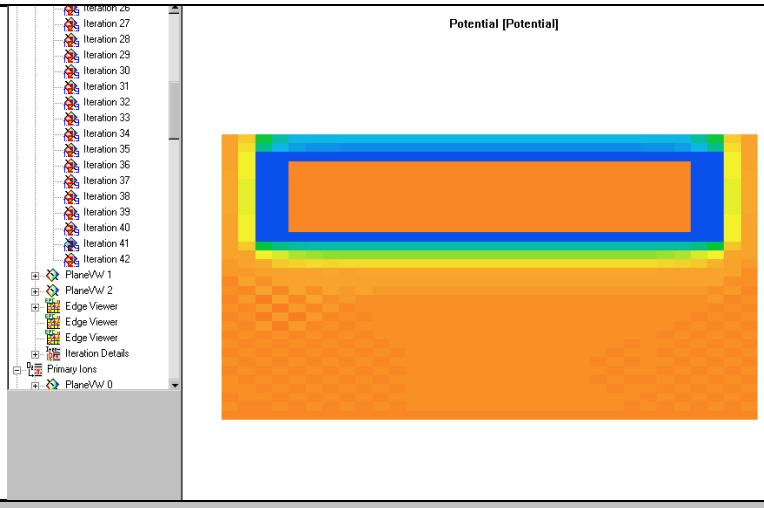

Figure 2.11. Distribution building at 42 iterations

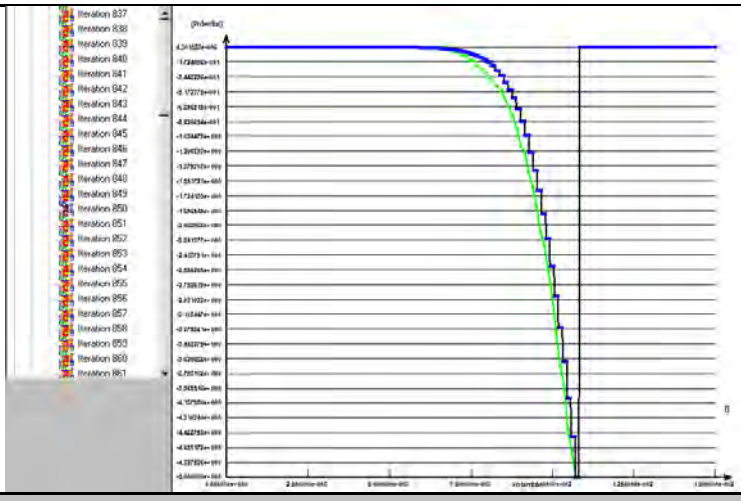

Figure 2.12. Distribution of building along the main axis

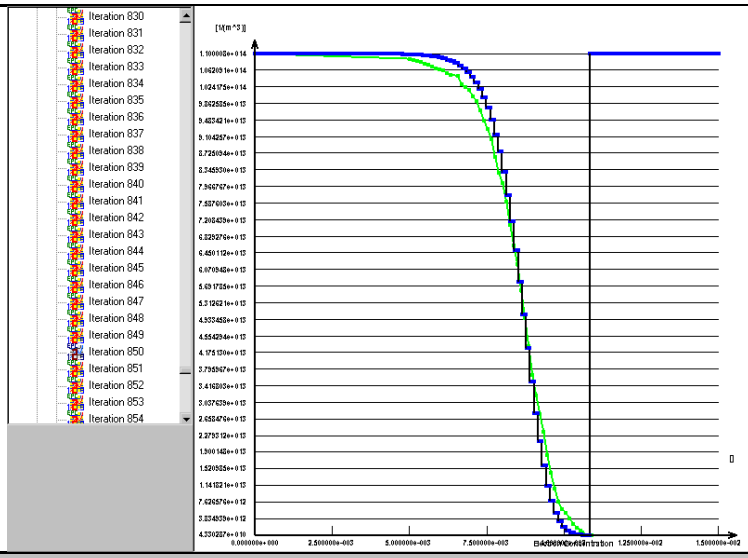

Figure 2.13. The distribution of electron density along the main axis

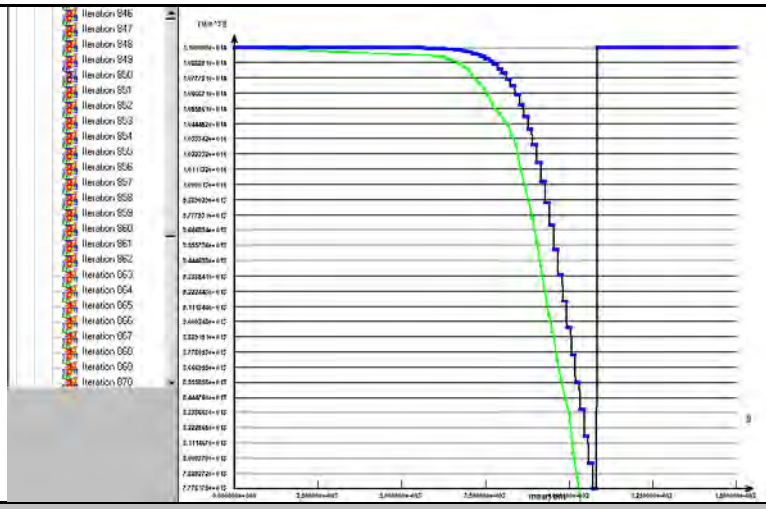

Figure 2.14. Distribution of ion concentrations along the main axis

Although we found differential approximation to determine the spatial distribution of plasma parameters in the wall layer, the practical realization of the model was very difficult because of the requirements for the grid area in a wall: a characteristic cell size should be 10 times smaller than the radius of Debye length.

2.4 Modeling of the magnetic field in the SPT

The external magnetic field in the SPT formed coils magnetization and magnetic system, so for his performance enough to conduct numerical modeling of the magnetic system, setting its dimensions and the currents in the coils. In the DM-based

SAP, delivered on board the spacecraft, the coil magnetization are included in the chain Base current, where there are variations. However, the number of turns in the coil is large, so it has enough inductance to the amplitude of fluctuations in the magnetic field was small. Thus, for engineering calculations of the magnetic field in the SPD with sufficient accuracy can be considered stationary. Therefore, the objective of the numerical description of a task magnetostatic.

To date, the task of calculating the static magnetic fields in various technical magnetic systems (IS) solution. There are a number of programs to calculate the MS (eg, [30,31,32]). Also, there are packages of software applications written specifically for the calculation of the magnetic system of the SAP [33]. In practice, research is often necessary to know the real magnetic field, taking into account the errors of manufacture and assembly of engine design and real differences of magnetic properties of materials from the IPU table. This task can be solved numerical modeling of the magnetic field with boundary conditions obtained experimentally.

In RIAME MAI was offered a similar method of settlement and experimental study of the magnetic field, which allows the engine to take into account the real structure and magnetic properties of real materials. In particular, a program that allows to calculate the magnetic field in the discharge chamber, with as boundary conditions were the measured values of magnetic induction. However, the program has some shortcomings, namely:

- Has been calculated assuming axisymmetric magnetic field;

- Do not use modern visualization of results.

In addition, the program was in beta form and methodology of the study was not worked by that do not allow a rapid analysis of magnetic fields in various models of the SPT. Thus, the complete methodology study the magnetic field in the SPT, taking into account the real structure and magnetic properties of real materials ICJ, which would include all the stages, from the collection of boundary conditions to the visualization of the results of the calculation of fields, including three in time for the start of the author did not exist.

2.4.1. Analysis of the trajectory of an electron off from the cathode-compensator in the vicinity of the outlet SPD

Because of the very small mass of electrons, they move strictly posilovym lines of the electromagnetic field. In this paper we study the motion of electrons along the magnetic field calculated in ELCUT [34].

ELCUT calculates only two axisymmetric, so we have to convert arrays of Br, Bz in three-dimensional, taking into account the axial symmetry of Bx, By, Bz.

The movement of electrons in an electromagnetic field described by the following equation:

$$m_e a_x = q(E_x + B_z v_y - B_y v_z)$$

$$m_e a_y = q(E_y + B_z v_x - B_x v_z) \qquad 2.3.41.$$

$$m_e a_z = q(E_z + B_y v_x - B_x v_y)$$

As for the trajectory of motion can affect the interaction with neutral atoms, ions accelerated in the engine, and reload the ions, as well as electron-electron interaction. All of these processes, we also consider using the ratio of intensity of the beam of electrons.

However, this calculation does not take into account the electric field, which in future can be entered using the experimental data, either by using the Boltzmann equation solutions.

Boundary conditions:

1) Cathode. The program interface allows you to start the cathode surface, and set the average energy of flight of particles. The direction of departure, we take on the normal to the start of, and determine the point at the start of the accident.
2) The trajectory of an electron off from the cathode: The next two drawings represent the conversion of magnetic induction field of ELCUT:

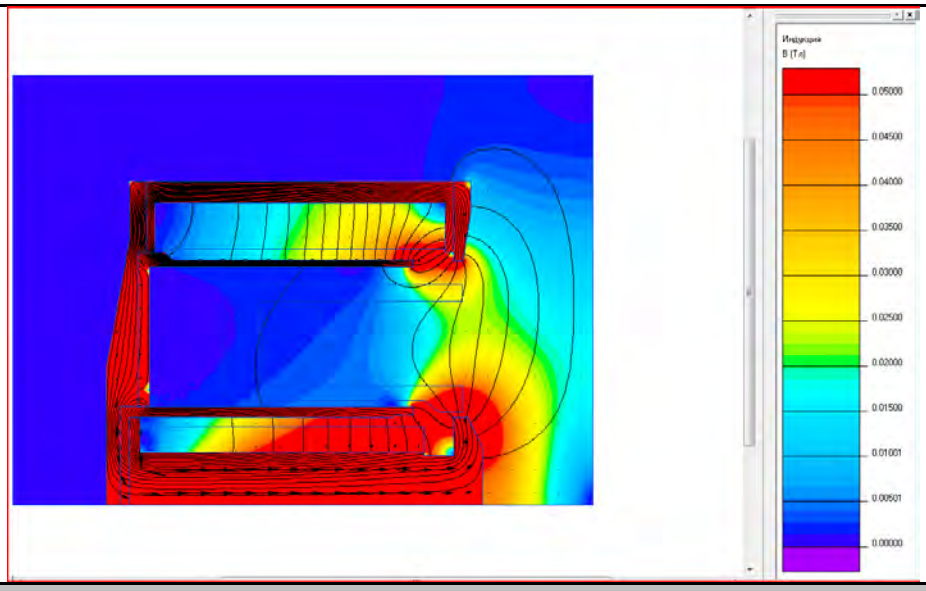

Fig. 2.15.B

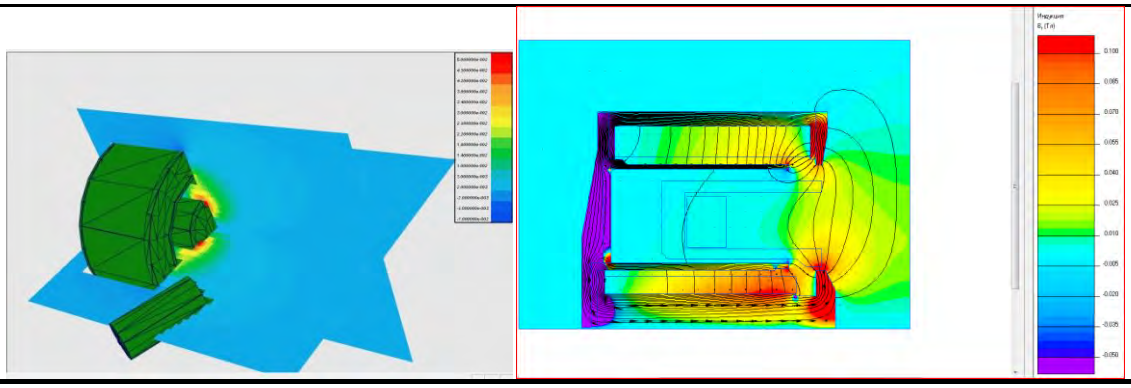

Fig. 2.16.Br

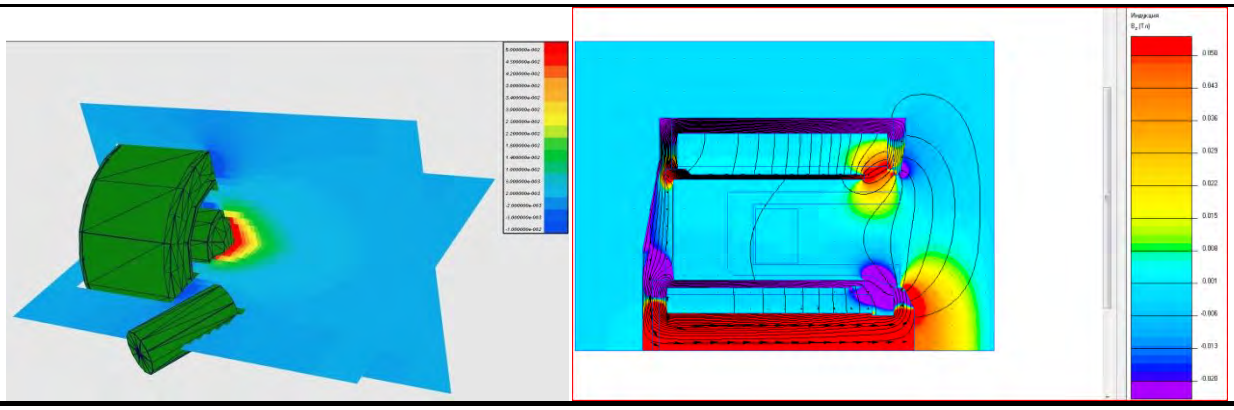

Fig. 2.17.Bz

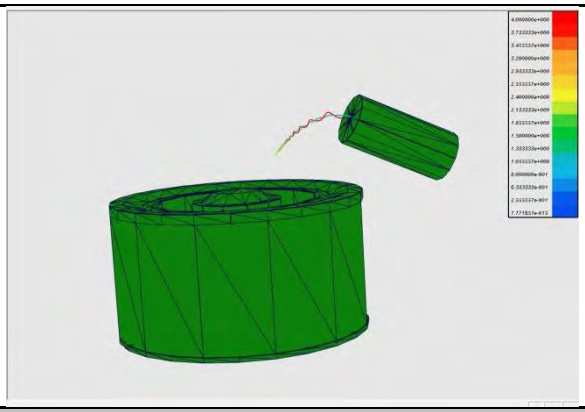

Fig. 2.18.Trajectory electron with starting energy 2eV

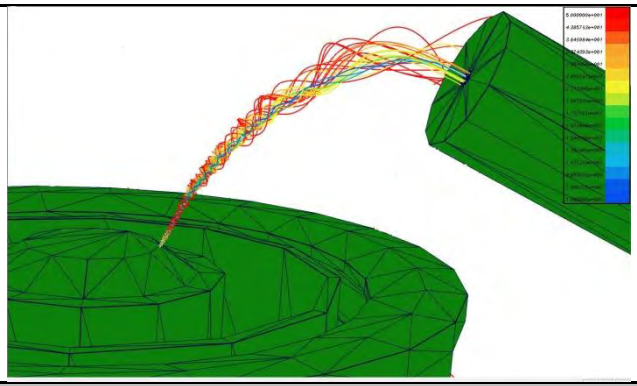

Fig. 2.19. Trajectories electrons in the beam (the average home energy elektrona12 eV)

Analysis:

In calculating the trajectories, it was observed that the electrons in strong magnetic fields in the zone of internal coils are deployed, and moved back to the same power lines, only with the energy of the order of 30-50 eV and a large radius of rotation around the power lines. What has also been observed in experiments.

3. The implementation of the mathematical model

3.1. Project Description

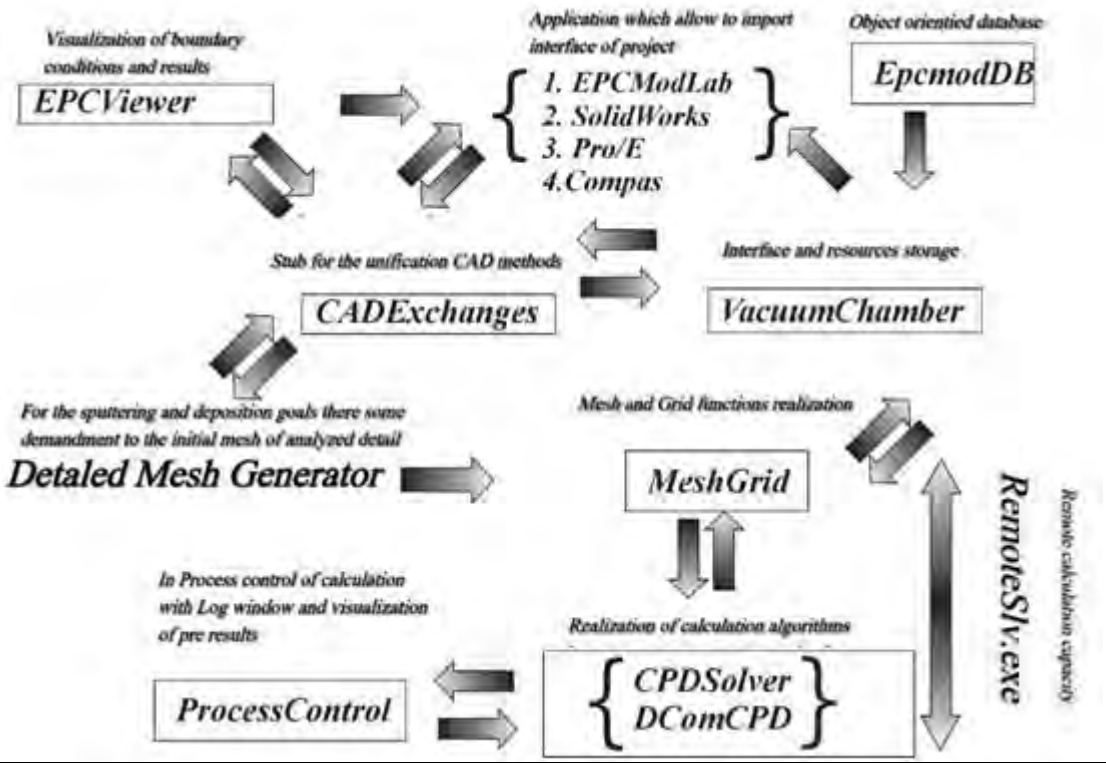

Fig. 3.1. Project Structure

1. Library VacuumChamber - implementation of the project tree, and dialogues, as well as parameters, and the main class project, conservation project settings and record the results. This is the main library PreProcessor'a.

2. Library CADExchanges - standardization of methods for working with CAD systems.

3. Library MeshGrid - which has preserved the objects surface and volume mesh. Contains the implementation of methods for working with grids. The implementation of the conservation of grids to a separate file. For the volumetric mesh has class to calculate the parameters of the cells in the input triangle shape lying in the cell. Calculate the volume of the body in the cell, the center of mass.

4. Component EPChartGl - ActiveX component that is designed to create dialogs and other objects, a basic class for which the base is a CWnd 1) the visualization of graphs, and 2) the distribution of any parameter in a given plane.

5. Component ElabView - ActiveX component that is implemented through the embedding of a tree project in the CAD system and application EPCLab.

6. Library EpcLabDB - contains the implementation of object-oriented database.

7. Application EpcLab - visualization of the grid, and container for wood project configuration OC.

8. Application DetailedMeshGenerator - surface mesh generator.

9. Application ProcessControl - monitoring the progress of calculation and display of interim results.

10. Application Registration - registers the objects and the way the project in the register of Windows.

11. Libraries CPDSolver DComCPD and stored in a realization of algorithms for the calculation, ie trajectory and magnetohydrodynamic model.

12. Library EPCMdlViewer unifies the visualization of the grid, boundary conditions, as well as the results of the calculations directly within CAD systems.

3.2 Determination of initial and boundary conditions

3.2.1. The initial and boundary conditions for calculating the distribution of neutral particles

Atomic mass of xenon 131

The temperature of the walls of the vacuum chamber 300K

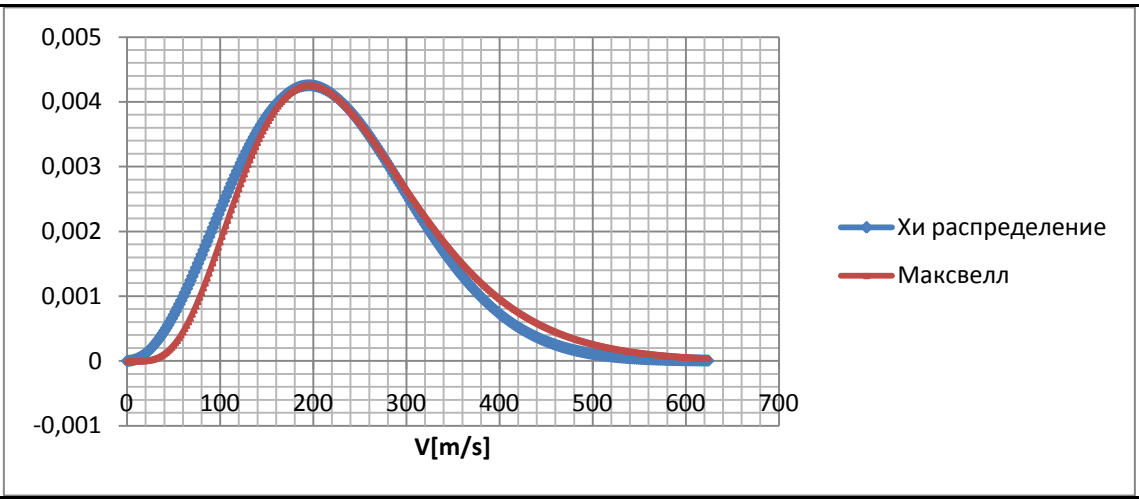

Fig.3.2. Approximation for modeling the velocities of neutral atoms of xenon after reflection from the walls of the vacuum chamber [m / s]

Engine № 1.1.

Mass flow rate of 2.35 mg / sec. The same angular distribution was measured using RPA probes, located on the beam at rasstoyanii0.4 meters from the engine.

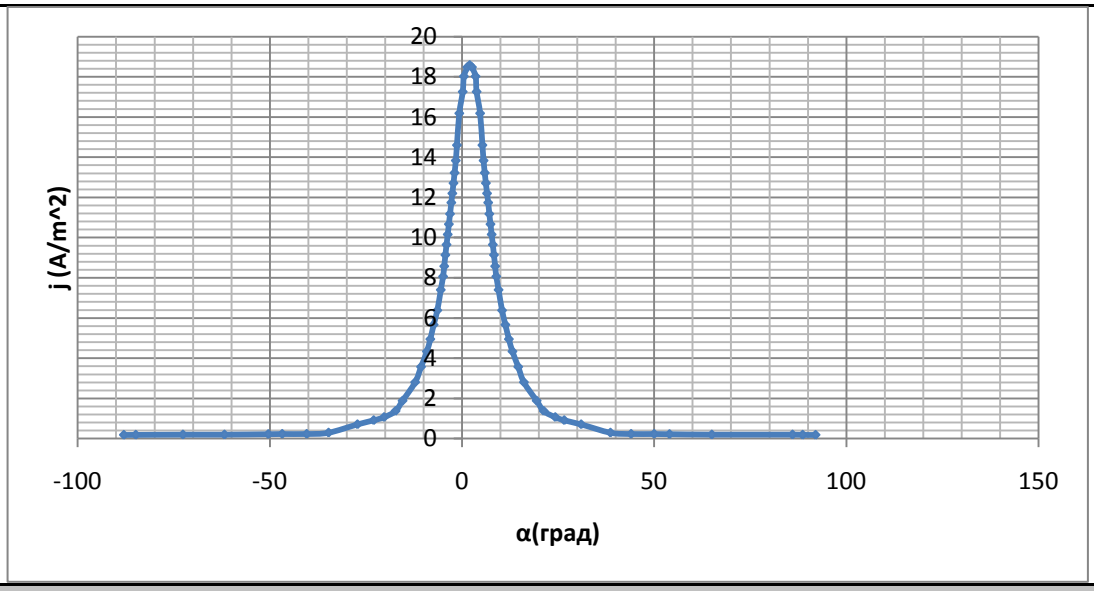

Fig. 3.3. Angular distribution of ion current density on the beam located at a distance of 0.4 m from the engine № 1.1.

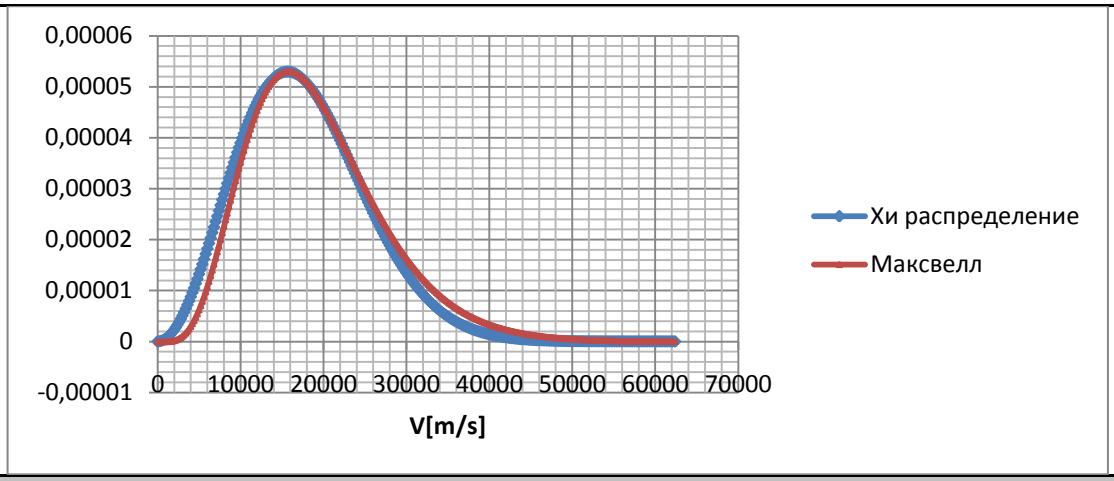

Fig.3.4. Approximation modeling for the primary ion velocity engine № 1.1. and № 1.2.

Engine № 1.2.

Mass flow rate of 2.35 mg / sec. The same angular distribution was measured using RPA probes, located on the beam at rasstoyanii0.4 meters from the engine.

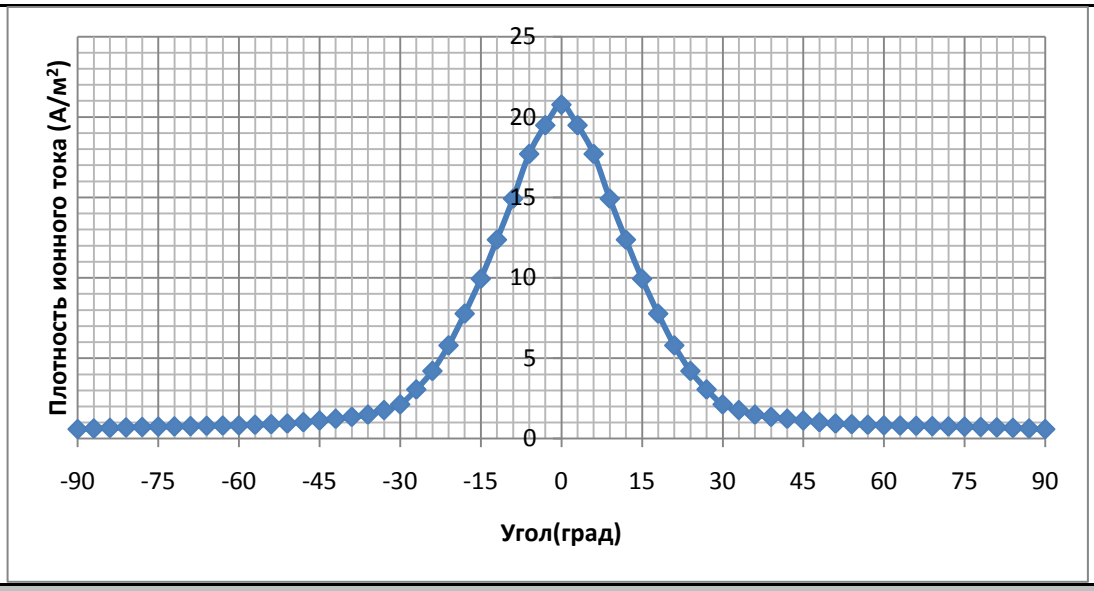

Fig. 3.5. Angular distribution of ion current density on the beam located at a distance of 0.4 m from the engine № 1.2.

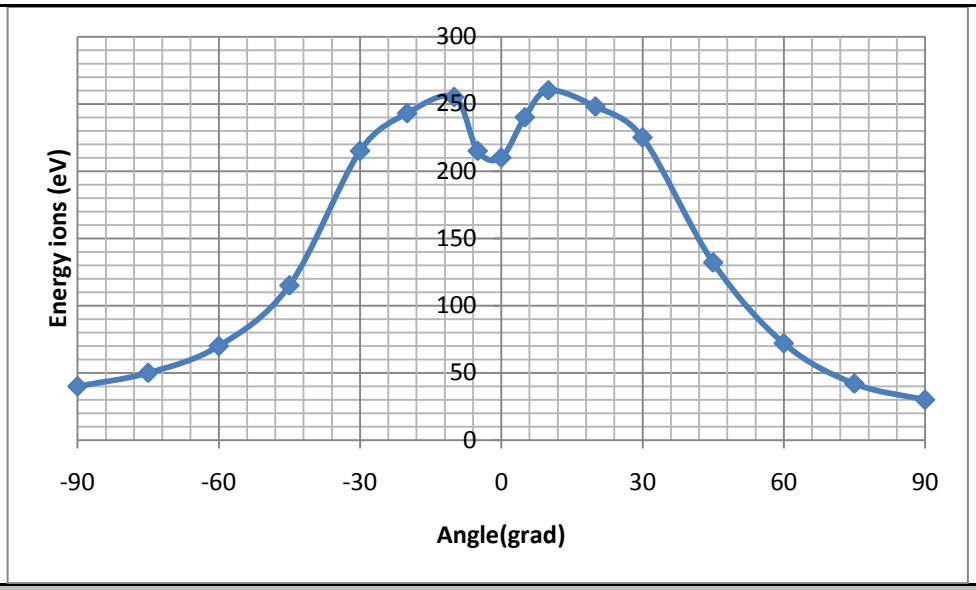

Fig. 3.6.Energiya ions from the angle of departure for engines № 1.1 and 1.2.

The engine number 2

Mass flow rate of 3.5 mg / sec. The same angular distribution was measured using RPA probes, located on the beam at a distance of 1 m from the engine.

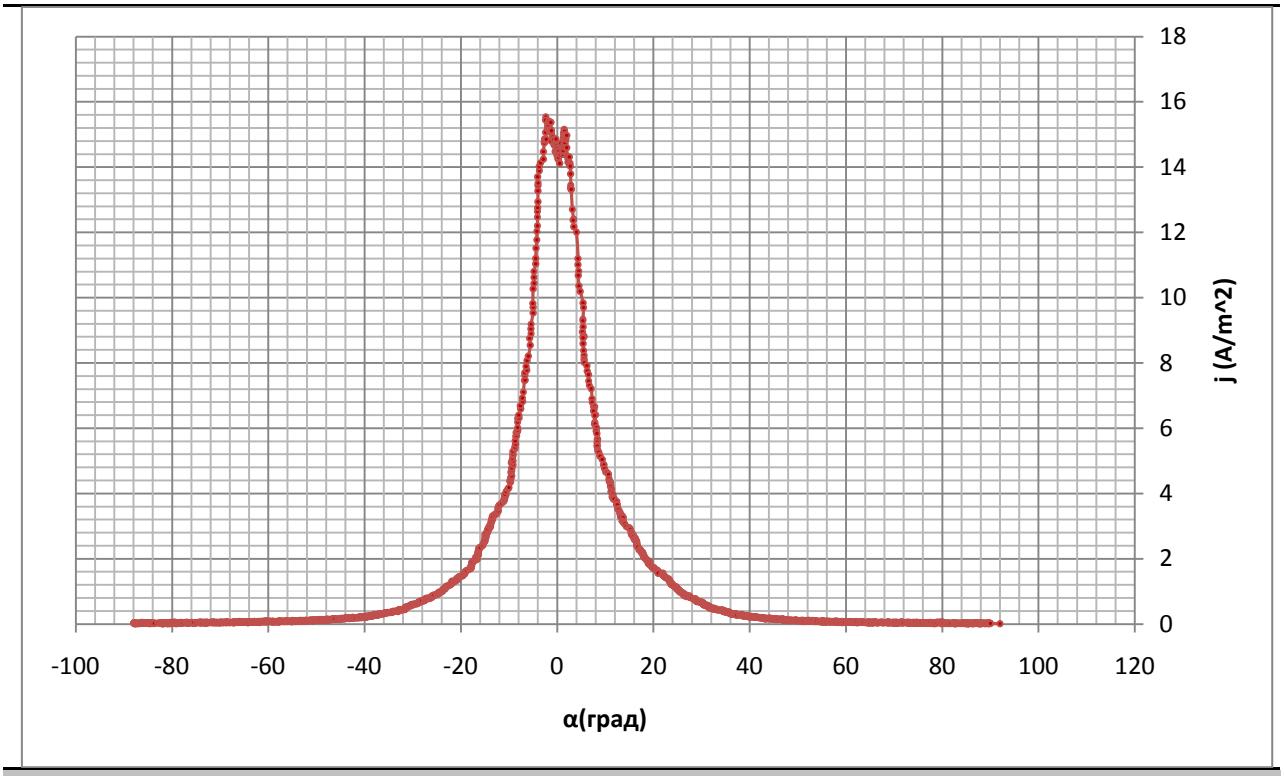

Ris.3.7 Angular distribution of ion current density on the beam located at a distance of 1m from the engine number 2

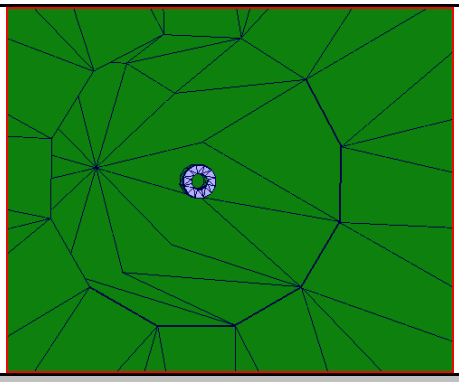

Fig. 3.8. Type of engine number 2 inside the vacuum chamber, which is emitted equiprobable primary ions

The engine number 3.

In [35] was published on the calculation of the concentration of neutral gas in the chamber Alta-IV. Also, there is given a drawing of the camera, so we were able to make it a model.

There have been building models 3kW motor with a mass flow rate of 5.4 mg / s, the average energy of ions of 250eV, and the distribution of ion current from the corner, we took as the model of the engine № 1.1.

The engine number 4.

In [8] calculated the accelerator BPT-4000 in a vacuum chamber AEDC 12V.

Mass flow rate 14.1 mg / sec.

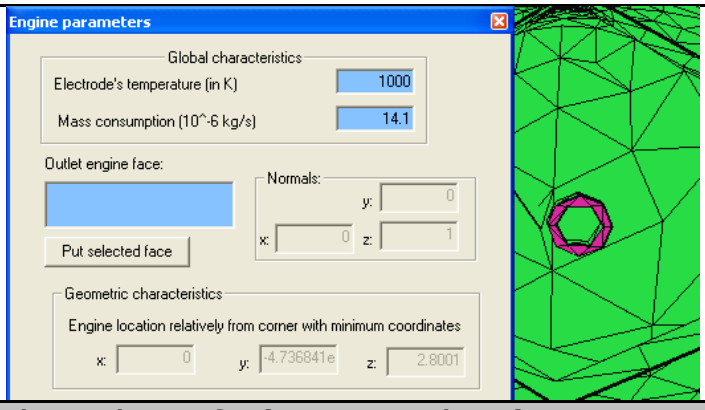

Fig. 3.9. The situation of the motor in the camera

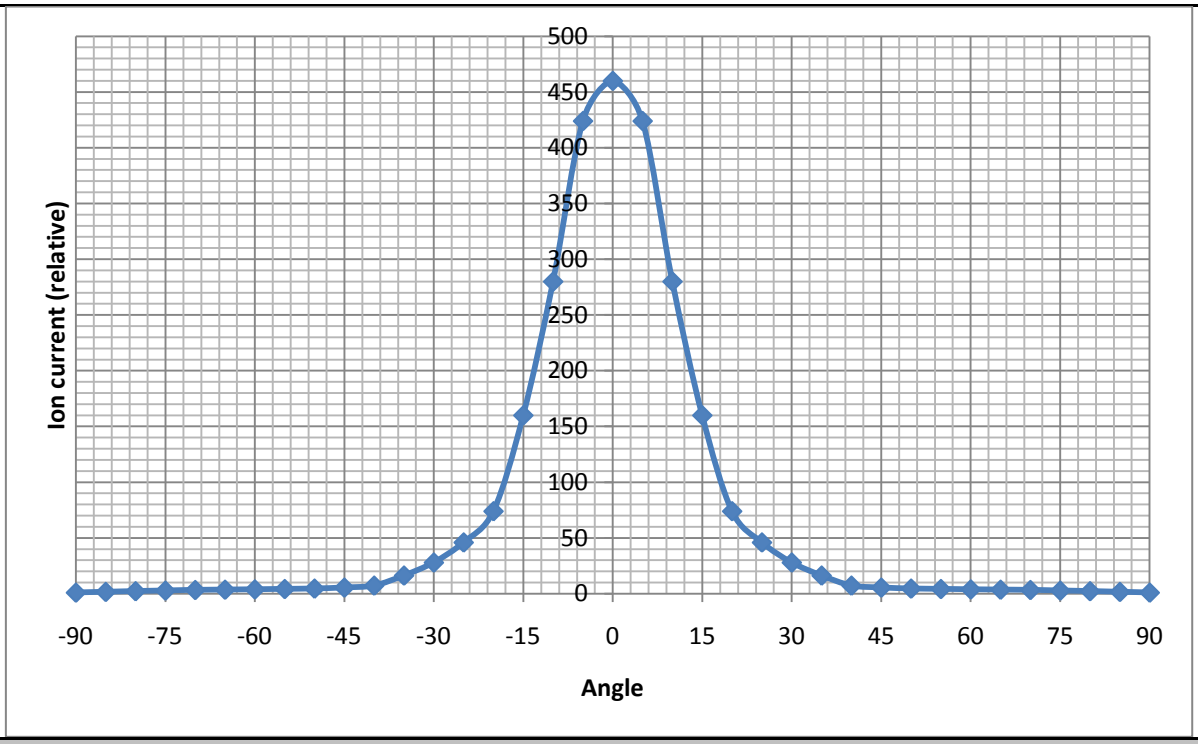

Fig. 3.10. Density of ion current from the accelerator

The engine number 5

In the experiments made in this work is supplied to the collector probe potential of 20 V, that does not transmit ions at low probe.

In our model, this distribution was unacceptable, so we took the distribution of [36], which were published by the distribution of current density ion SPT-100, under various pressures in a vacuum chamber.

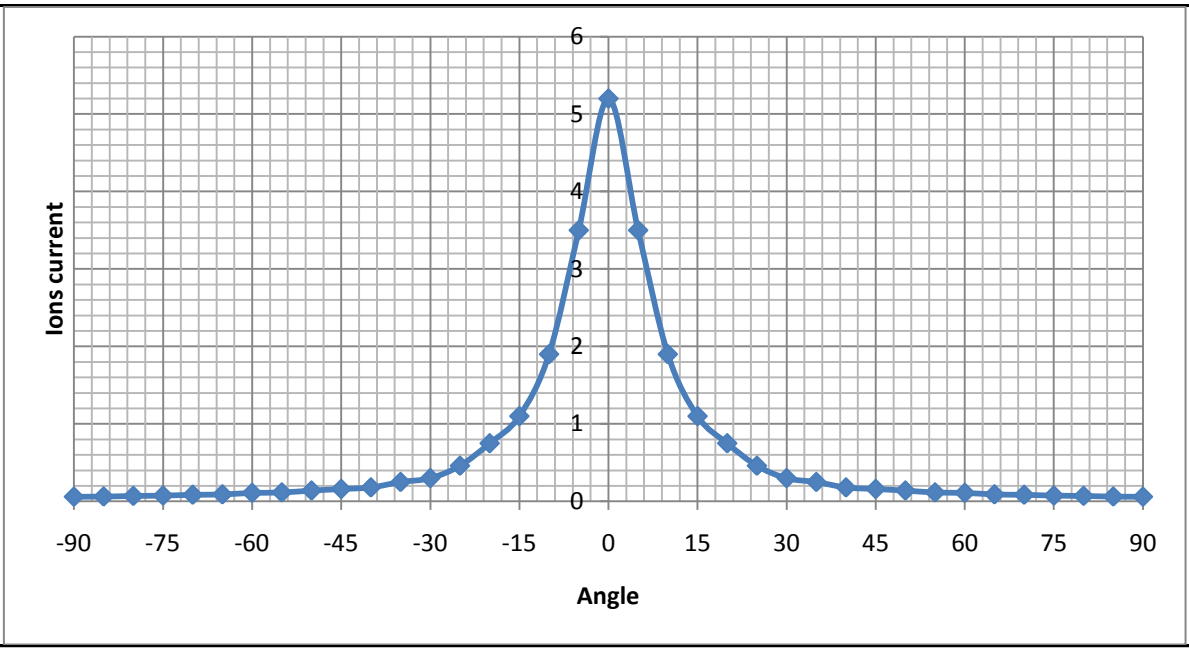

Fig. 3.11. Distribution of current density for the SPT-100 at a pressure of 2.5e-5 Tor.

3.2.2. The initial and boundary conditions for calculating the distribution of primary ions

Also measured volt-ampere characteristics at angles of 0, 5, 10, 20, 30 and 40 degrees for the engine number 2.

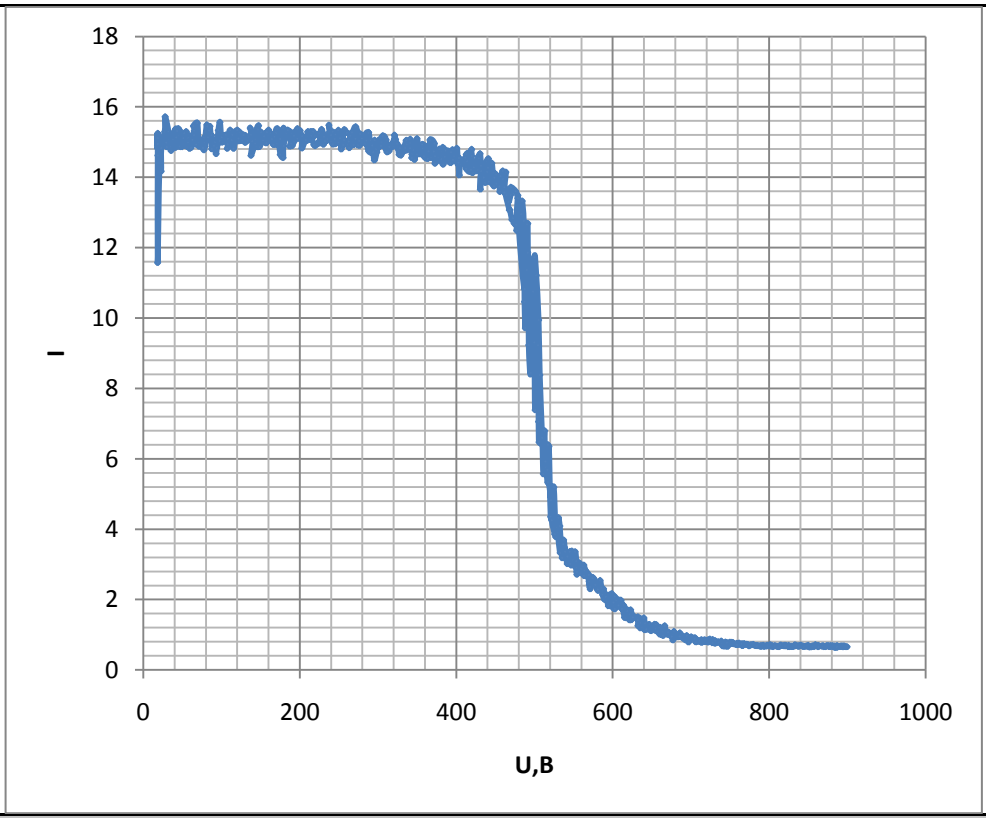

Fig.3.12. Volt-ampere characteristic for the angle of 0 degrees

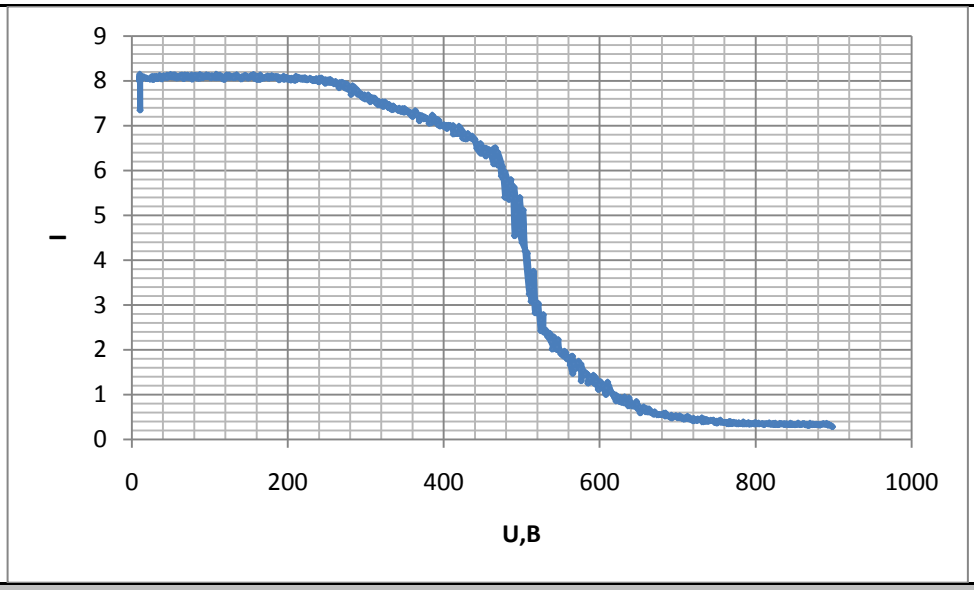

Fig.3.13. Volt-ampere characteristic for the angle of 5 degrees

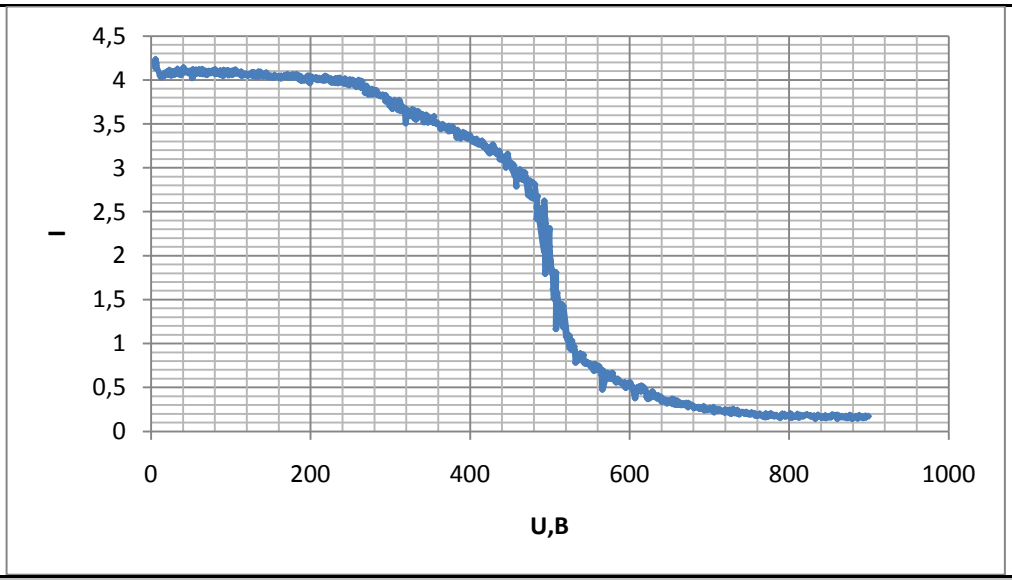

Fig.3.14. Volt-ampere characteristic for an angle of 10 degrees

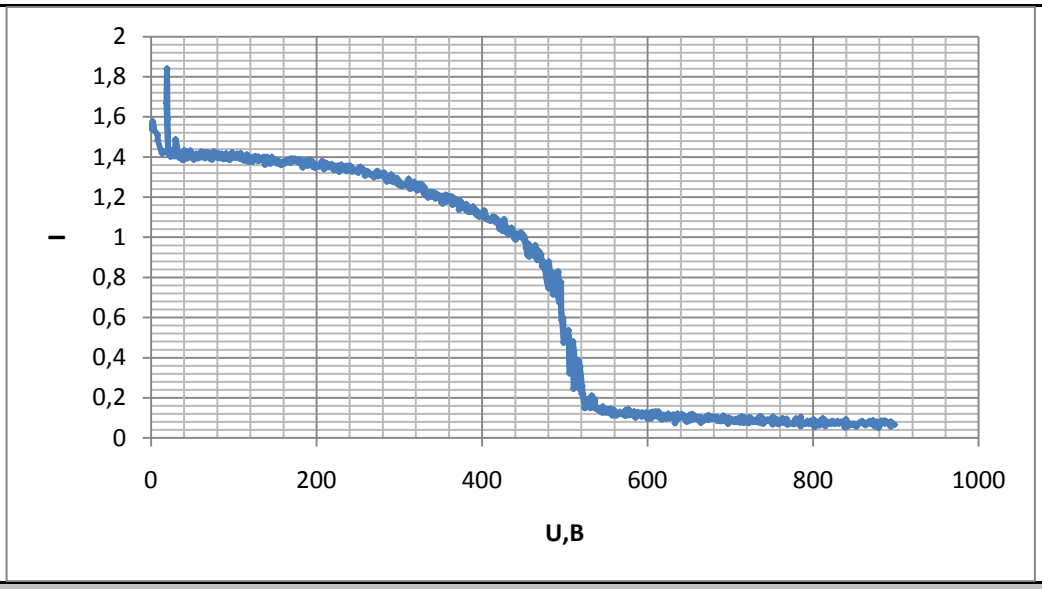

Ris.3.15. Volt-ampere characteristic for the angle of 20 degrees

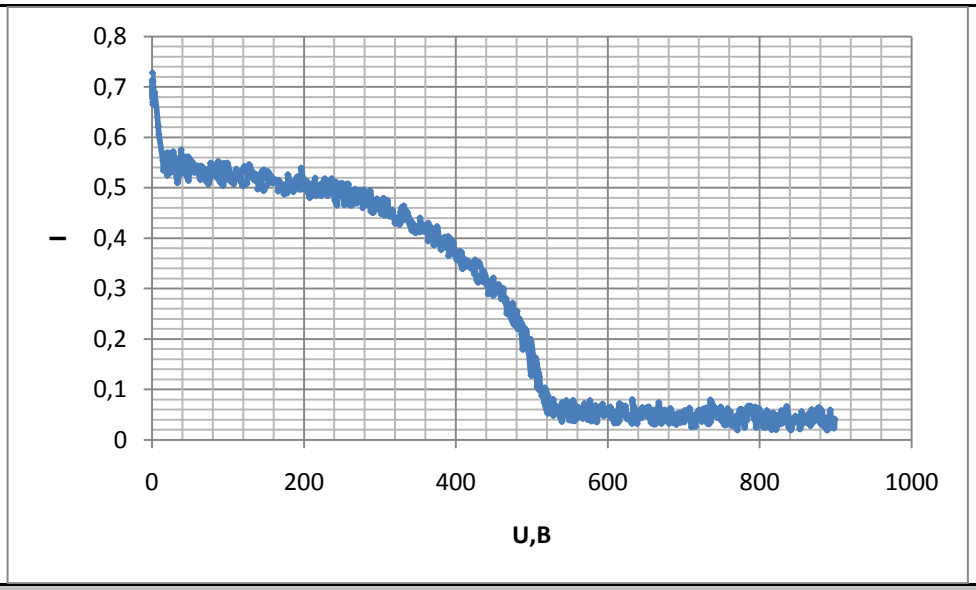

Fig.3.16. Volt-ampere characteristic for the angle of 30 degrees

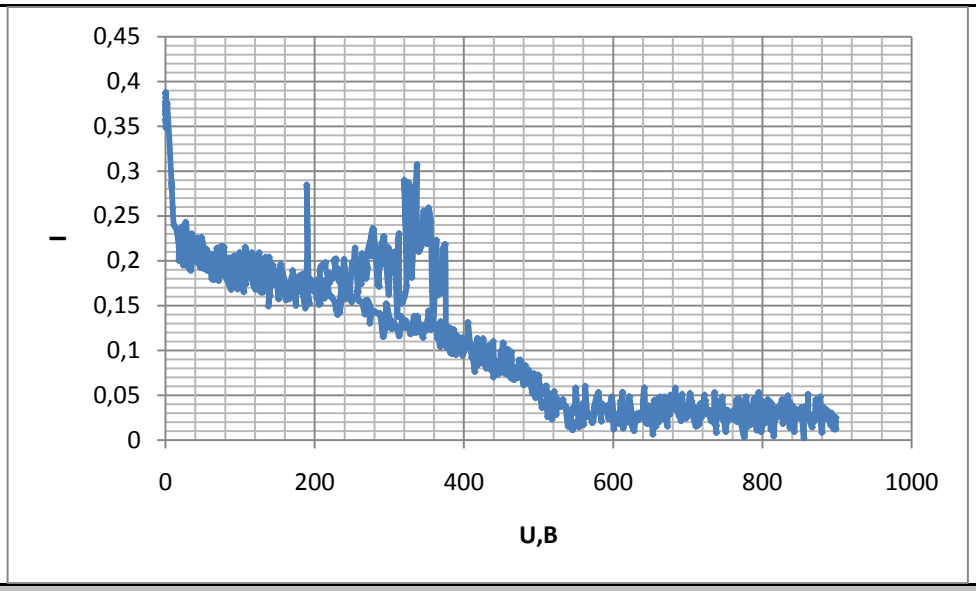

Fig.3.17. Volt-ampere characteristic for the angle of 40 degrees

Processing of volt-ampere characteristics

The following formula was used to obtain a volt-ampere characteristics of the distribution of energies:

$$\frac{dN}{dE} = \left[\frac{\frac{dj}{dU}_{i+1}}{\sqrt{U_{i+1}}} + \frac{\frac{dj}{dU}_{i}}{\sqrt{U_i}}\right](U_{i+1} - U_i)/2 \qquad 3.1$$

The following images are presented the results of the processing to the respective corners.

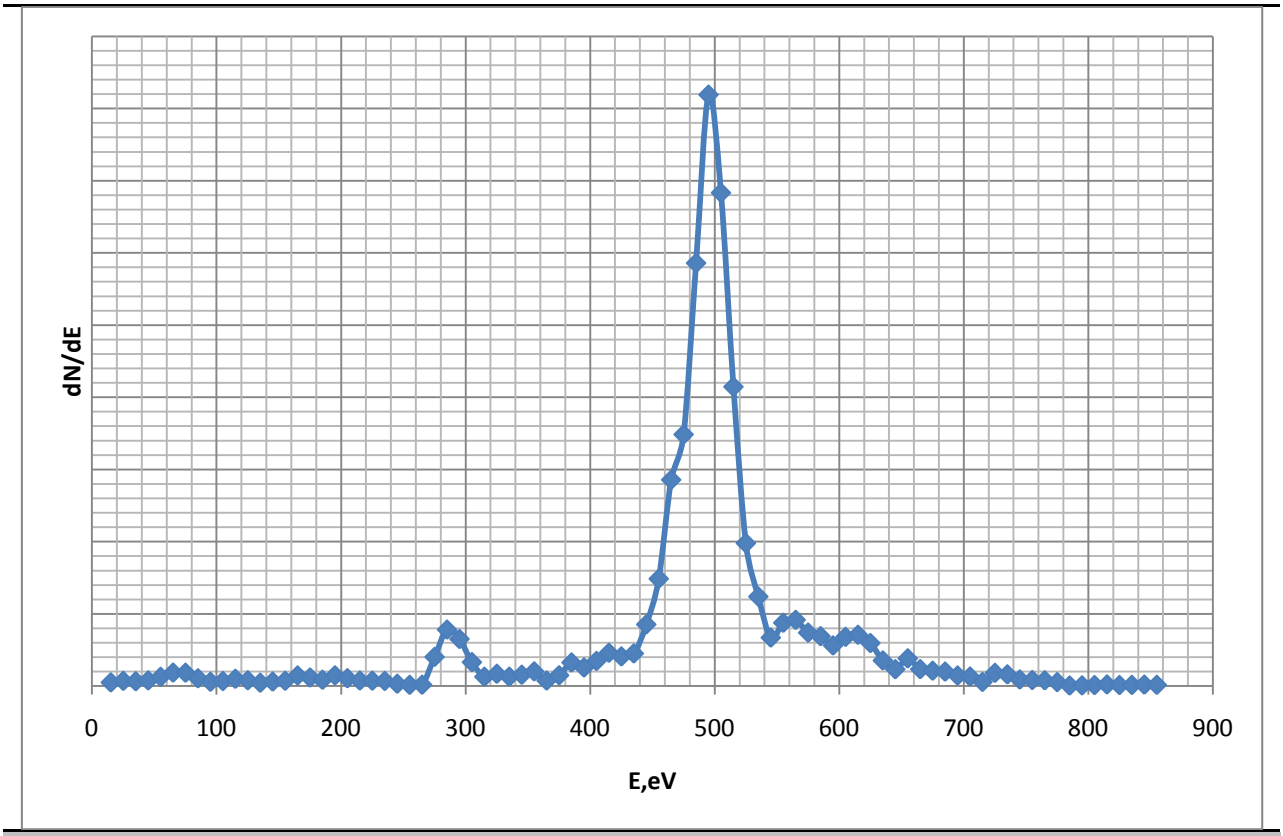

Fig.3.18. The distribution of energies of ions in the jet at an angle of 0 degrees from the axis of the engine

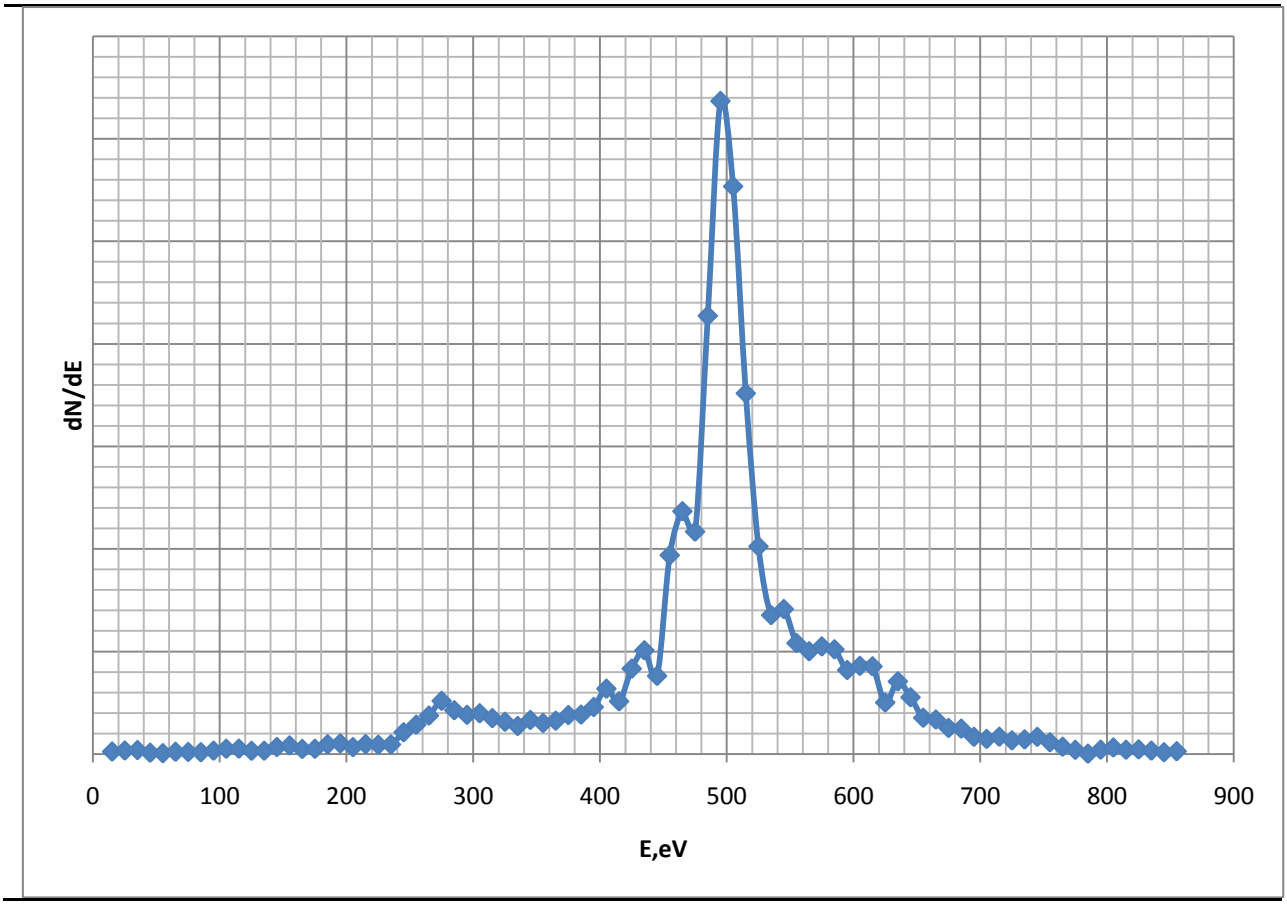

Fig.3.19. The distribution of energies of ions in the jet at an angle of 5 degrees from the axis of the engine

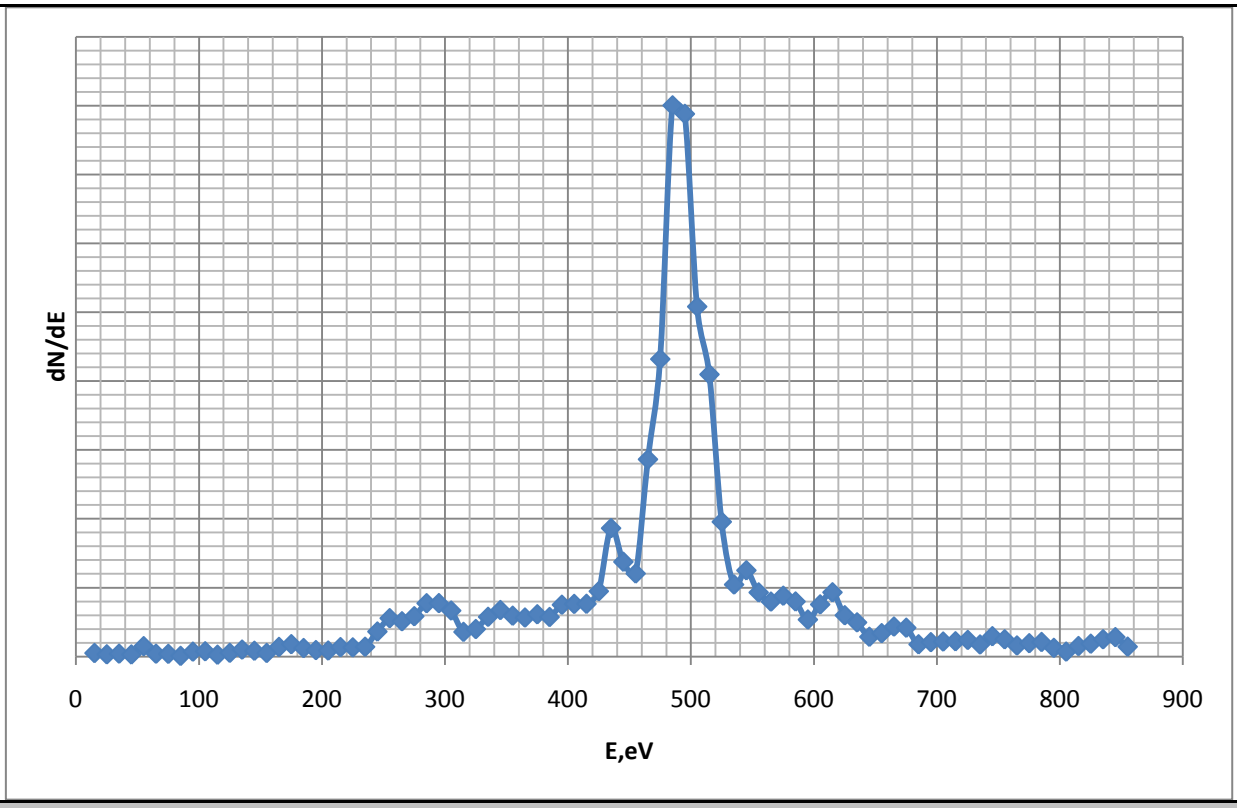

Fig.3.20. The distribution of energies of ions in the jet at an angle of 10 degrees from the axis of the engine

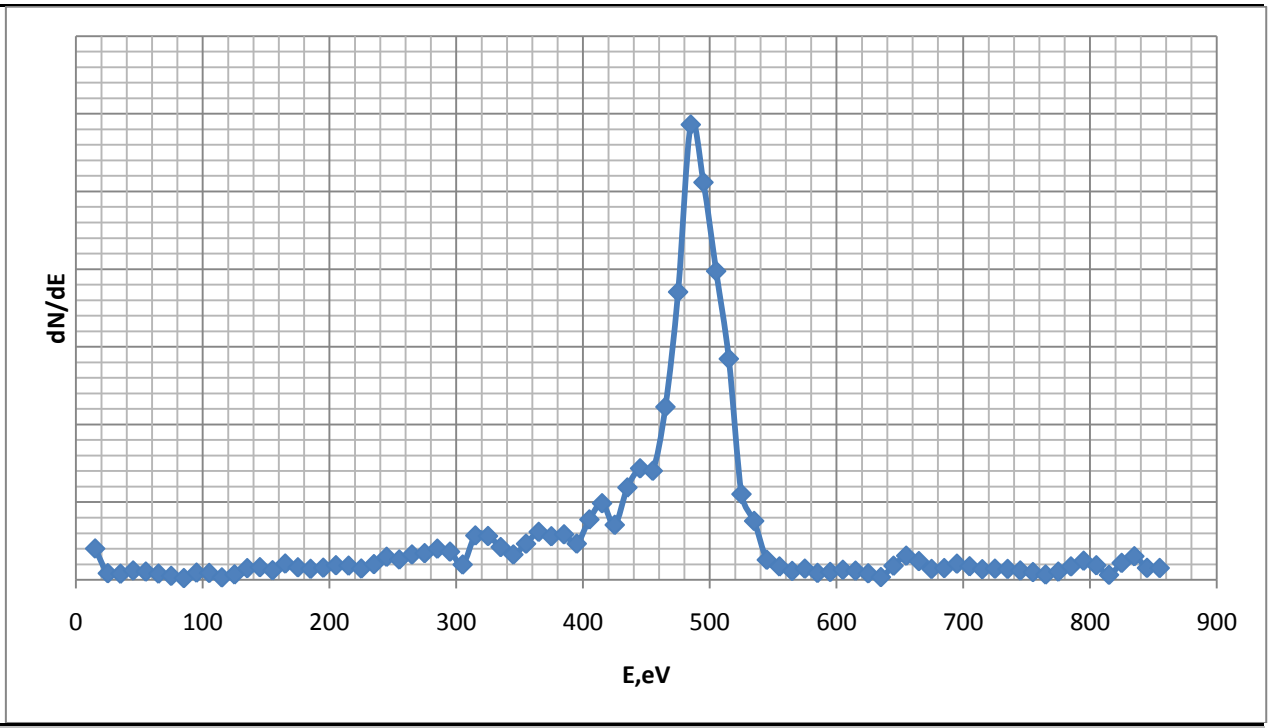

Fig.3.21. The distribution of energies of ions in the jet at an

angle of 20 degrees from the axis of the engine

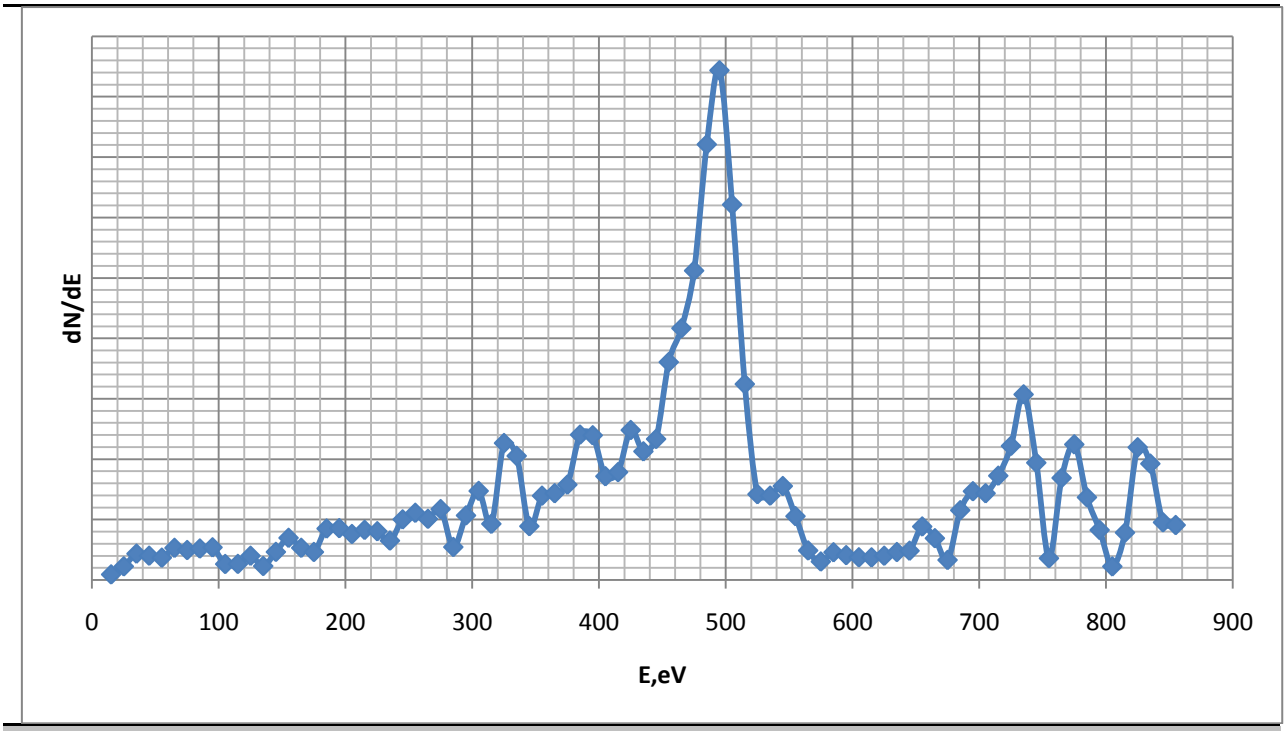

Fig.3.22. The distribution of energies of ions in the jet at an angle of 30 degrees from the axis of the engine

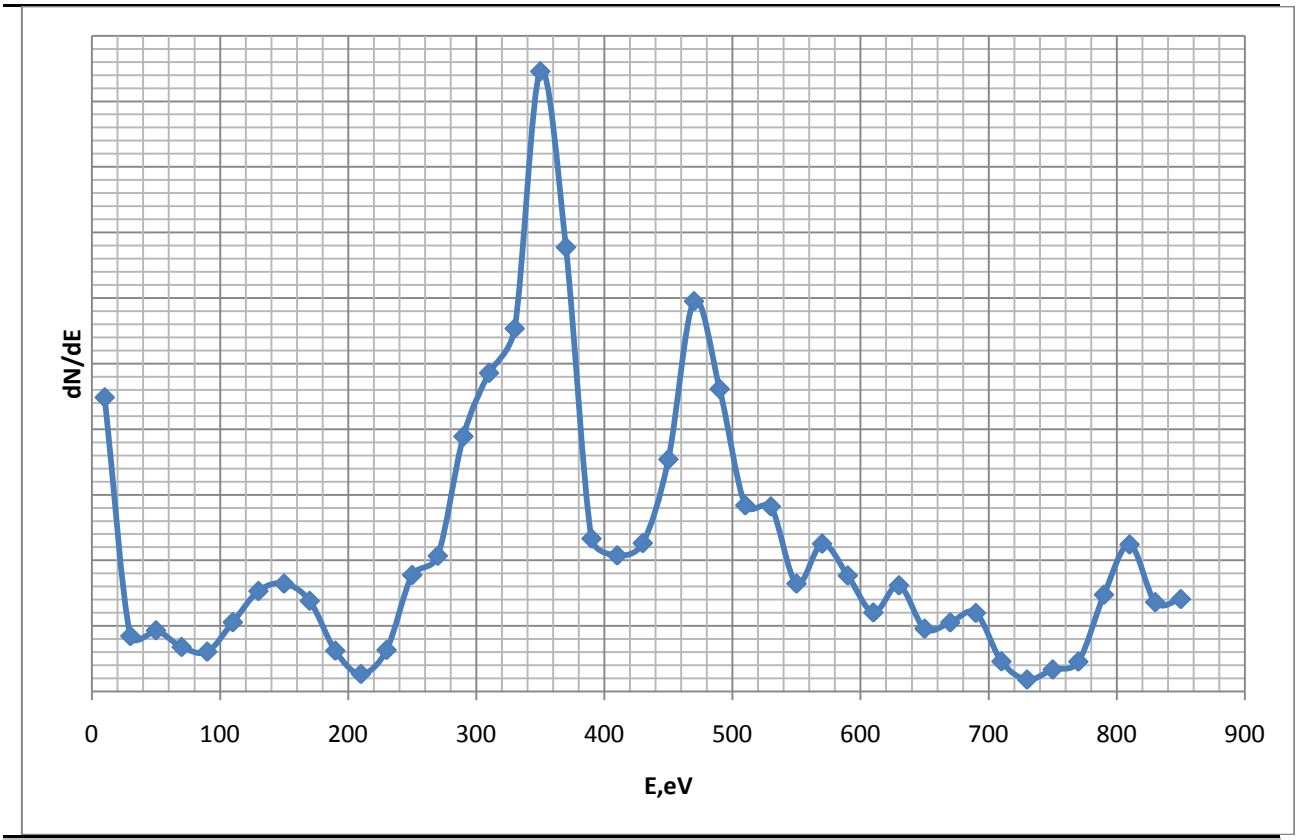

Fig.3.23. The distribution of energies of ions in the jet at an

angle of 40 degrees from the axis of the engine

The energy distribution for the engine number 5 In this experiment we used a different model of jets: the distribution of ions to energies were taken by probe measurements shown in the following illustrations.

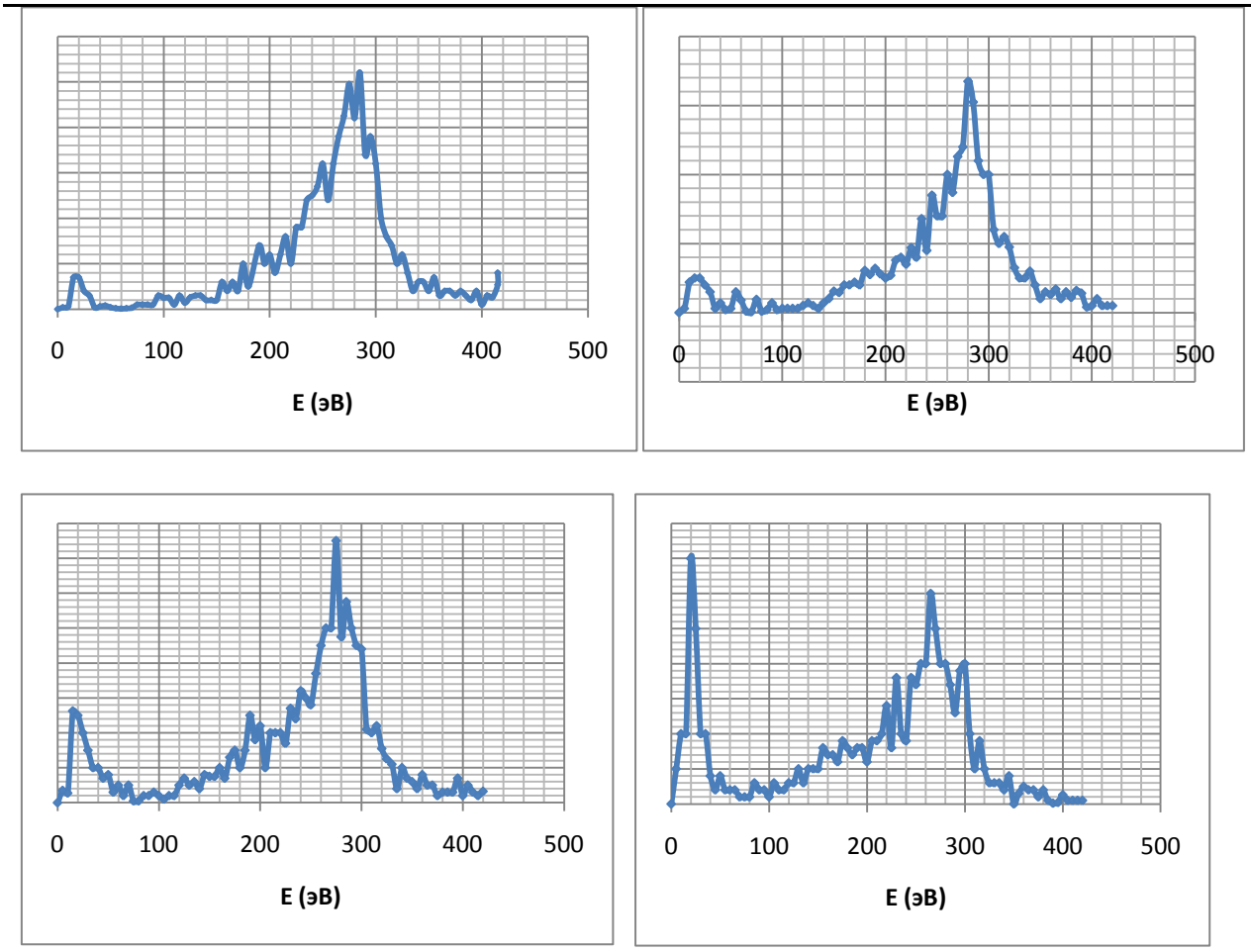

Fig. 3.24. Energy distribution of ions in the jet at 0,7.5,15,22.5 degrees from the axis of the engine.

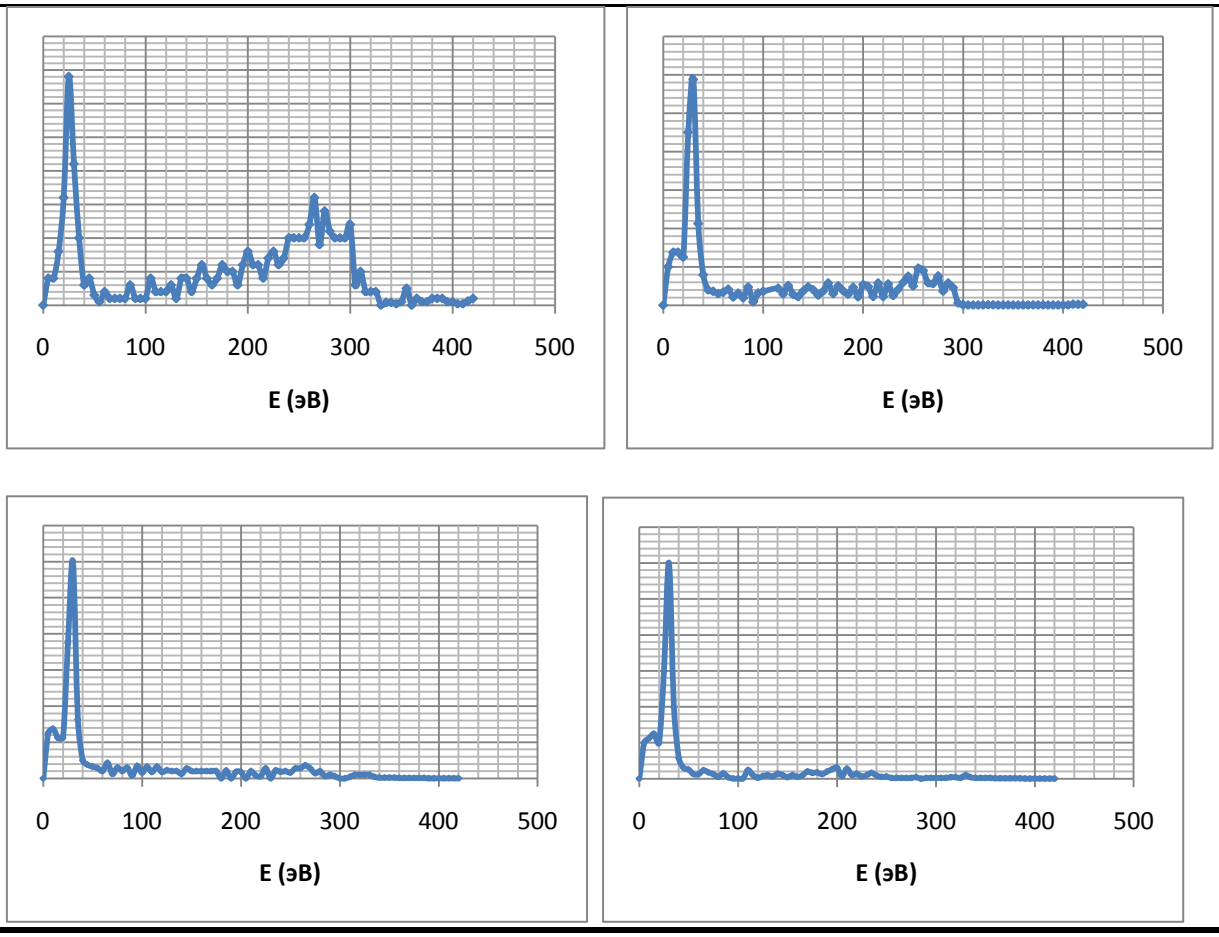

Fig. 3.25. Energy distribution of ions in the jet at 30,37.5,45,52.5 degrees from the axis of the engine.

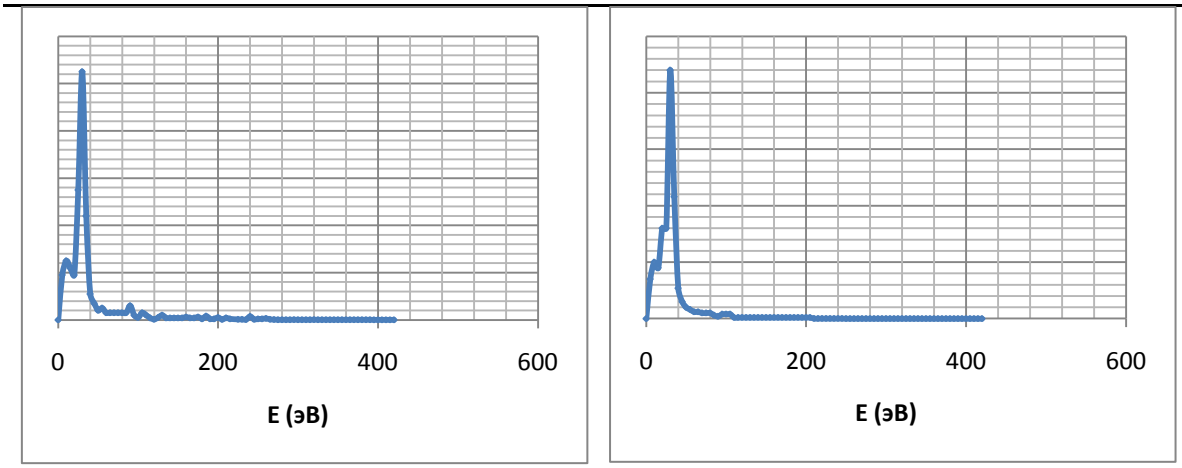

Fig. 3.26. Energy distribution of ions in the stream at 60 and 67.5 degrees from the axis of the engine.

3.2.3. The initial and boundary conditions for calculating the distribution of recharge of ions formed by the interaction of the jet with the gas in the vacuum chamber

Section $Xe-Xe^+$ we calculated using the following formula $(175.6-11.812*\log(E))*10^{-20}$, where E - energy of the primary ion in eV. [37]

3.2.4. The initial and boundary conditions for calculating the distribution of sputtered particles with the walls of the vacuum chamber

In the approximation may be taken according to the dispersion of iron ions Xe. In general, the rate depends on the angle of incidence of ion Y (a) (fig.3.27) and ion energy Y (E) (fig.3.28).

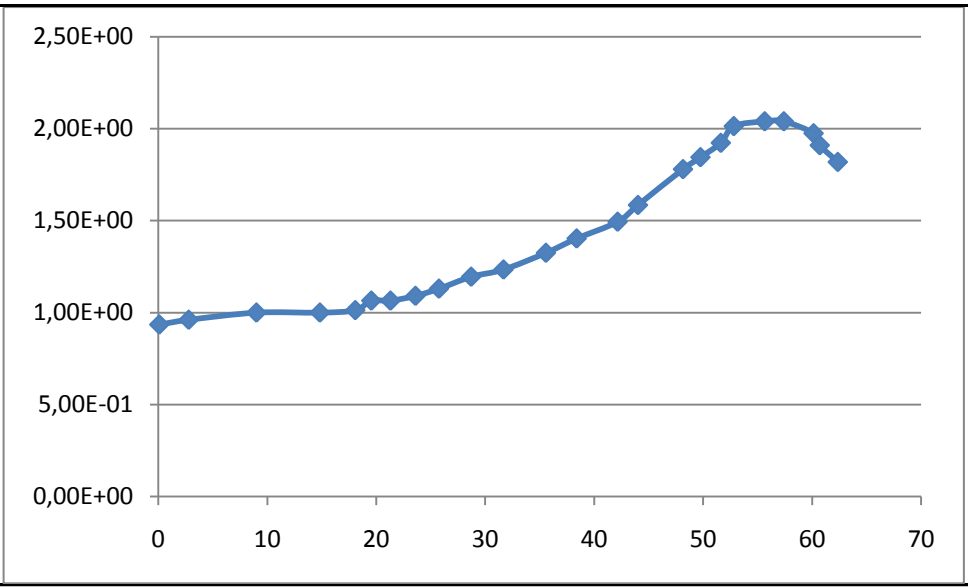

Fig.3.27. The dependence of the coefficient of dispersion of the angle of incidence normal to the particle surface

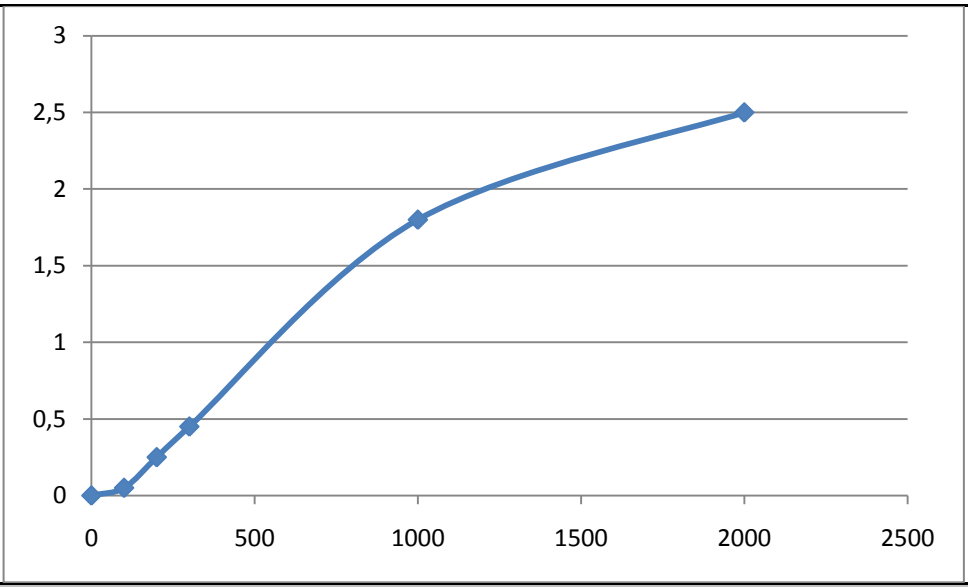

Ris.3.28. The dependence of the coefficient of dispersion for Fe from falling energy ion Xe

Distribution by volume sputtered particles is not uniform, most of it depends on the angle of incidence of particles and it can be experimentally measured dependences are shown in Fig.

3.29 ÷ 3.32.

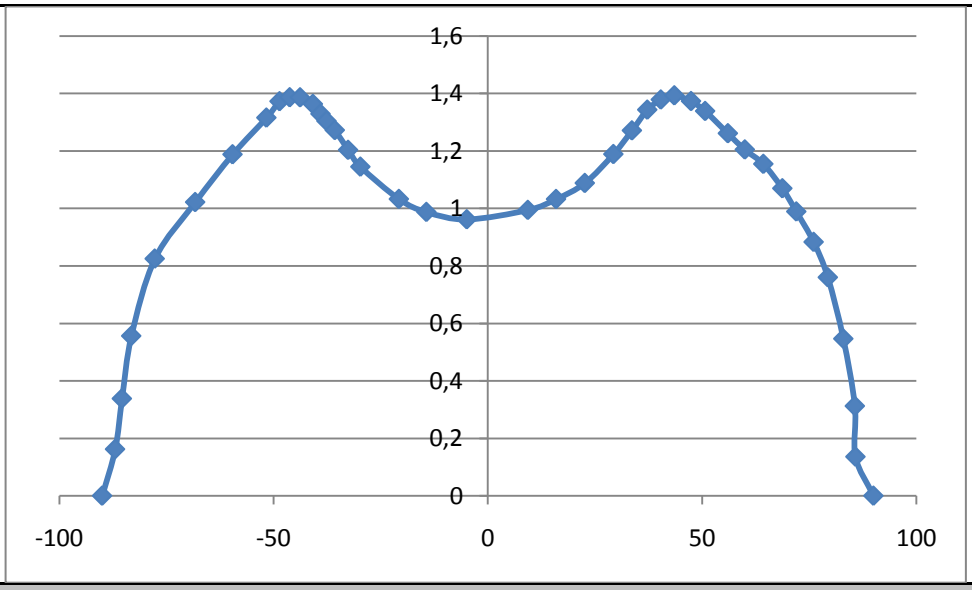

Fig.3.29. The distribution of sputtered particles at an angle to the normal jet track 0 degrees

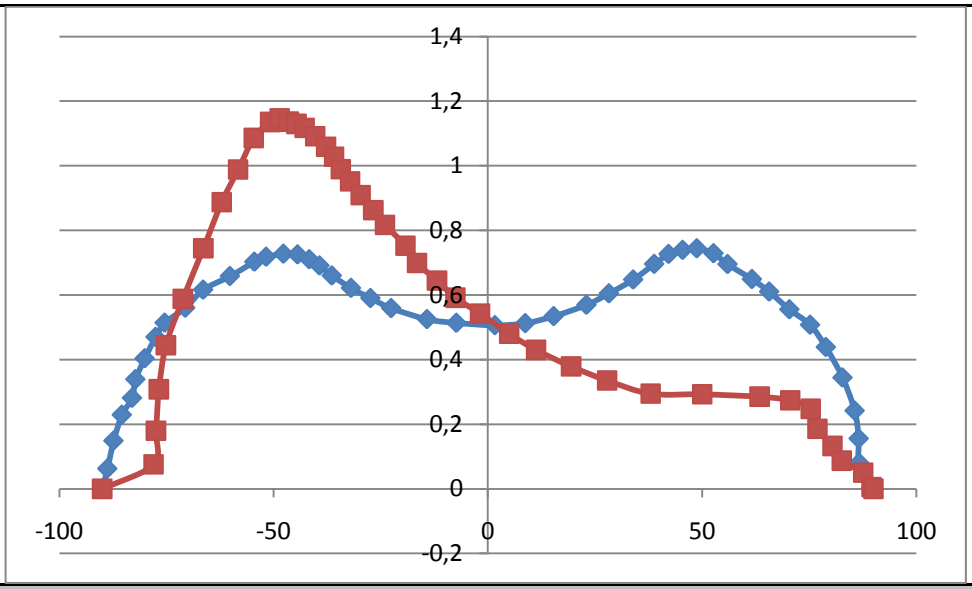

Fig.3.30. The distribution of sputtered particles at an angle to the normal jet track 20 degrees

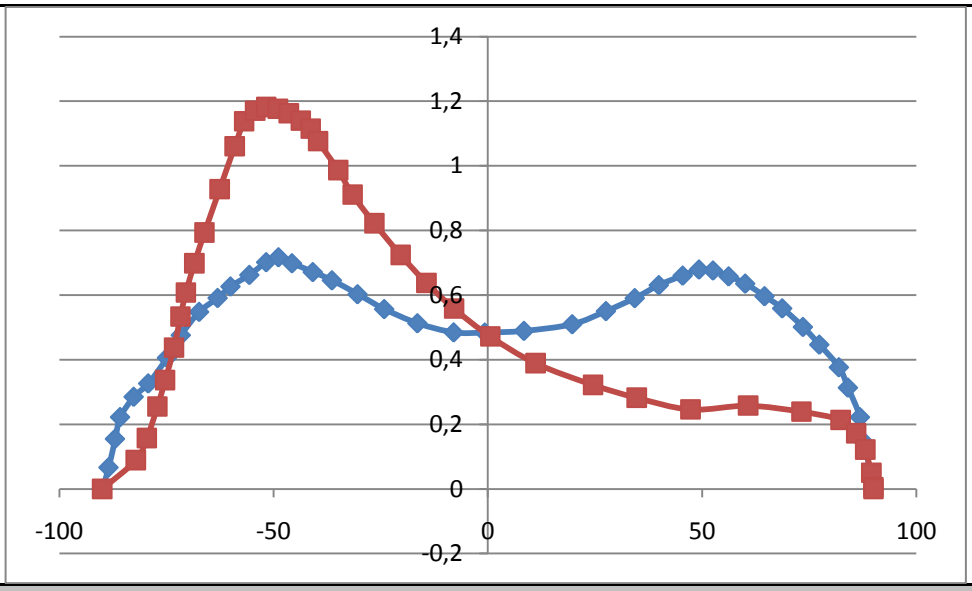

Fig.3.31. The distribution of sputtered particles at an angle to the normal jet track 40 degrees

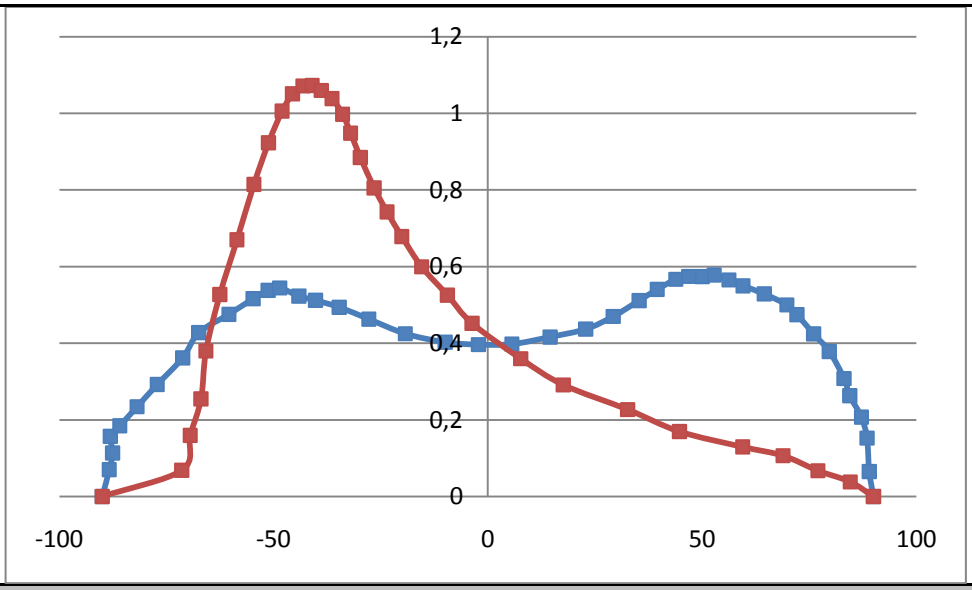

Fig.3.32. The distribution of sputtered particles at an angle to the normal jet track 60 degrees

3.3 The method for determining surface characteristics using mathematical analysis (SMA)

3.1. Determination of pressure on a given surface of SMA

$$p = 2\frac{\dot{m}}{S*N(\text{общ})}\sum_{i=1}^{N}(V_{i(z)}) \qquad 3.2$$

3.2. Determination of traction

To determine the traction engine was used the following method: put the measuring section in a few cm from the engine so

that it overrides all section of the chamber, hit the floor of accelerated ions fixed to the ion velocity and the cosine of the angle between the direction of motion of the ion to the normal track for absolute value. Thrust into this case will be equal to:

$$F = \frac{\dot{m}}{N(\text{общ})} \sum_{i=1}^{N} (V_i * Cos(\alpha_i)) \qquad 3.3.$$

3.3. Determination of current density of primary ions

In the process of modeling the surface probe enters N simulated particles, the mass carried by each simulated particle per second time m ˙ / N (total), where N (total) - total number of simulated particles. Each simulated particle its velocity Vi, taken to the Maxwell distribution. Current density on the probe will be determined from the formula:

$$j = \frac{N\dot{m}FZ}{\mathrm{N}_{(\text{общ})}MS} \qquad 3.4.$$

where the F-constant Farradeya; M - molar mass of xenon; S - area of the probe; Z - ion valency. Since SMA installed at some distance from the engine, modeled ion beam passing through the medium of neutral atoms in a vacuum chamber is weakened, as reflected through the reduction factor. Also, the ions formed by re-invest its share of the total current.

3.4. Determination of current density ion recharging

After modeling the distribution of primary ions in a vacuum chamber knows the total number of ions formed as a result of recharging of the camera, as well as in individual cells. After gathering information on the number of ion rechargeable cells, each cell in the algorithm is a source of ion rechargeable. Sufficient ion rechargeable emitted by a given distribution lines, and speeds. Their trajectories are constructed, taking into account the equations of motion.

In the modeling shown in red surface probe gets conditional particles N, N-˙_пер total number of ions formed as a result of recharging of the camera. Nobsch, the total number of simulated trajectories. Current density on the probe will be determined from the formula:

$$j = \sum_{i=1}^{N} \left\{ \frac{\dot{N}_{\text{пер}}\mathrm{e}}{S * N_{\text{общ}}} \right\}, \qquad 3.5.$$

where e - elementary charge, S - space probe.

3.4 Visualization of results

3.4.1. The trajectories of particles

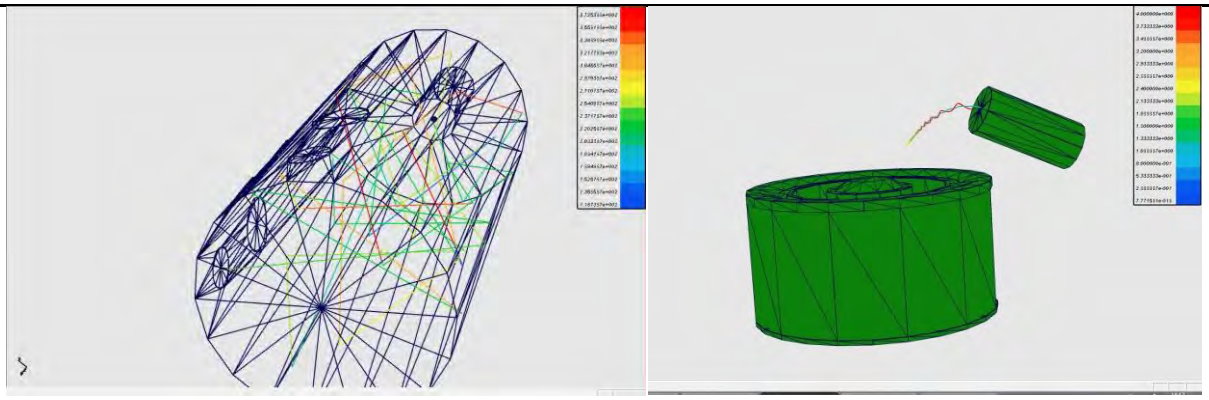

Fig.3.33. Trajectory of ions (the initial velocity of 220m / s (300 K)), the color corresponds to the speed in m / s) (left) Trajectory of an electron in a magnetic field (right).

3.4.2. Distribution of parameters in a selected `plane`

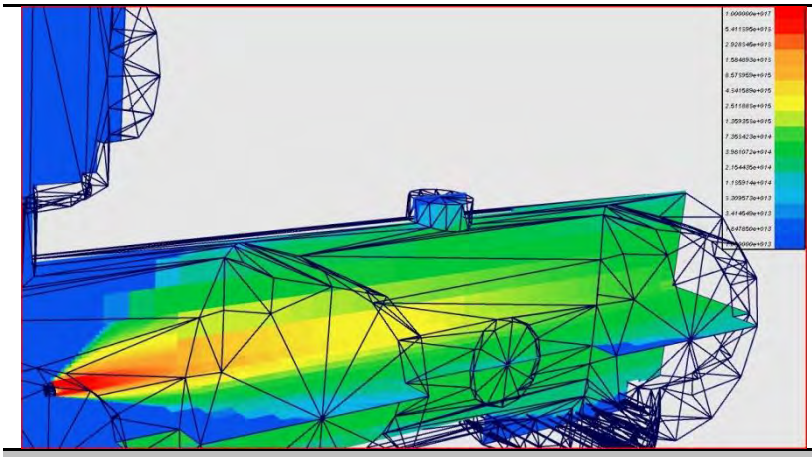

Fig. 3.34. The distribution of primary ions in the two selected planes

3.4.3. The distribution of the parameter along the parametric curve

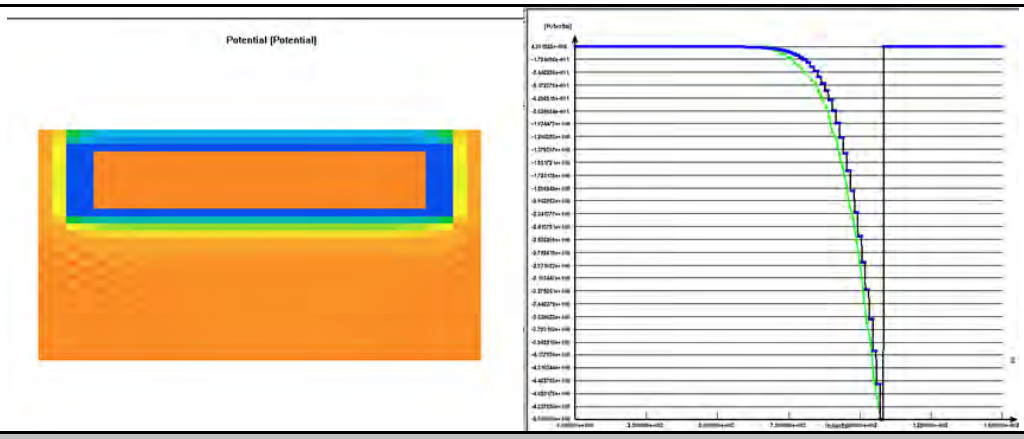

Fig. 3.35. Allocation of capacity along the central line

In addition, ActiveX component to display graphs, shown in risisunkah above, has an option to export data to Microsoft Excel 2007 that allows you to enjoy the functionality of Excel for processing and data visualization.

3.4.4. Distribution of parameters on surfaces phone

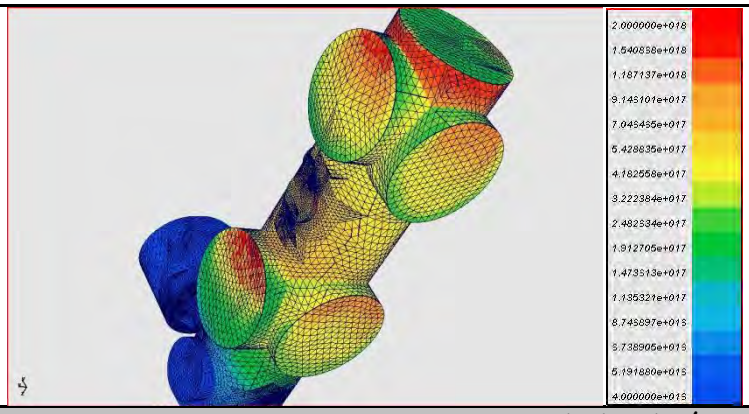

Fig. 3.36. Distribution perepyleniya Engine № 1.1 [1 / s].

3.5 Analysis of cross sections of elastic interaction between atoms of xenon

In the above analysis will be given 4 models to assess the cross-section of elastic interaction:

T1 - The model of hard spheres

T2 - The model of hard spheres of variable diameter

T3 - The model with the potential interaction of the Lennard-Jones

T4 - The model with the potential for the repulsive Born-Mayer

T1:

The interaction between the atoms represented in the form of solid balls.

Cross section of the elastic interaction is described by the formula:

$$\sigma = \pi R_0^2 \qquad 3.6.$$

R0-gazokineticheky radius of the elastic collision

The error models: the uncertainty in knowing the value Gasokinetic collision radius R0, depending on the method of determining the

amounts to 0.1-1 A. This determines the accuracy of all the other variables.

Comments:

In the geometric representation of the collision of two identical molecules - Gasokinetic the value of hard spheres of radius numerically equal to the diameter of the molecule.
The model of hard spheres are widely used when considering the dynamic characteristics of collisional processes in gas and plasma-level assessments of probabilities, cross sections and rate constant processes in any approximation.
T2:

Assignment model

Determination of elastic collisions of neutral particles in the method of direct statistical simulation (DSMC)
Assumptions

A solution of the elastic collision of particles in the framework of classical mechanics

The model is a generalization of the model of hard spheres and a model with a power potential of repulsion. Unlike the model of hard spheres of radius R0 Gasokinetic value depends on the relative velocity of particles in a collision. The value of R0 is proportional to the distance the greatest convergence of molecules for a power capacity of $V(R) = AR^{-\nu}$ in the frontal impact and is determined from the relations:

$$\sigma = \pi R_0^2 \qquad 3.6.$$

A and ν - coefficient and exponent in the degree of potential interaction

α - constant for identical particles equal to 1

u - the relative velocity of particles

The error model:

The real dependence of the average cross section of elastic scattering σ0 of temperature is not a power function. The smallest deviation σ0 (T) of the power functions are in the range 300 <T <1000 K (with an error of about 5% at T = 1000 K). At higher temperatures the error uncertain.

Comment:

The model of hard spheres of variable diameter are widely used to solve the dynamics of a rarefied gas by the direct simulation (DSMC).
T3:

Assumptions

A solution of the elastic collisions of particles are considered in the framework of classical mechanics with the approximation results The interaction of the colliding particles is described by the Lennard-Jones potential

$$V(R) = 4\varepsilon_m \left[\left(\frac{\sigma}{R}\right)^{12} - \left(\frac{\sigma}{R}\right)^{6}\right] \qquad 3.8.$$

The potential curve V (R) changes sign at R = σ, with R = σ √ (6 & 2) passes through a minimum, the depth of the potential well is εm.
Limits

Collision energy ε and the gas temperature T from the bottom condition is limited consideration of the applicability of the classical motion of particles when the de Broglie wavelength is much less than the typical range of molecular forces.

Restrictions on approximations for the average cross section of 1 <kT / ε_m <25 in the case of xenon gas temperature is limited to 220 <T <5507 (K).

Comments:

The parameter σ Lennard-Jones potential is also called the diameter of the molecule. This value corresponds to a value of R, where V (R) = 0, ie head-on collision of molecules with extremely low energy

T4: Assumptions:

A solution of the elastic collisions is considered within the framework of classical mechanics with the approximation results.
We consider the exponential potential of the Born - Mayer V (R) = V_0 exp (-αR), Modeling forces of repulsion, which occur at close distances of the colliding particles.
V0 - the pre-exponential factor of the Born - Mayer
α - the opposite of the radius of interaction the Born-Mayer

Limitations:

The model describes the collision of particles without taking into account the forces of attraction and is valid at the energy ε> εm, in the case of xenon T> 220 K.

The error model:

In the area of applicability of the model at temperatures of approximately 3000K the error is less than 1%. With a decrease in temperature error increases (10-15% at T = 300K) in the direction of overstatement σ0 (T).

Commentary

Model of the Born - Mayer used to describe the interaction of particles at high energies the collision. Parameters of the model are determined from the data on scattering of fast beams, and the results of quantum-mechanical calculations of interaction energy of atoms and molecules.

In the calculation used the formula and the coefficients of [38]. In the model of hard spheres of variable diameter of the formula and coefficients are taken from [39]. The model with the repulsive potential of the Born-Mayer coefficients are taken from [40].

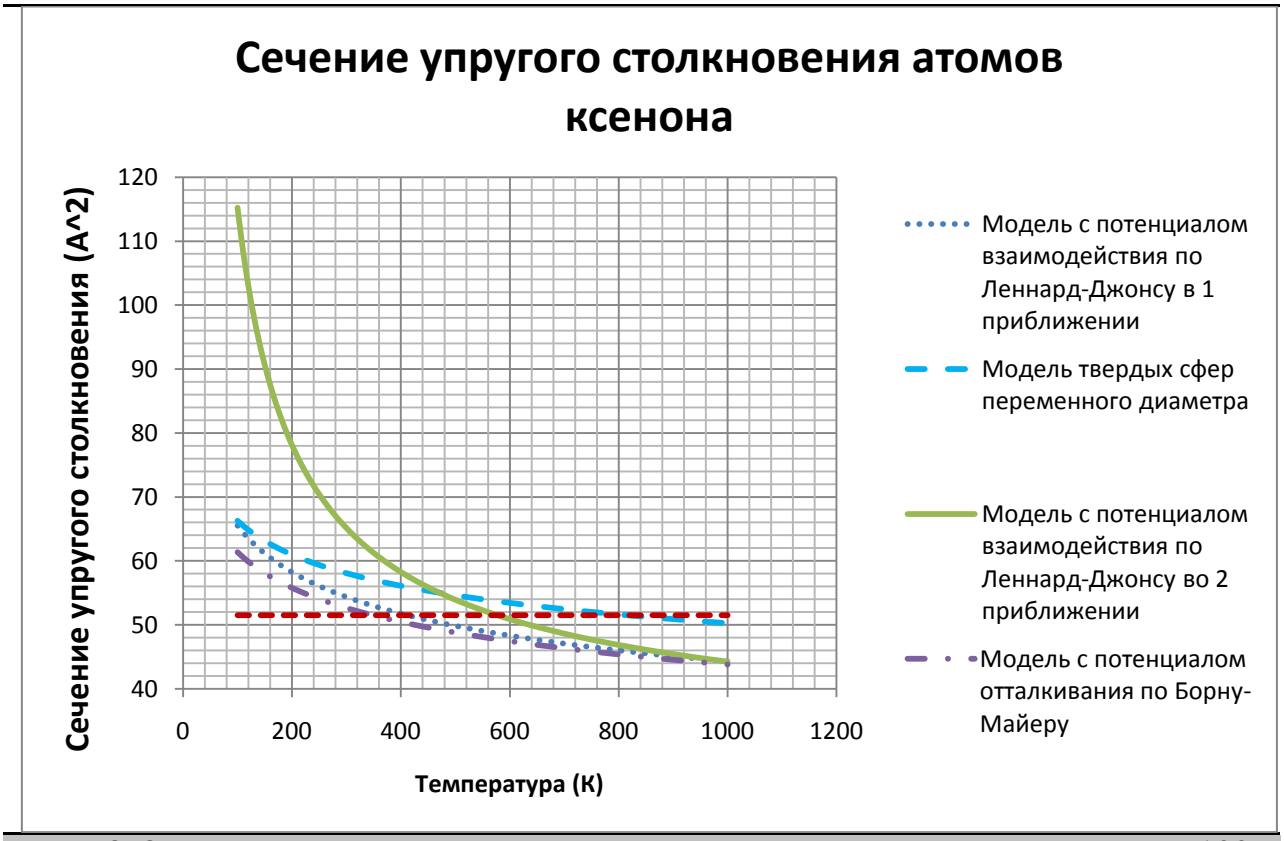

Fig. 3.37. The cross section of elastic collisions of xenon atoms (100 to 1200K)

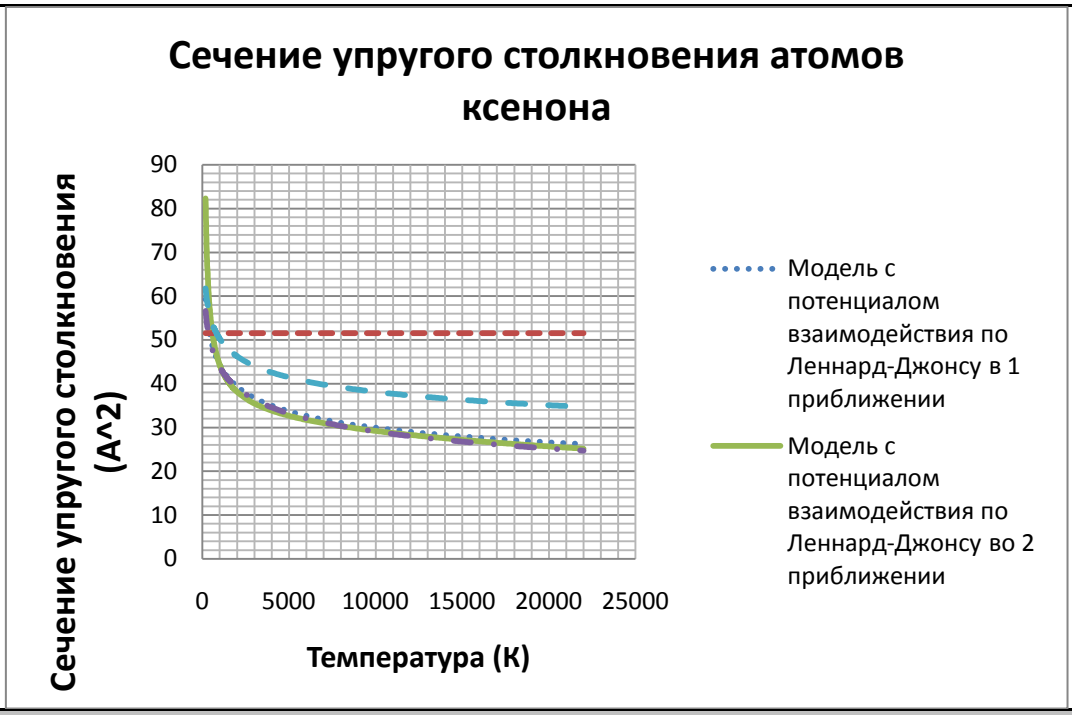

Fig. 3.38. The cross section of elastic collisions of xenon atoms (1000 to 22000K)

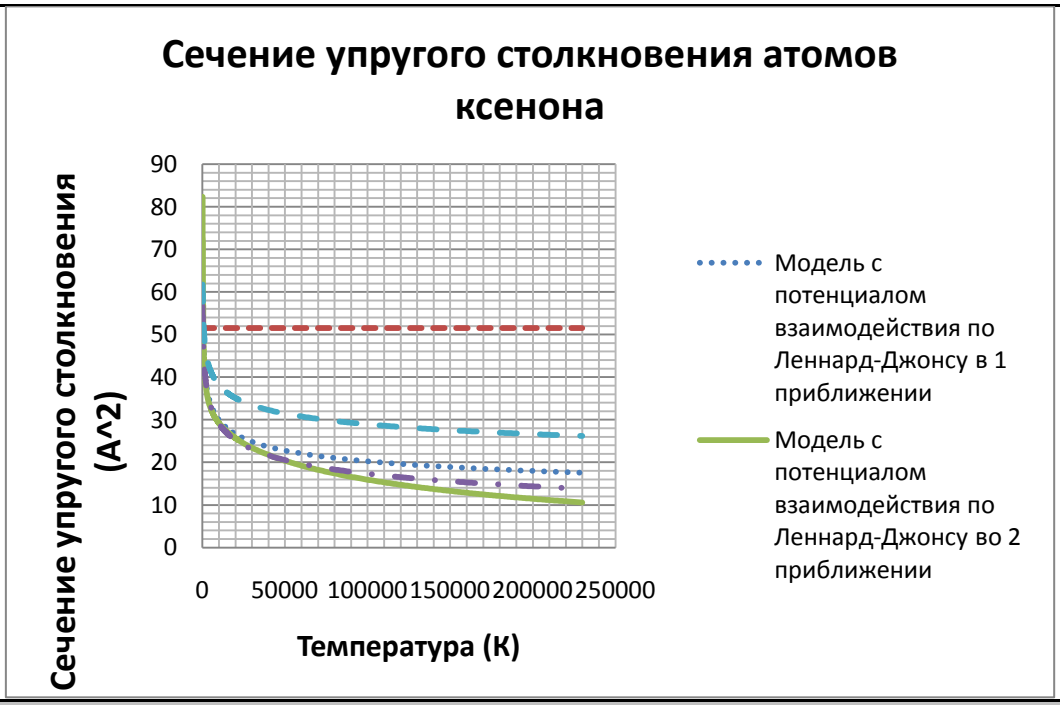

Fig. 3.39. The cross section of elastic collisions of xenon atoms (10000 to 220000K)

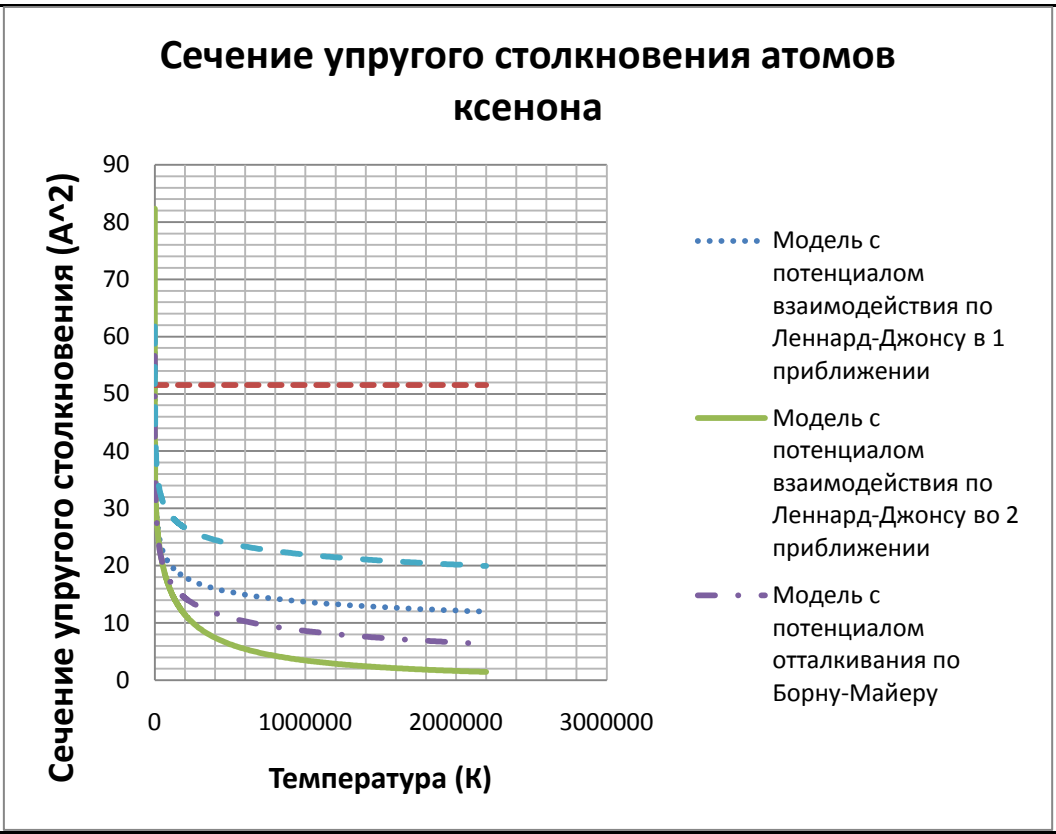

Fig. 3.40. The cross section of elastic collisions of xenon atoms (100000 to 2200000K)

Based on the assessments and kommetariev error model is the best combination of methods, such as at temperatures less than 1000K model of hard spheres, and at high temperatures the model with the potential for the repulsive Born-Mayer.

3.6 Analysis of the probability distribution of the direction and speed of xenon atoms after collision with an atom of xenon environment with an average temperature of 300 K using solid spheres

Description:

Two round smooth elastic ball moves faster and. Need to find the speed after the ball is elastic noncentral collision. Weights and balls. To simplify the description look 2 dimensional approximation, following the withdrawal of the final turn to the three-dimensional formulas.

Decision.

The task of discussing the SALW coordinate axis OX and OY which lie in a horizontal plane, with the axis OX is directed from the centers of balls at the time of collision (Fig. 1). Then the momentum of balls in the process of interaction continues, and here - pulse washers before and after the collision.

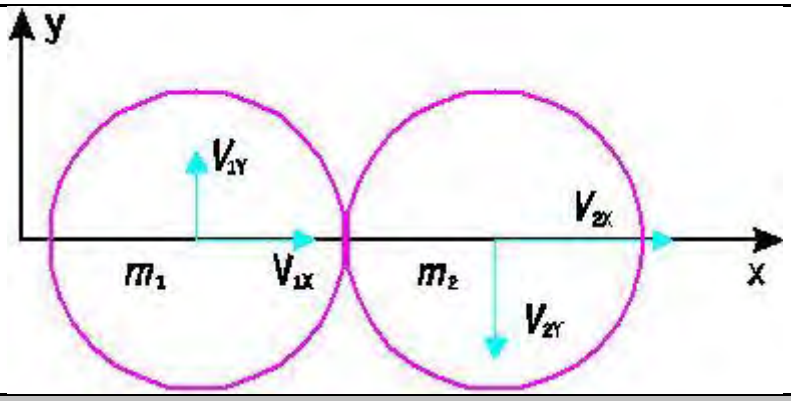

Fig. 3.41. Schematic drawing collision balls

Because the balls perfectly smooth, the impact of internal forces - the forces of elastic interaction of balls - are aimed only at the axis OX. These forces do not change the Y-components of momenta balls. Then from, find the Y-component of the velocity of balls after the collision, ie in projection on the axis OY speed of balls as a result of collision not changed.

Find the X-component of the velocity of balls after the collision is elastic. With this collision of stored kinetic energy of

$$\frac{m_1\left(V_{1X}^2+V_{1Y}^2\right)}{2}+\frac{m_2\left(V_{2X}^2+V_{2Y}^2\right)}{2}= \\ =\frac{m_1\left(\left(V'_{1X}\right)^2+\left(V'_{1Y}\right)^2\right)}{2}+\frac{m_2\left(\left(V'_{2X}\right)^2+\left(V'_{2Y}\right)^2\right)}{2}. \qquad 3.9$$

Given the equality Y-component of the velocity of balls before and after the collision last equality takes the form.

$$\frac{m_1V_{1X}^2}{2}+\frac{m_2V_{2X}^2}{2}=\frac{m_1\left(V'_{1X}\right)^2}{2}+\frac{m_2\left(V'_{2X}\right)^2}{2}. \qquad 3.10.$$

Let us turn to the law of conservation of momentum and move on to the projections of pulses balls on the axis OX

$$m_1V_{1X}+m_2V_{2X}=m_1V'_{1X}+m_2V'_{2X} \qquad 3.11.$$

Thus, the original problem is reduced to the problem of the absolutely elastic central impact: it is this type of legislation would save the energy and momentum, if the speed of balls have been sent by the centers. The resulting nonlinear system of equations can be reduced to linear. To do so, (as in the previous problem) in both equations on the same side of the sign of equality to combine the components related to the first ball, but on the other - for the second, and divide the obtained

relationship to each other. This leads to the linear equation form. Solving the system of the last two equations, we find

$$V'_{1X} = \frac{(m_1 - m_2)V_{1X} + 2m_2V_{2X}}{m_1 + m_2}, \quad V'_{2X} = \frac{2m_1V_{1X} + (m_2 - m_1)V_{2X}}{m_1 + m_2} \quad 3.12.$$

Given that in our case the mass of balls are equal, then the problem reduces to To find the point of intersection of balls in the interaction and the external normal to the surface of the ball at the point of intersection. This is normal and the x axis in our description. Then construct a projection of velocity on this axis, and then calculated by the formula of speed along the x-axis after the interaction. Then translate them into the current system.

Description of simulation environment: Set design area (on the pictures shows a large area). In this area is given equal starting point and direction of motion of the atom environment at a speed corresponding to an average 300K.
Simulated an atom moves from point (0,0, z (min)), a t (0,0,0) if the velocity of an atom is less than the modeled 220 m / c (Central sootv. to 300K) at a rate set by the user, the direction for all atoms is strictly along the axis z, vector (0,0,1).

The user also specifies the number of interactions, to produce a true picture of the distribution. All the following pictures were analyzed by 1000 interactions for each speed.
The following pictures blue arrow shows the direction of movement of the atom environment, a red arrow, the direction of the modeled atom. Green indicated by an arrow normal to the surface of the sphere at the point of interaction.

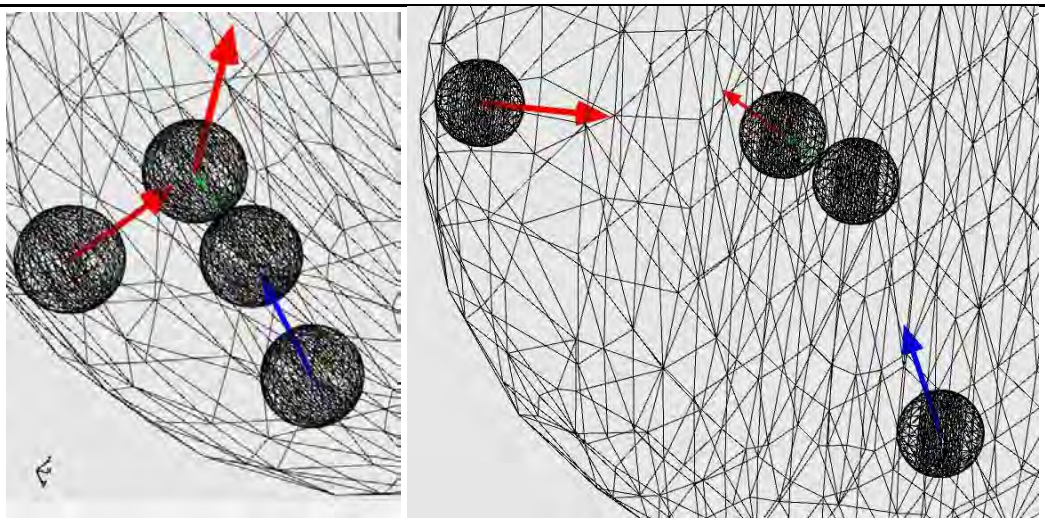

Fig.3.42. 300 K (env) 250m / c (free-atom)

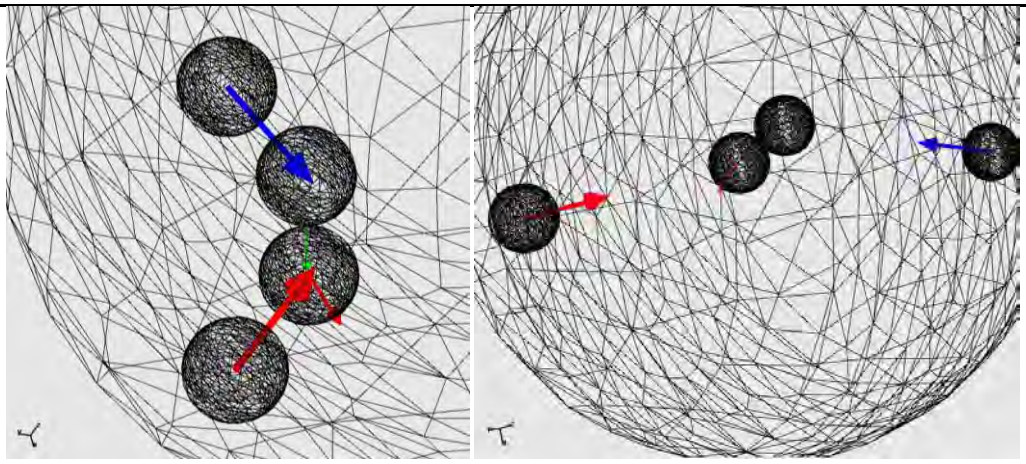

Fig.3.43. 300 K (env) 250m / c (free-atom)

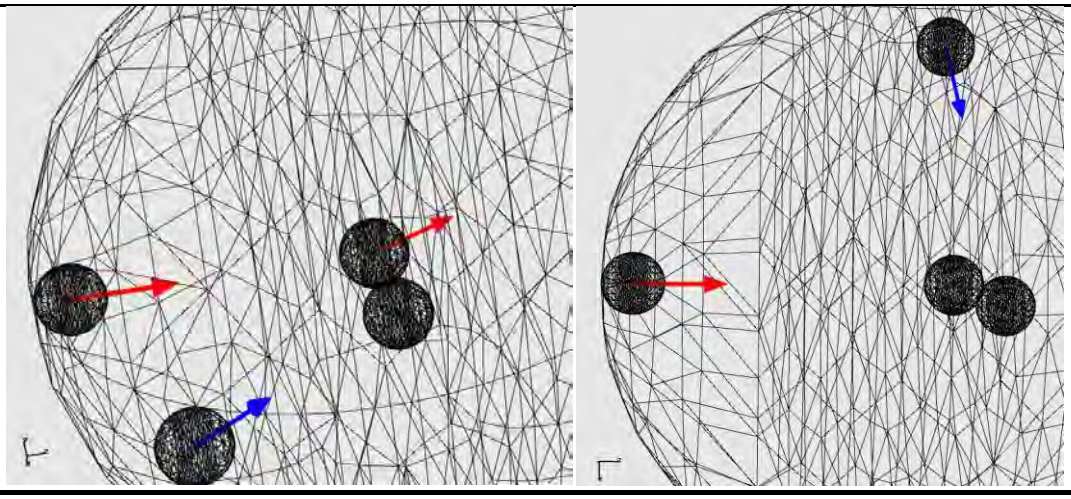

Fig.3.44. 300 K (env) 250m / c (free-atom)

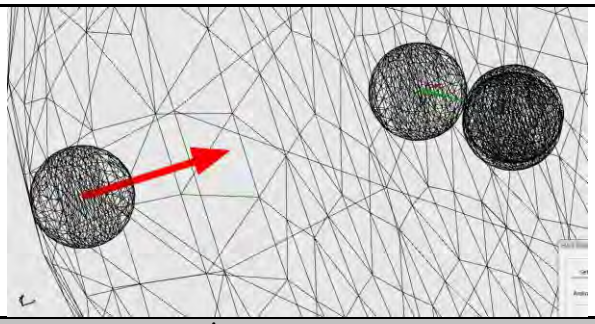

Fig.3.45. 300 K (env) 10000 m / s (free-atom)

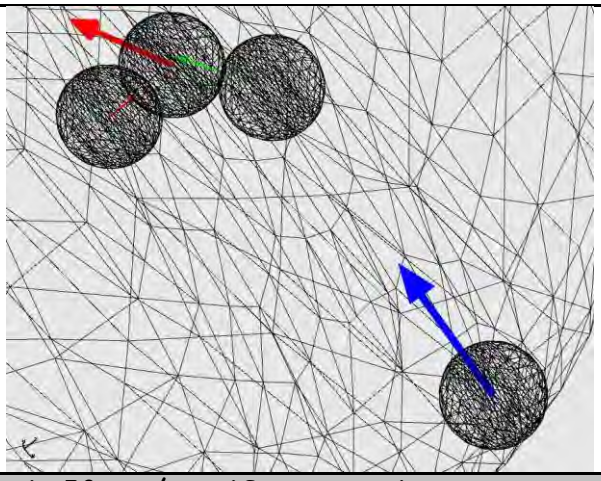

Fig.3.46. 300 K (env) 50 m / s (free-atom)

The following figure shows the probability of a color motion of atoms in a given direction the arrow corresponds to the value set in the interface to the external radius of the sphere. Also on the panel interface on the pictures gives the average speed after the interaction.

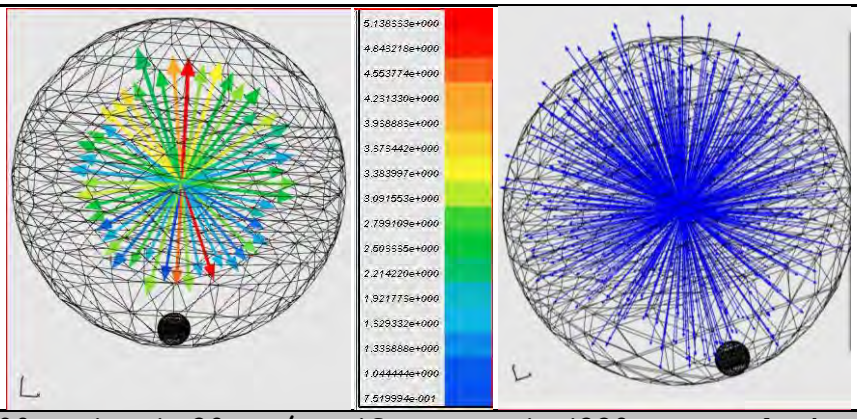

Fig.3.47. 300 K (env) 20 m / s (free-atom) (220 m speed visualization / s)

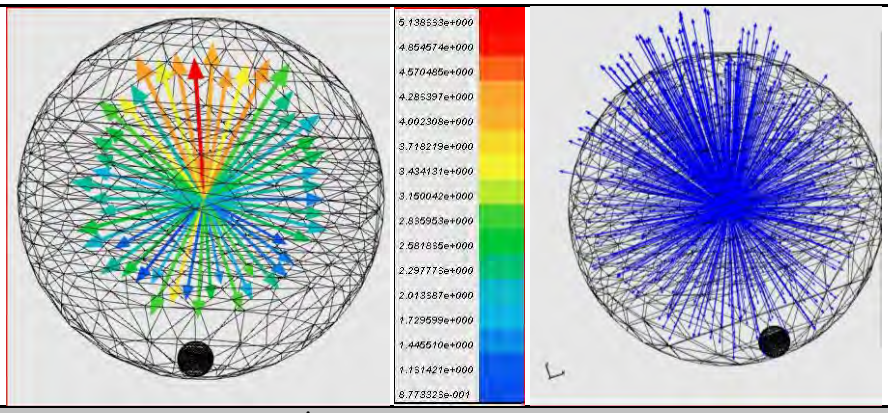

Fig.3.48. 300 K (env) 40 m / s (free-atom) (220 m speed visualization / s)

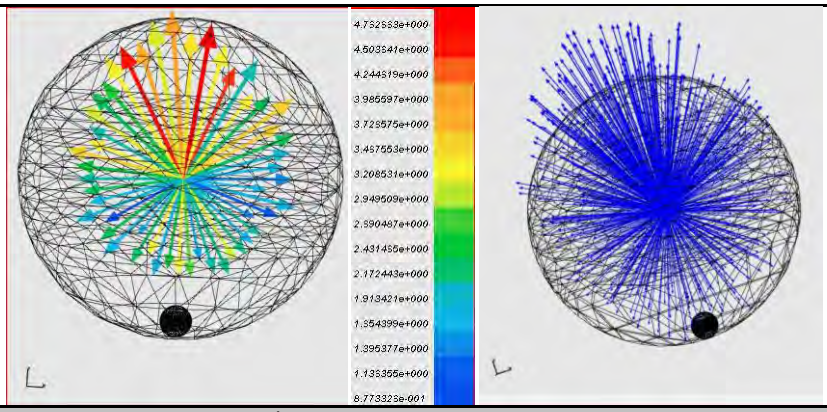

Fig.3.49. 300 K (env) 60 m / s (free-atom) (220 m speed visualization / s)

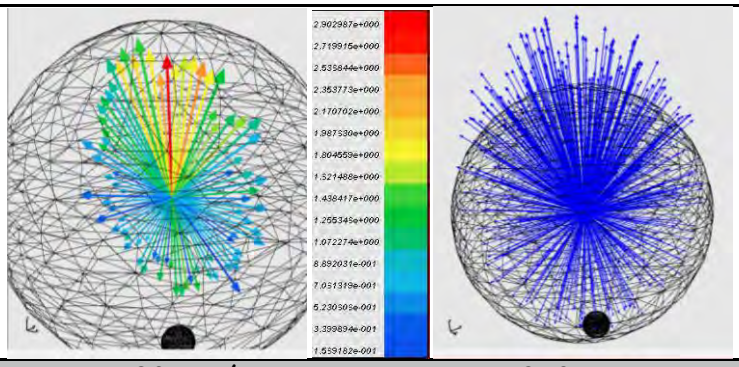

Fig.3.50. 300 K (env) 80 m / s (free-atom) (250 m speed visualization / s)

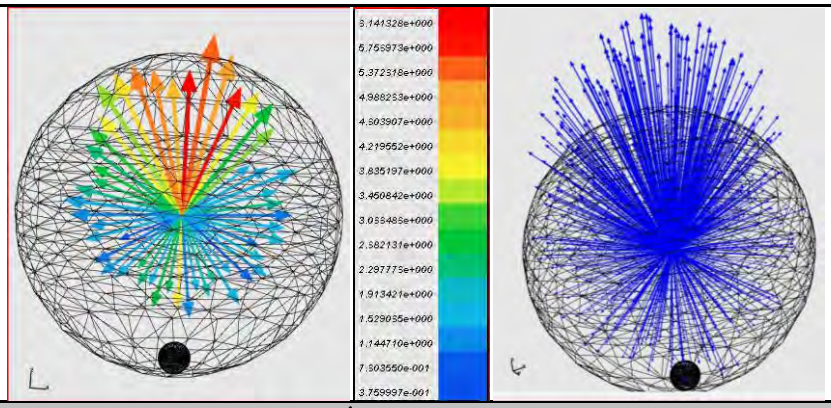

Fig.3.51. 300 K (medium) 100 m / s (free-atom) (220 m speed visualization / s)

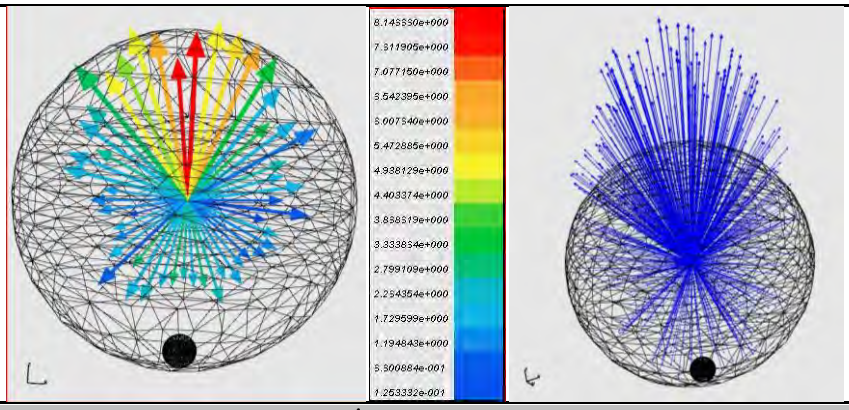

Fig.3.52. 300 K (medium) 150 m / s (free-atom) (220 m speed visualization / s)

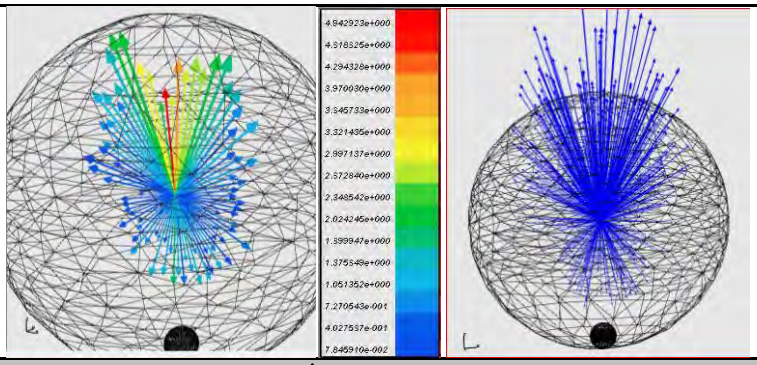

Fig.3.53. 300 K (medium) 200 m / s (free-atom) (250 m speed visualization / s)

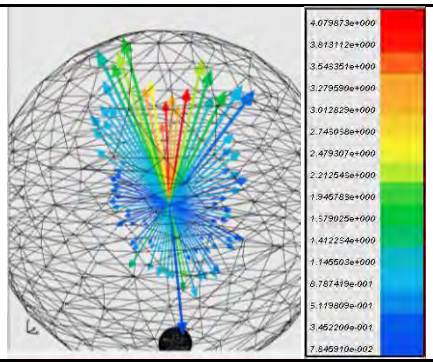

Fig.3.54. 300 K (medium) 250 m / s (free-atom) (250 m speed visualization / s)

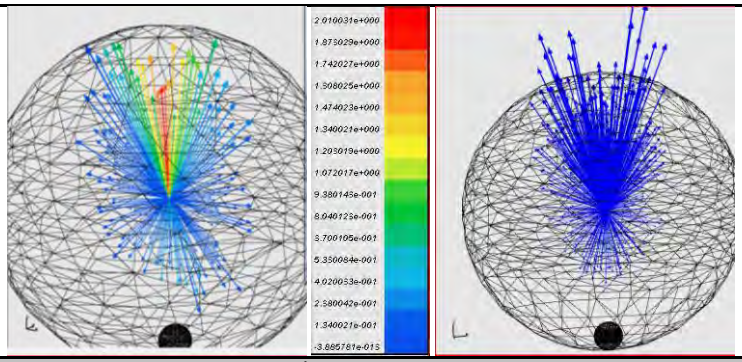

Fig.3.55. 300 K (medium) 300 m / s (free-atom) (250 m speed visualization / c) (speed of the visualization 400 m / s) (right)

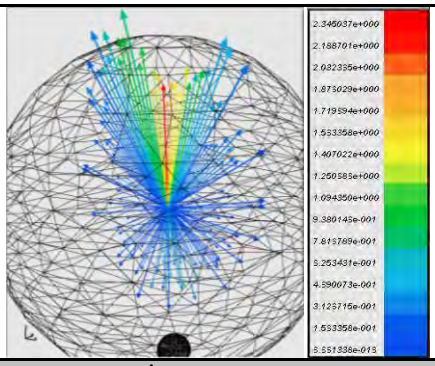

Fig.3.56. 300 K (medium) 350 m / s (free-atom) (250 m speed

visualization / s)

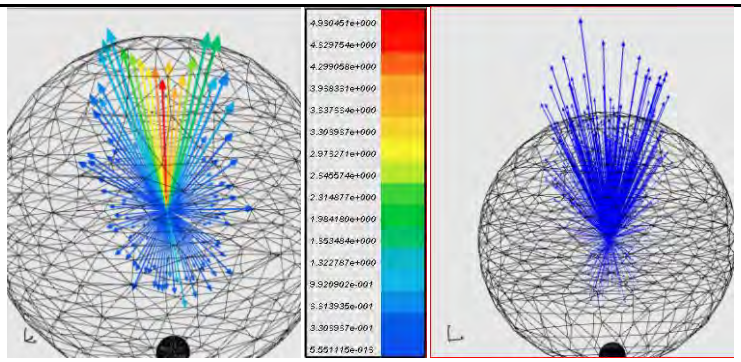

Fig.3.57. 300 K (medium) 400 m / s (free-atom) (250 m speed visualization / s) (speed of the visualization 400 m / s) (right)

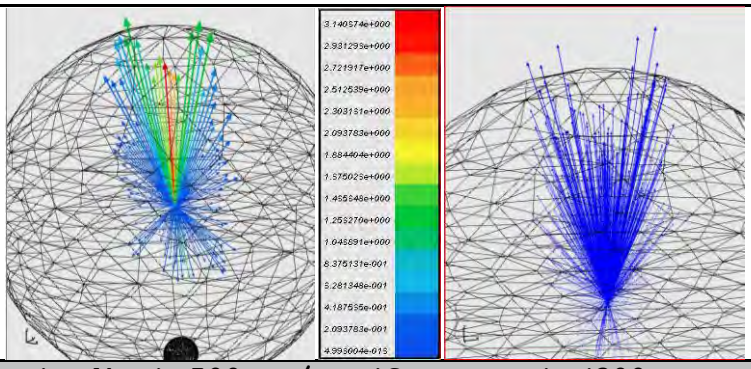

Fig.3.58. 300 K (medium) 500 m / s (free-atom) (300 m speed visualization / s) (speed of the visualization 600 m / s) (right)

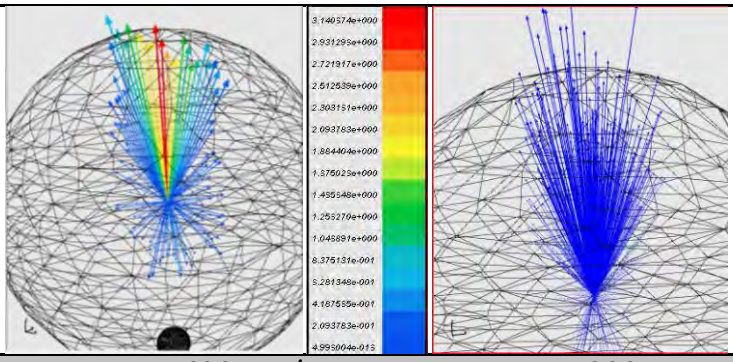

Fig.3.59. 300 K (medium) 600 m / s (free-atom) (300 m speed visualization / s) (speed of the visualization 600 m / s) (right)

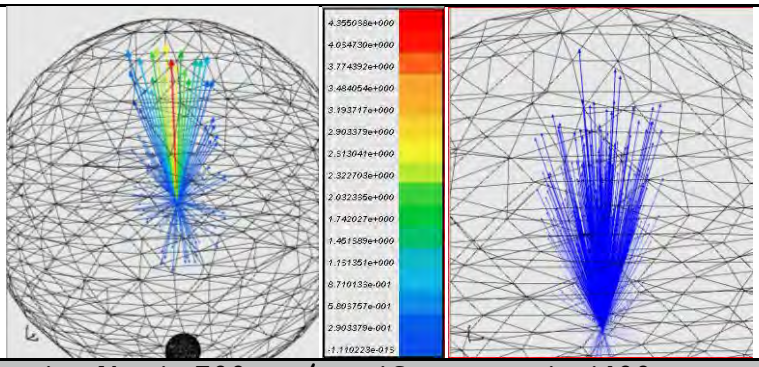

Fig.3.60. 300 K (medium) 700 m / s (free-atom) (400 m speed visualization / s) (Speed Visualization 1000 m / s) (right)

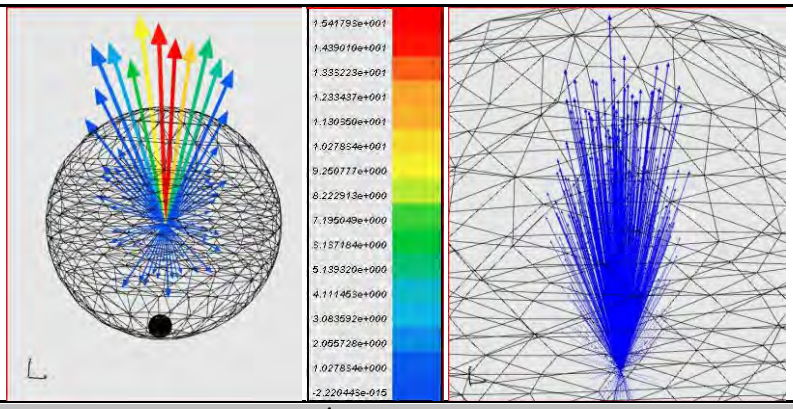

Fig.3.61. 300 K (medium) 800 m / s (free-atom) (220 m speed visualization / s) (Speed Visualization 1000 m / c) (right)

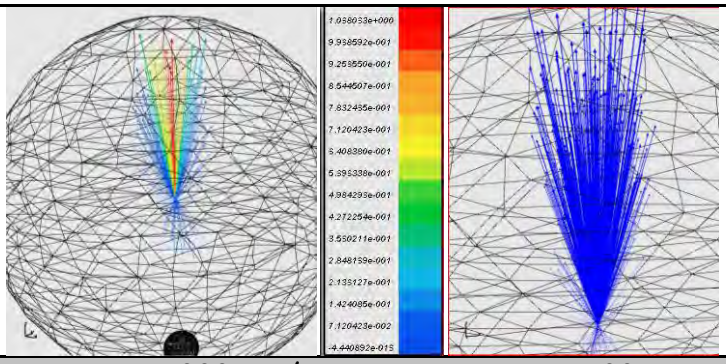

Fig.3.62. 300 K (medium) 900 m / s (free-atom) (500 m speed visualization / s) (Speed Visualization 1000 m / s) (right)

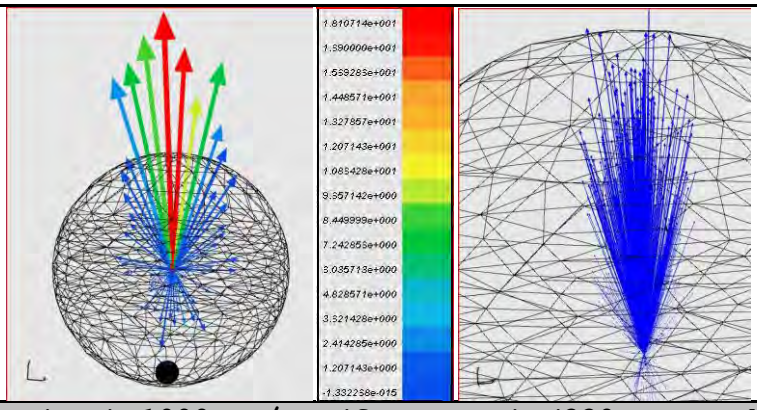

Fig.3.63. 300 K (env) 1000 m / s (free-atom) (220 m speed visualization / s) (Speed Visualization 1000 m / s) (right)

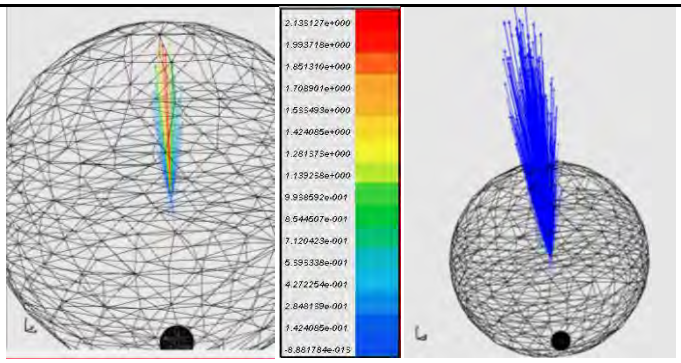

Fig.3.64. 300 K (env) 2000 m / s (free-atom) (Speed Visualization 1000 m / s) (speed of the visualization 800 m / s) (right)

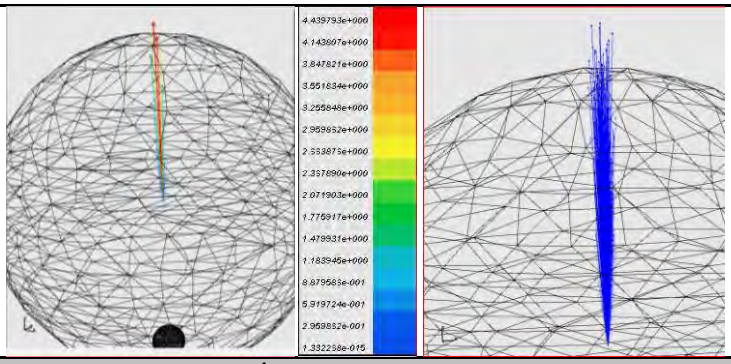

Fig.3.65. 300 K (env) 5000 m / s (free-atom) (Speed Visualization 2000 m / s) (Speed Visualization 4000 m / s) (right)

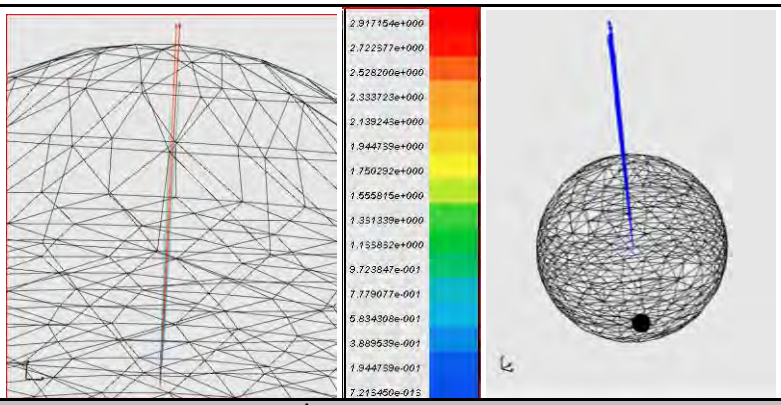

Fig.3.66. 300 K (env) 20000 m / s (free-atom) (Speed Visualization 8000 m / s)

3.7. Calculation of the coefficients Klauzinga for tubes of different cross section

To verify the algorithms for calculating the summary-molecular gas flow was promodelirovano svobodnomolekulyarnoe gas flow in pipes of different lengths. This surface is one of the ends of tubes were set as the start and it equiprobably emit particles. Tracking the trajectory of the particles along the channel, calculated the number of particles off of the pipe and returned to the starting surface. Coefficient Klauzinga that was: W = Nvyletevshih / N, where Nvyletevshih - the number of particles off of the pipe. N - total number of emitted particles. L - length of pipe, r - its radius. Figures 3.67 ... 3.69. shows comparison of results with known data (lines are theoretical curves, taken from work [41], but the point - that the calculation algorithm to create the appropriate length).

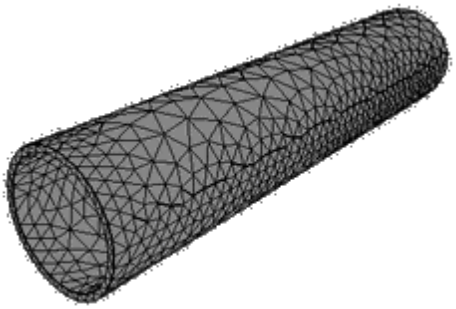

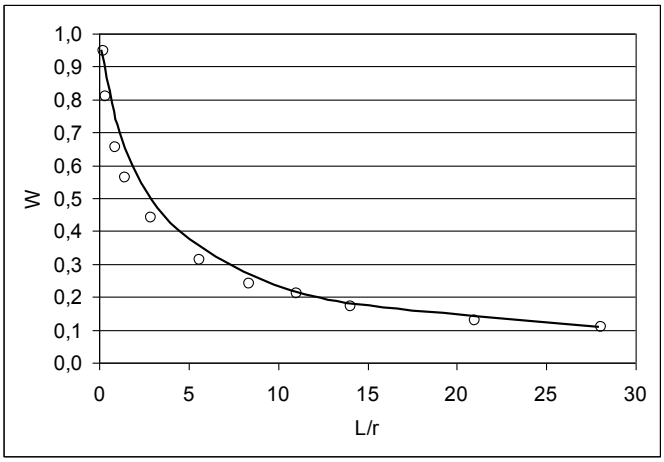

Fig.3.67. Pipe

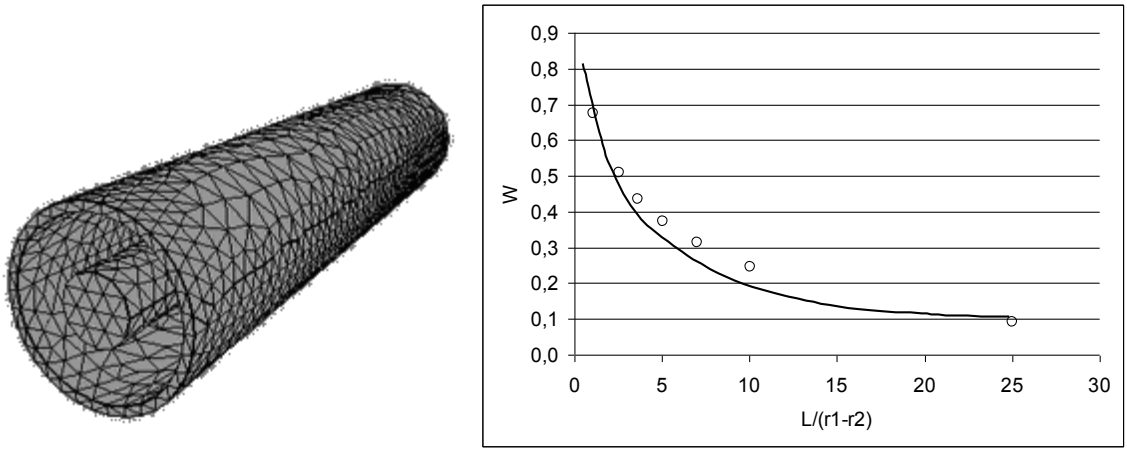

Fig.3.68. The pipe with the inner cylindrical plugs (the ratio of the radii of tubes equal to r1/r2 = 0.4)

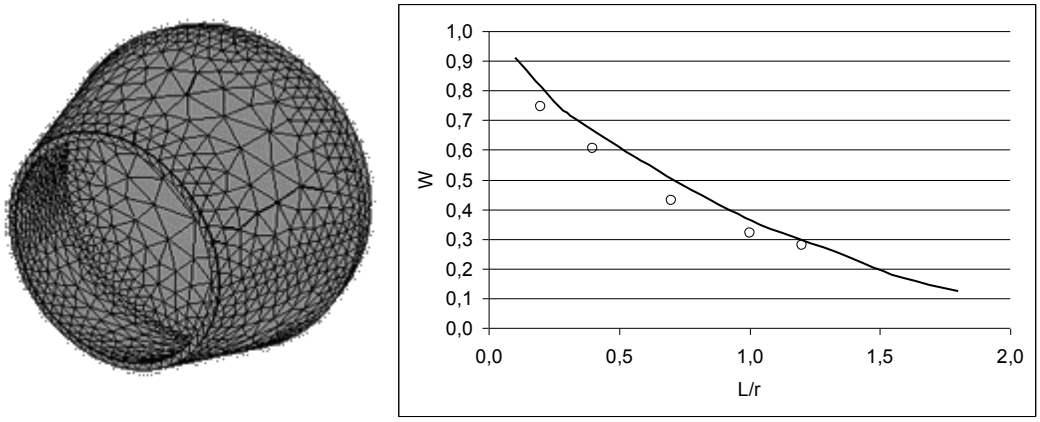

Fig.3.69. Taper with angle at the top of 20 degrees

As can be seen from the figures, for all cases received a satisfactory convergence of the calculated results with the theoretical curves.

3.8. Testing models deposition on the hemispherical

This section presents the results of testing model perepyleniya, a description which can be viewed in gl.2. For testing, we took the hemisphere, which, under different angles were the sources of ions, they were placed so that the ions are emitted perpendicular to the surface of the flight, came straight to the center of hemisphere, then we analyzed the spatial distribution of particles perepylennyh on the status of ion source, as well as their quantitative distribution in the beam with the PMA.

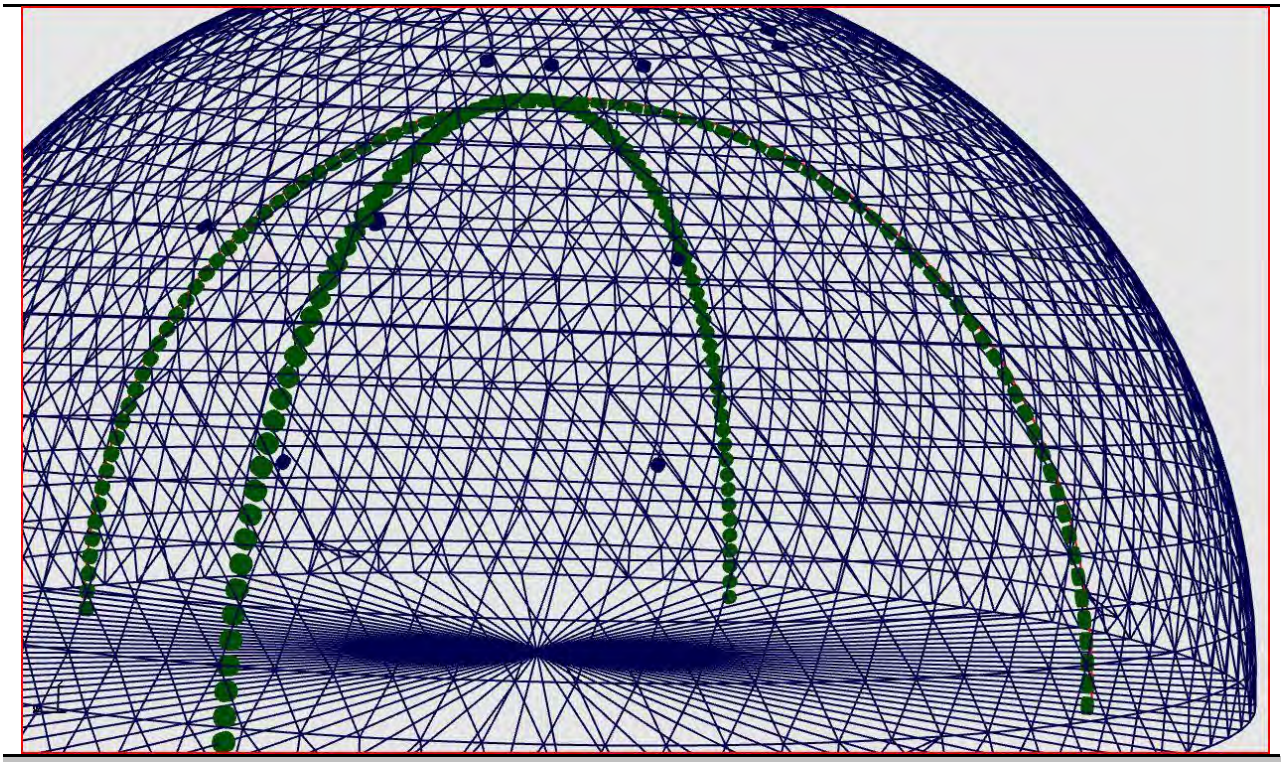

Fig. 3.70. Beam with SMA in the longitudinal and transverse planes

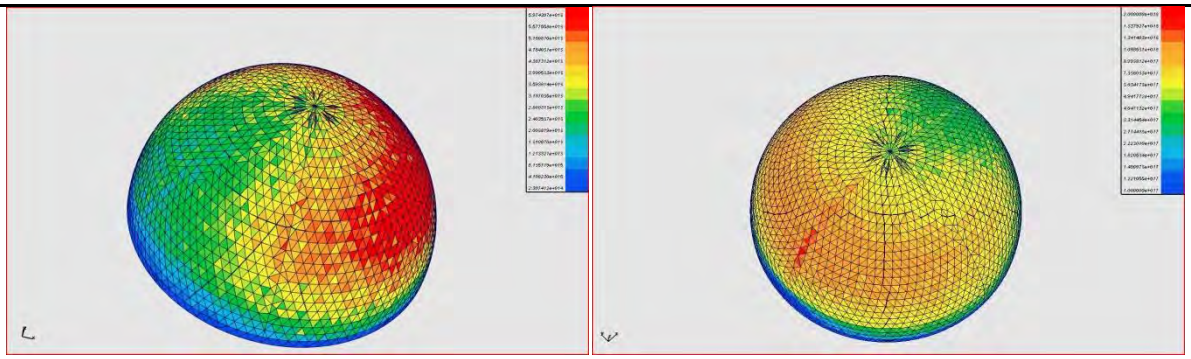

Fig.3.71. Example of spatial distribution deposition chatits

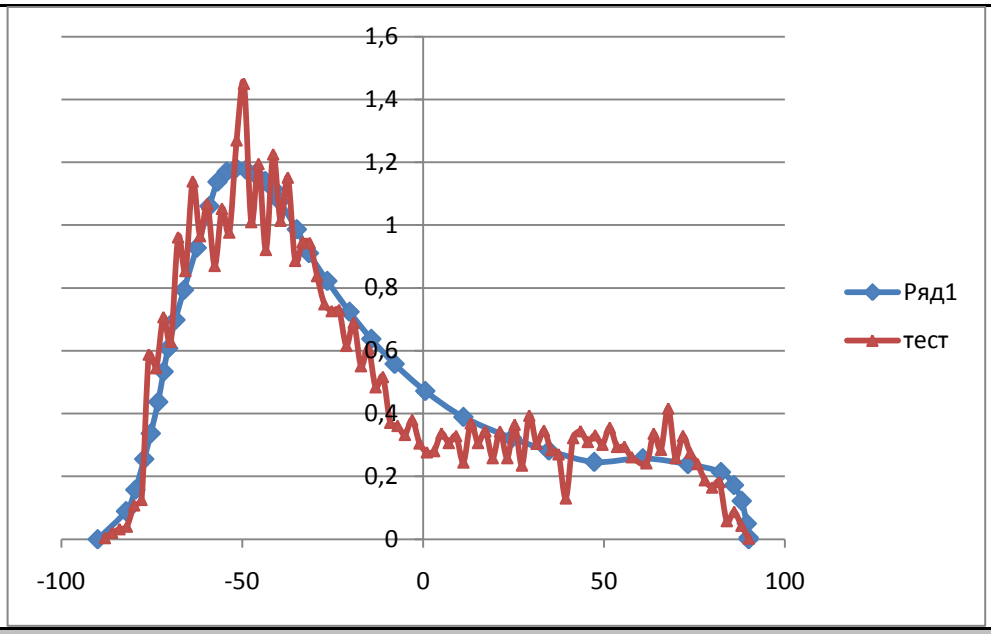

Fig.3.72. Comparison of a given distribution of particles off the data, the SMA to 20 degrees

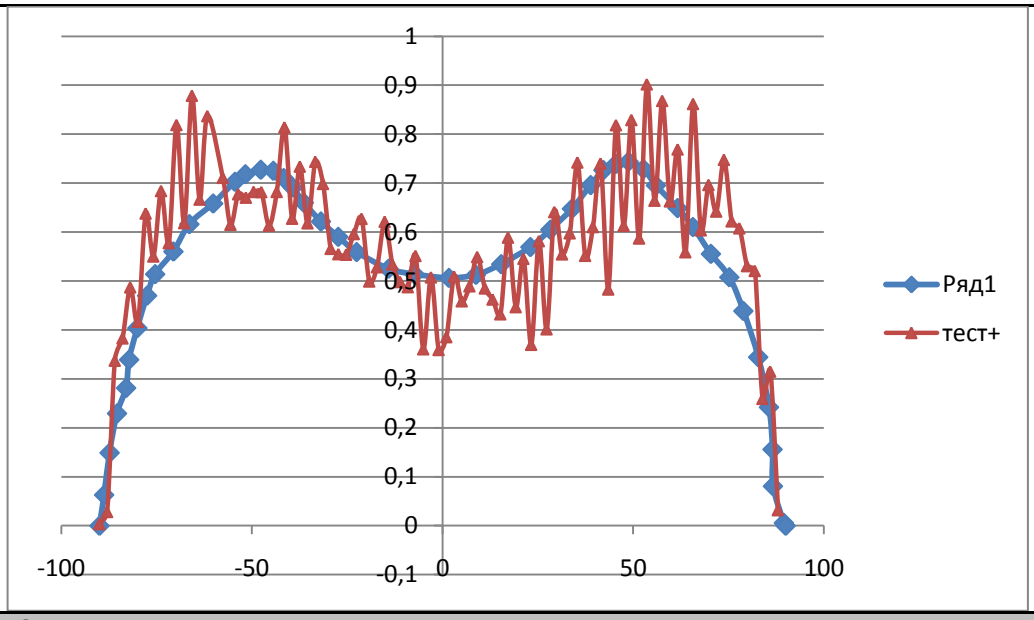

Fig.3.73. Comparison of a given distribution of particles off the data, the SMA to 20 degrees

4. Simulation results in different cells

4.1. The calculation of dynamic pressure

4.1.1. Stand MAI

The experiment was carried out in one of the MAI stands for testirovki software. In experiment 2, we removed the distribution of ions in the beams and the pressure in the chamber at a given point. The first ion beam current was measured at a distance of 400 mm from the accelerator. The second beam was in the plane of the output cross section of the accelerator and was filmed in the main current of ions recharge. Because of the fact that the length of the beam was only 100 mm, we performed two measurements.

The experiment used two probe Faraday. The first beam probes have a diameter of 7mm, and the second 18.2 mm.

Baseline data for the calculation:
1) The temperature of the wall of the camera 300K.
2) The only gas in the chamber - it is xenon, we do not take into account the static vacuum.
3) mass flow from the anode 2.2 mg / s
4) mass flow from the cathode 0.22 mg / s
5) 5% of the total mass of the anode - anode neutrals with temperature 1000K
6) The average energy of ions from the corner was taken from work [42].

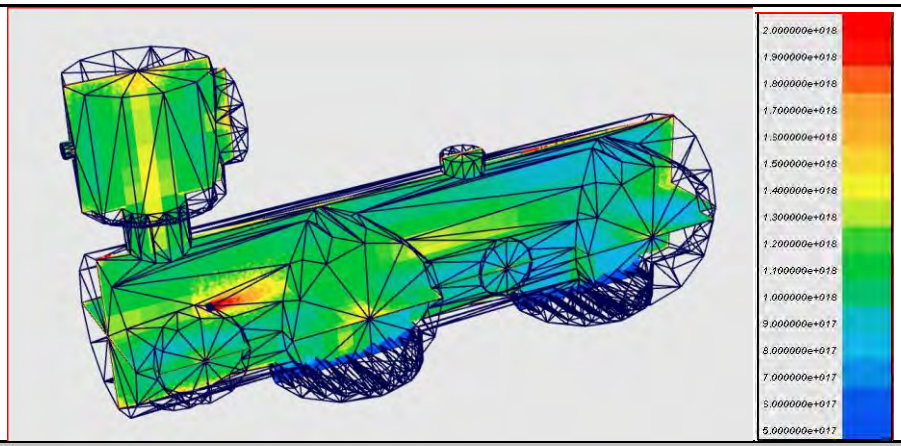

Figure 4.1. The calculated concentration of neutral particles (general view) (1/m3)

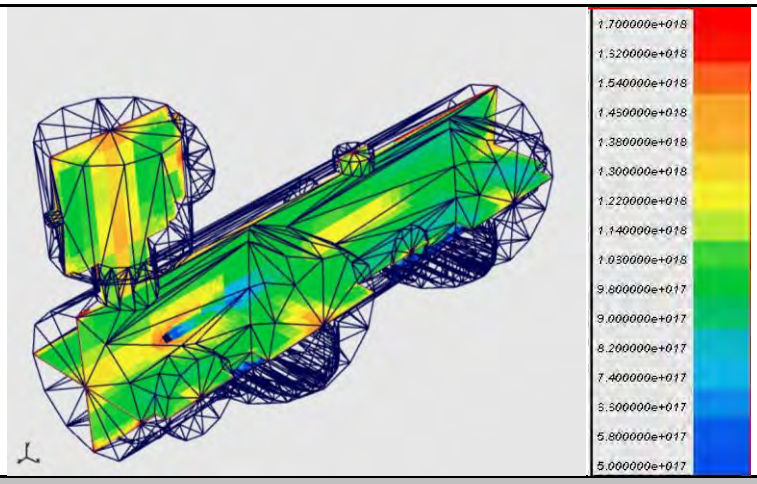

Fig.4.2. The calculated concentration of neutral particles (taking into account the burnup of neutral atoms in the interaction of a jet) (1/m3)

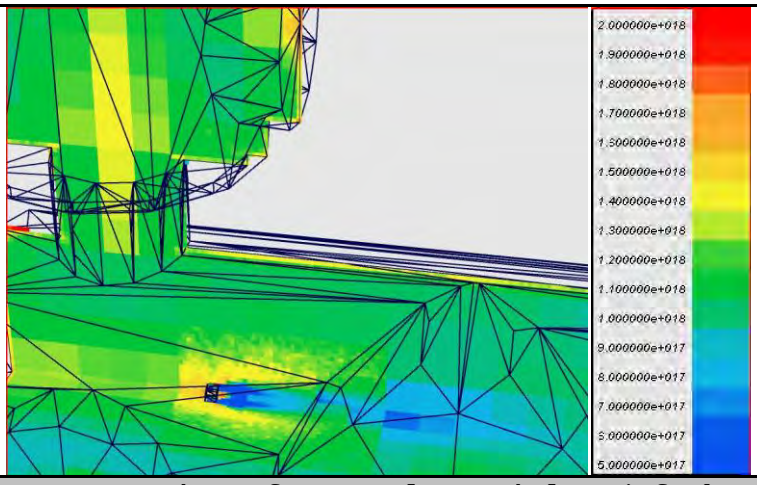

Fig. 4.3. The concentration of neutral particles (of the accelerator and the vacuum sensor) (1/m3)

Analysis of pressure in the chamber

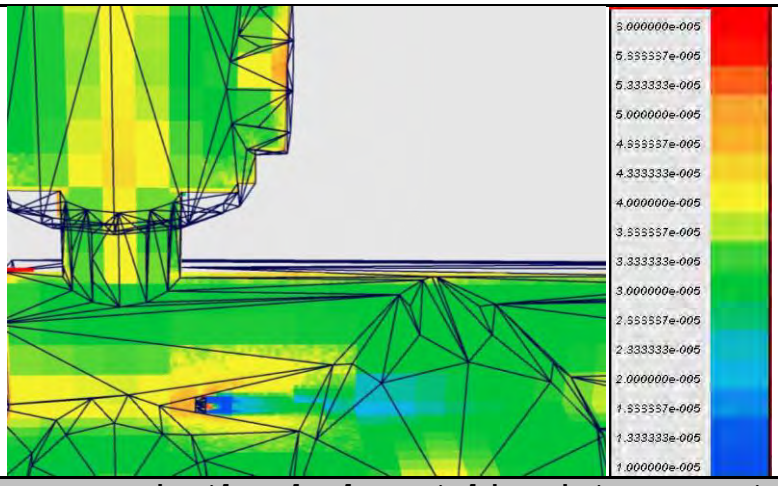

Fig.4.4. The pressure in the chamber, taking into account the burnup

of neutral atoms in the interaction with the jet

Experimental measurement of pressure in the chamber ranged from 5 * 10^{-5}Tor to 6.2 * 10^{-5}Tor with an engine.
The testimony of the sensor with the engine switched off (static void) also ranged from 0.7 * 10^{-5}(Tor) to 1.2 * 10^{-5}(Tor)
The calculated pressure values in general in the volume of the chamber, depending on the location varied from 3 ÷ 5 * 10^{-5} Tor. The value of pressure on the walls and increases equal to 4.2 * 10^{-5} Tor in place of the provisions of the sensor vacuum.
P (calculated) = 4.2 * 10-5 (Tor).
P (experiment) = [(5.0 ÷ 6.2) - (0.7 ÷ 1.2)] * 10-5 = [3.8 ÷ 5.5] * 10-5 (Tor)

4.1.2. Stand in the center of Keldysh

The input data for the problem:

The engine number 2. The wall temperature 300K.

A brief description of the model:

The problem is solved in 2 iterations: 1) using the primary model for tracking the specified number of particles. 2) The method of direct statistical modeling method for analyzing the impact of solid spheres made recalculations.

In the first iteration of trace ions in the probability of a given corner of the angular distribution obtained experimentally. After the ion collision with the wall, he goes with the speed taken from the probability distribution of the Maxwell to the most probable velocity of 194 m / c (300K). Then, tracing continues until not touch the surface of the pump. Example trace is shown in fig.4.5 and 4.6.

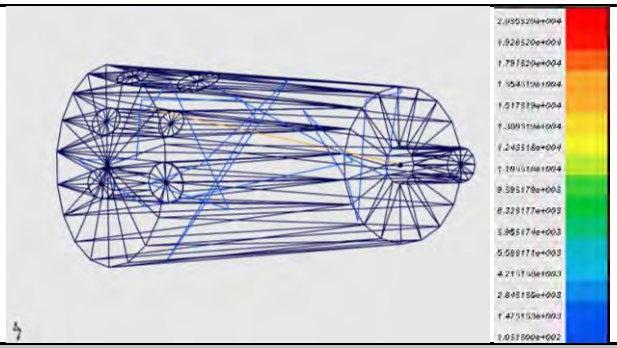

Fig.4.5. (Trajectory of ion (the initial velocity of 20000m / s (250eV)), the color corresponds to the speed in m / s)

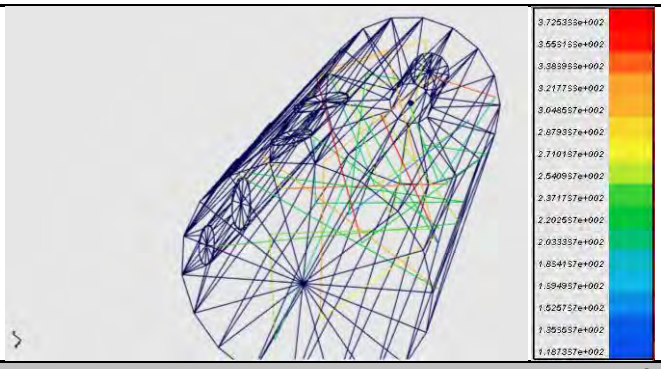

Fig.4.6. (Trajectory of ion (the initial velocity of 220m / s (300 K)), the color corresponds to the speed in m / s)

In the second model, we used the model with the potential interaction of the Lennard-Jones in the first approximation to calculate the cross section of elastic interaction. A velocity field after the interaction we had with the help of hard spheres. Knowing the speed of the modeled atom, the concentration of particles calculated in the first iteration, and the average temperature of gas in the camera is first cross-section of elastic interaction, then the length of free run. Knowing the length of the modeled trajectory of a particle in a cell, is the probability of particle collisions modeled with neutral gas particles. Trassiruem particle until the total probability is not equal to 1. By predraschetam is the direction and value of the velocity vector after the collision.

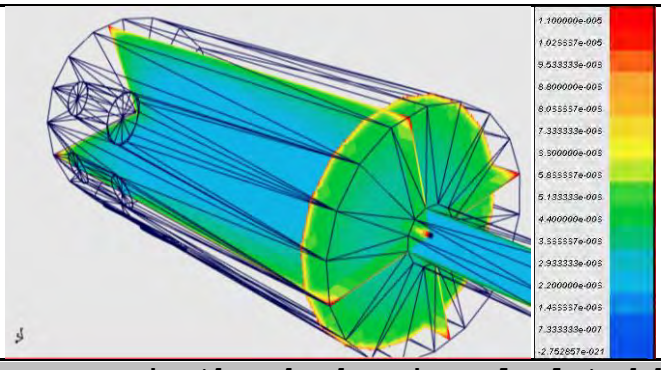

Figure 4.7. The pressure in the chamber is calculated by the first model in Tor (reflection from the walls of equiprobable)

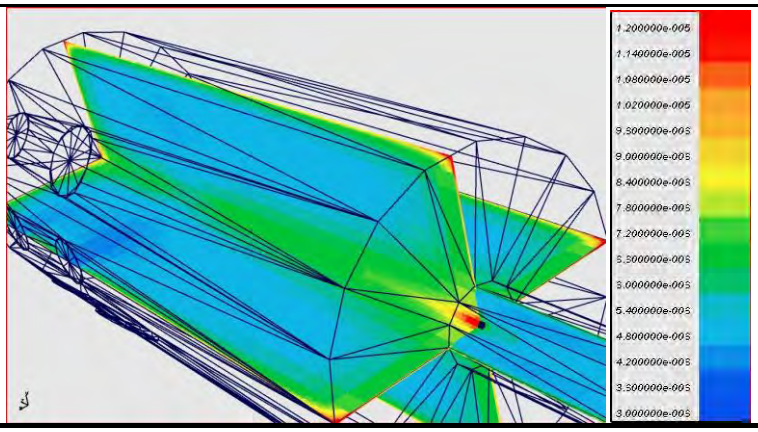

Figure 4.8. The pressure in the chamber is calculated by the second model in Tor (reflected from the wall under the law of full cosine

It should be noted that in the first model, we used equiprobable reflection (reflection on the field, ie, if the hemisphere around the point to describe the reflection of the probability of departure will be equal, and the probability of departure of the reflected particles with an angle less than 30 degrees to the surface will be 50%, which is why concentration of particles near the surface in the first model, much more).

Generally reflect the law is the law of cosine, in any case, the material for the walls of the chamber. Therefore, the second model we used them, and differences in the calculation is mainly due to various factors determining the law reflected from the surface. The same high concentration of particles in the center of the camera is due mainly because of the law of reflection, and not because the engine of the flying neutral particles.

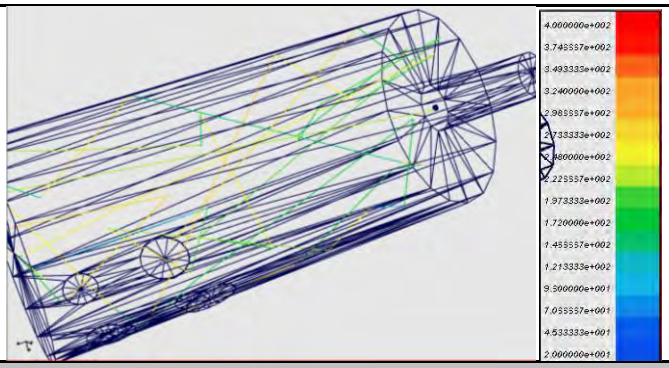

Figure 4.9. Movement of the modeled particles on the second model, taking into account the impact (the color corresponds to the speed in m / s)

Comments:

The experiment had two vacuum, one at the edge of the camera, approximately at the intersection of planes in Fig. 4.7. Second in the rear compartment of the chamber.

On the vacuum gauge reading was 8.8 * 10^{-6} Tor. The second vacuum 8.4 * 10^{-6} Tor.
There is a very good convergence of the model on the first results of the calculation of vacuum (9 * 10^{-6} Tor). Moreover, our model does not take into account the static pressure that is present when the engine disconnected, but at the same time along the edge at which the vacuum is rapidly reducing the concentration, so it is difficult to confidently assert the exact value calculated by the model, it is somewhere in the region of 8 * 10^{-6} to 10^{-5} Tor
In the rear compartment of convergence is not observed. In the second model, 6.5 * 10^{-6} Tor In my own geometry of the rear compartment is different from the one that is specified in the model, so the accuracy of the model is better judged by the results of the first vacuum.
Since the free path length of particles in the cell, commensurate with the size of the camera, do not have a significant impact effect on the overall distribution of neutral particles in the chamber.

4.1.3. Stand 71-3-90 in KB «Torch»

This stand was interesting for us, as it were lifted energy parameters of the jet of ions at different angles from the axis of the engine. Comparison of these characteristics may be quite clear to the accuracy of the magnetohydrodynamic model. Although in this experiment we did not have complete information, we can still show only the principles.
a) The geometry of the camera:

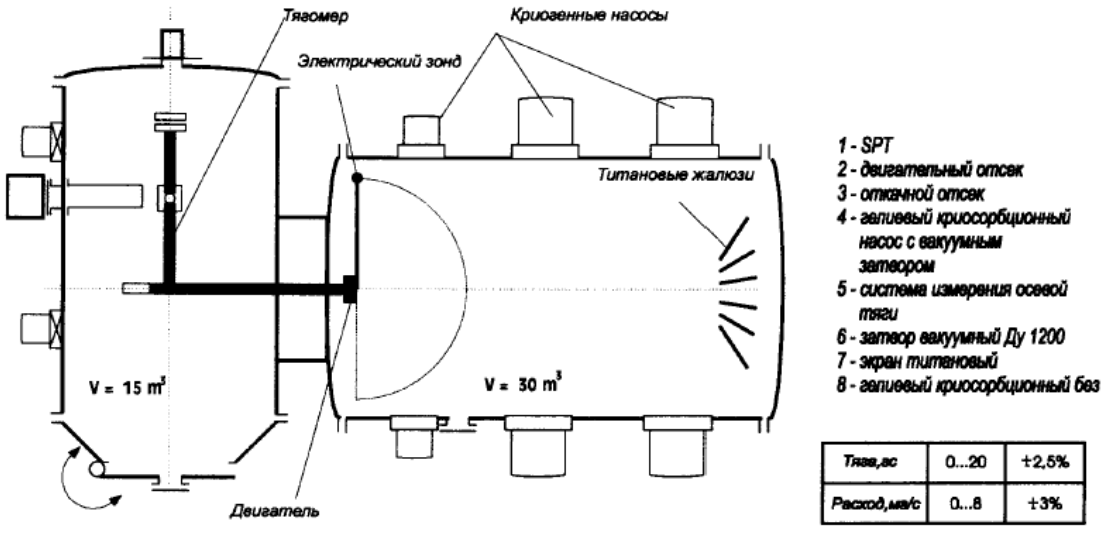

Рис. 21. Схема и параметры стенда 71-3-90 с криогенной откачкой

Fig. 4.10. Initial geometry

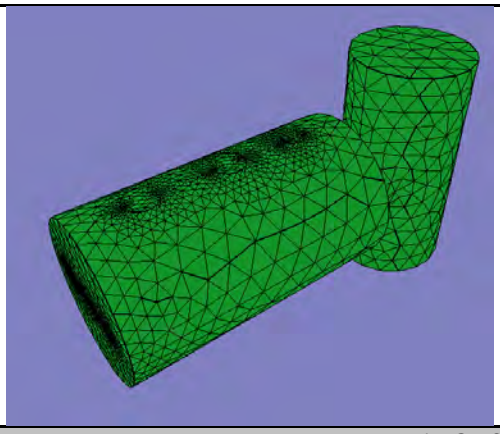

Fig. 4.11. 3-dimensional model of the stand 71-3-90.

Fig. 4.12. the distribution of neutral particles in the vacuum stand 71-3-90 for the engine number 5.

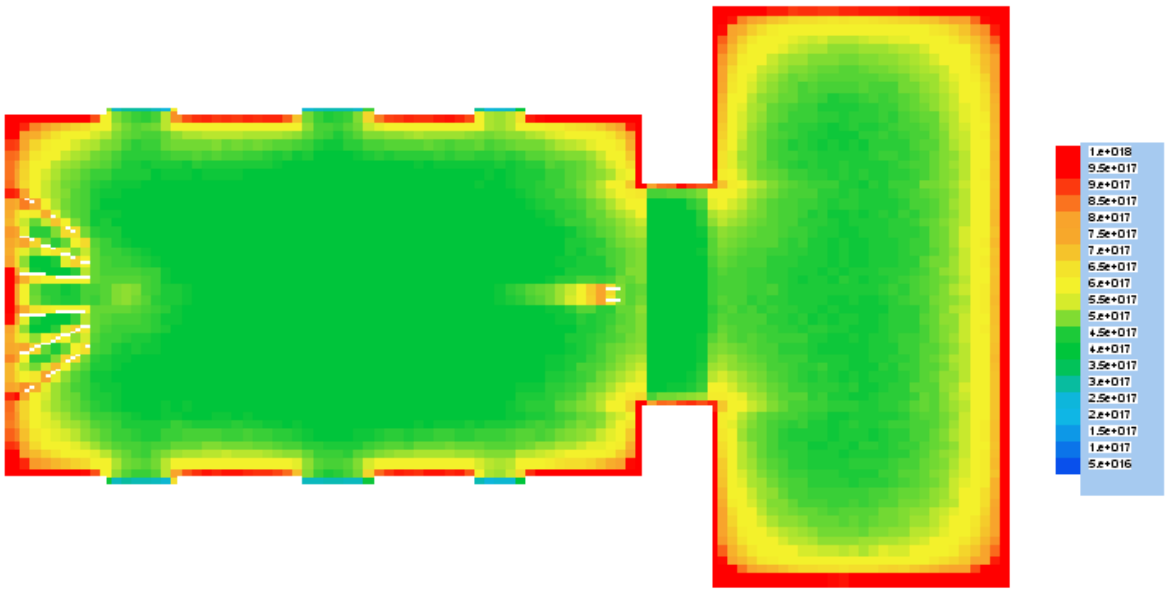

Fig. 4.12. The distribution of particles when the engine without taking into account the static vacuum.

4.1.4. Comparison with the calculation of Alta

The model used the engine number 3.

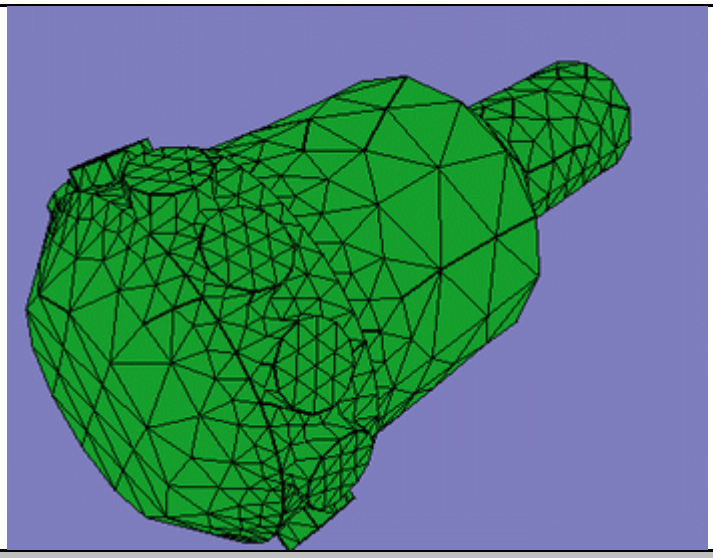

Fig. 4.13. 3D model of the vacuum chamber.

Results for 600,000 emitted ions and neutrals 30,000 (5%), as well as the grid in this calculation was 40x40x80.

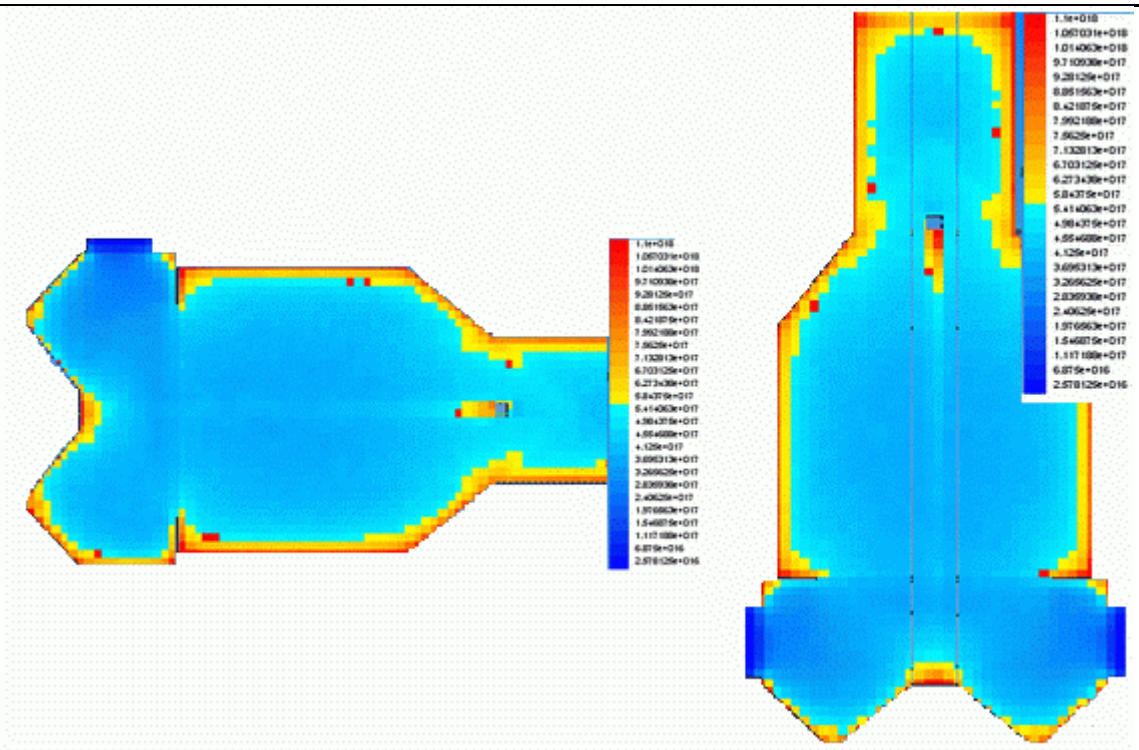

Fig. 4.14. The concentration of neutral particles

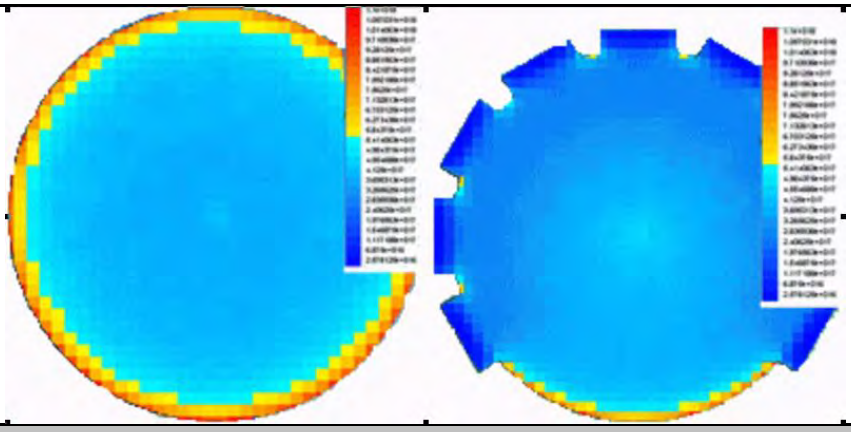

Fig. 4.15. The concentration of neutral particles (cross section in the middle of the camera and in the pumps) [1/m3]

The following figure shows the point where the model is compared with that used in [43]:

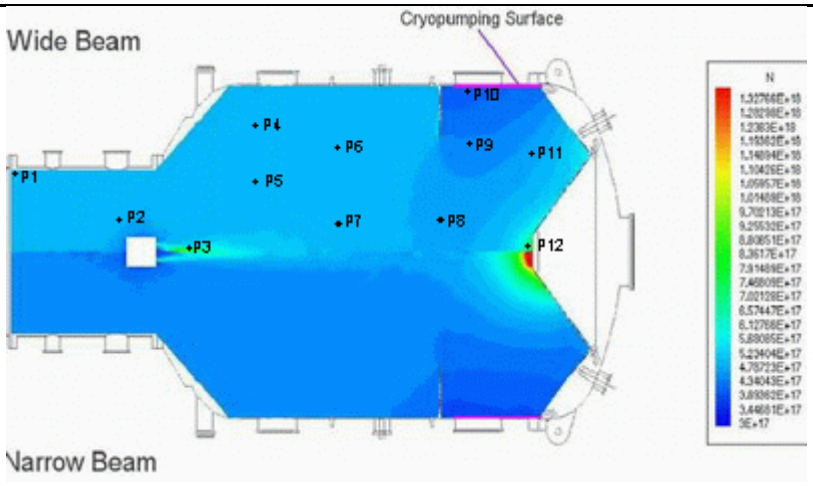

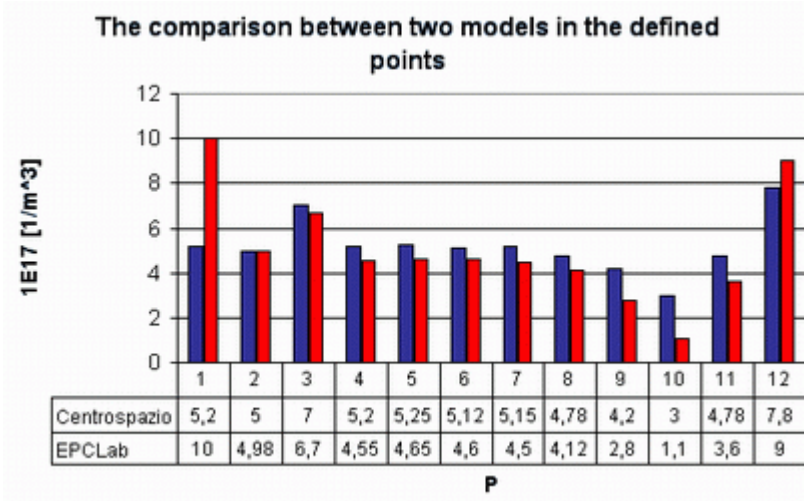

Fig.4.16. Points for comparison and a comparison

This calculation was carried out under the assumption that the reflection from the wall occurs equiprobable. The generally accepted assumption is a reflection of the cosine. With its use of concentration at the edges of the camera does not increase so much as in our model, but its tendency to increase, there is (see the comparison for Sand in the East. Keldysh) of approximately 1.3 times. Therefore, at point 1, our evidence is too high.

4.1.5. Comparison with simulations carried out by [8]

The model used the engine number 4

1. 3D model based on the given article size

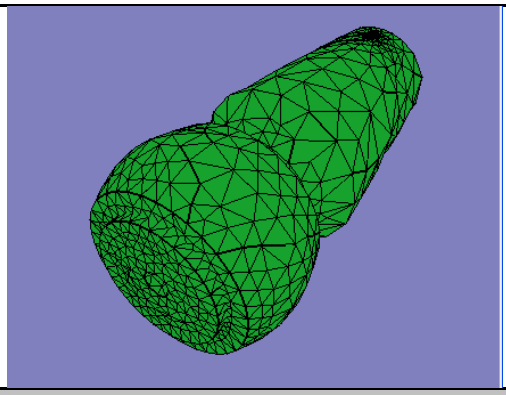

Fig.4.17.Trehmernaya camera model

2. Configuration and space cryogenic panels given at Arnold Engineering Development Center [44].

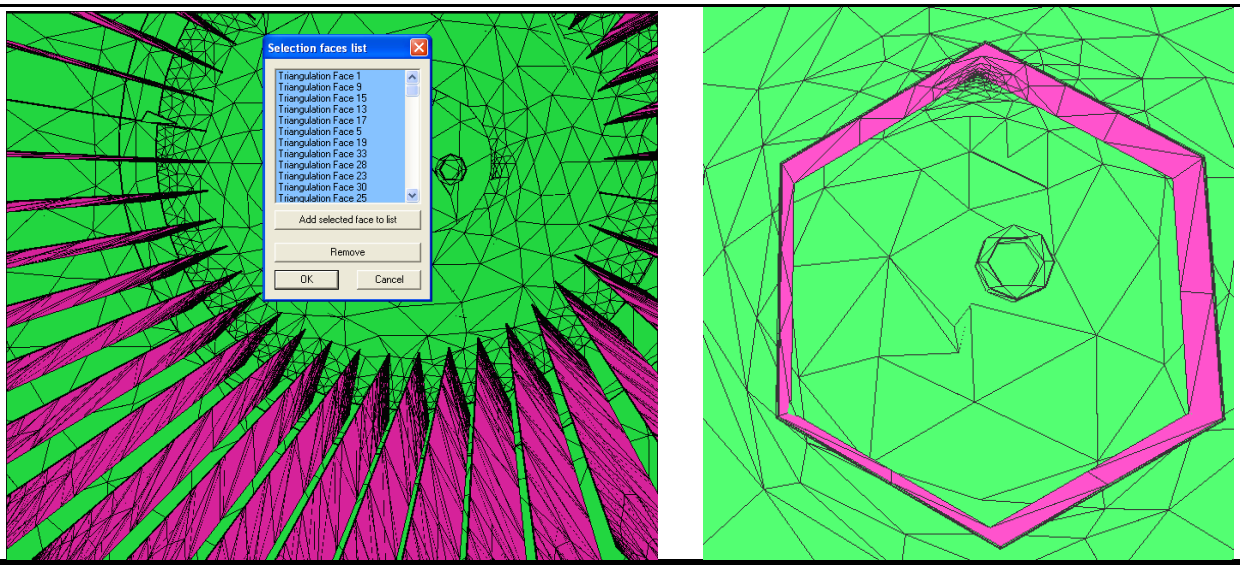

Fig. 4.18.Cryogenic cover the upper and lower pumps in the cell

.

Analysis of results

1. Analysis of the dynamic vacuum in the chamber

For this camera, in this experiment we did not have accurate information on the location of the sensors vacuum, the article said only that the vacuum chamber in order 10^{-6} Tor, measured experimentally.

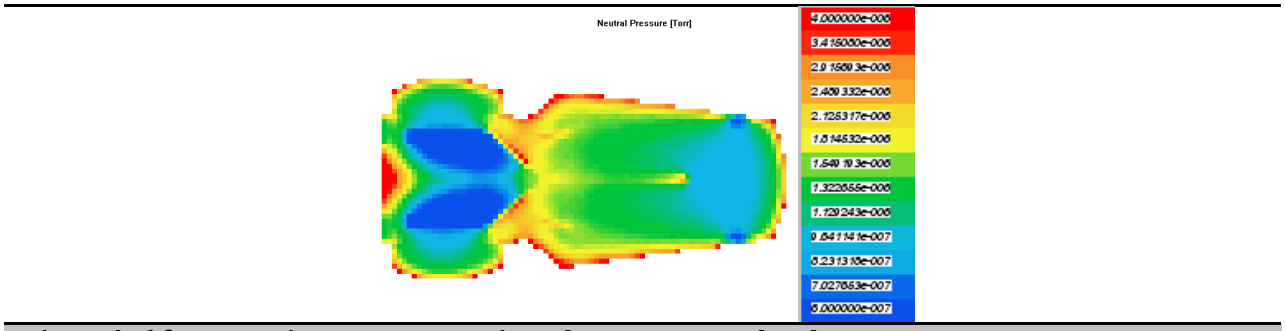

Fig. 4.19.Dynamic pressure in the vacuum chamber.

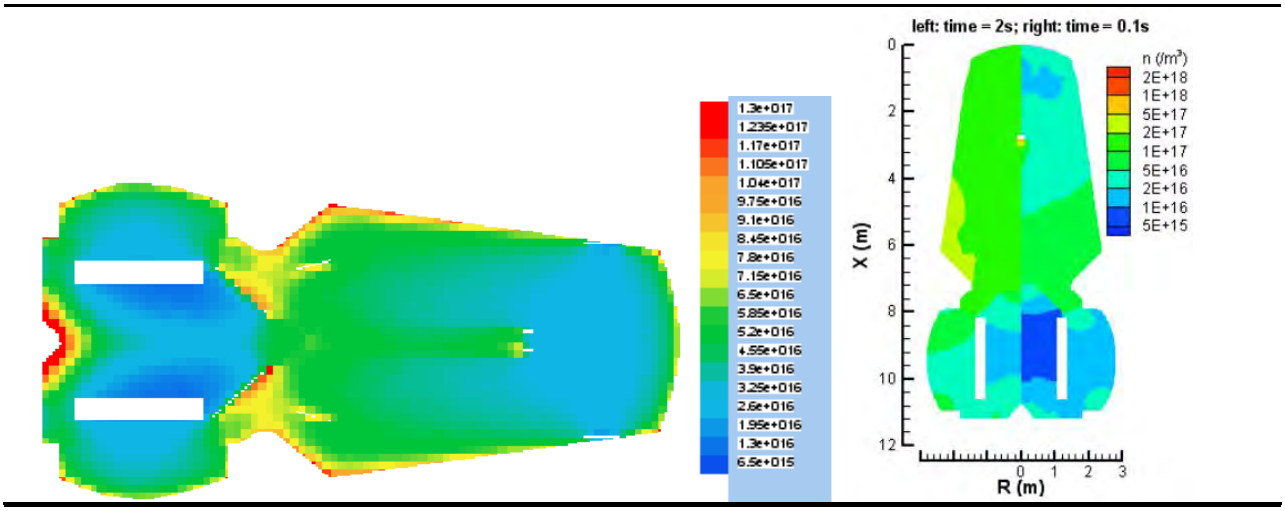

Fig. 4.20.Sravnenie concentration of neutrals. (Top EpcLab; lower Boyd)

4.1.6. Calculation of the area near the engine

This calculation is interesting because it is possible to estimate the proportion of neutral particles flying from the engine compared to their shares, which came out of the vacuum chamber.
It was asked the initial concentration of particles of 5 * 10^{17} [1 / m ^ 3] (1.66 * 10^{-5} Tor) for the entire computational domain. There were emmitted from the virtual cathode (distance 25 mm from the anode), a neutral particle. Mass flow rate of 0.15 mg / s, about 5% of the total mass flow.

Calculated distribution:

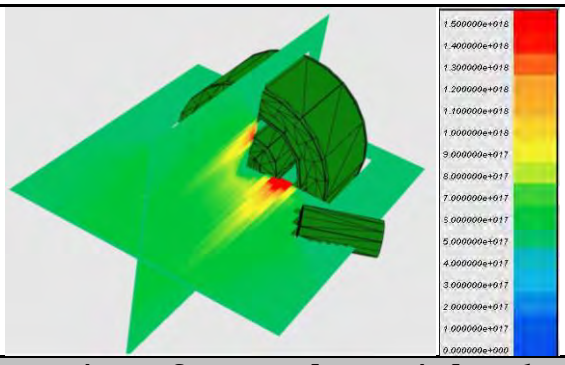

Fig.4.21. The concentration of neutral particles 1 / m ^ 3

4.2. The calculation of the distribution of primary ions

4.2.1. Stand in the MAI

The calculations for the lifting of simulated parameters of the jet used by the two beams with the probes: one with the real size of probes for every 2.5 degrees. The second probes with 35 mm located at 6 degrees. The first was used for removal of ion current. Second for the lifting of the energy distribution.

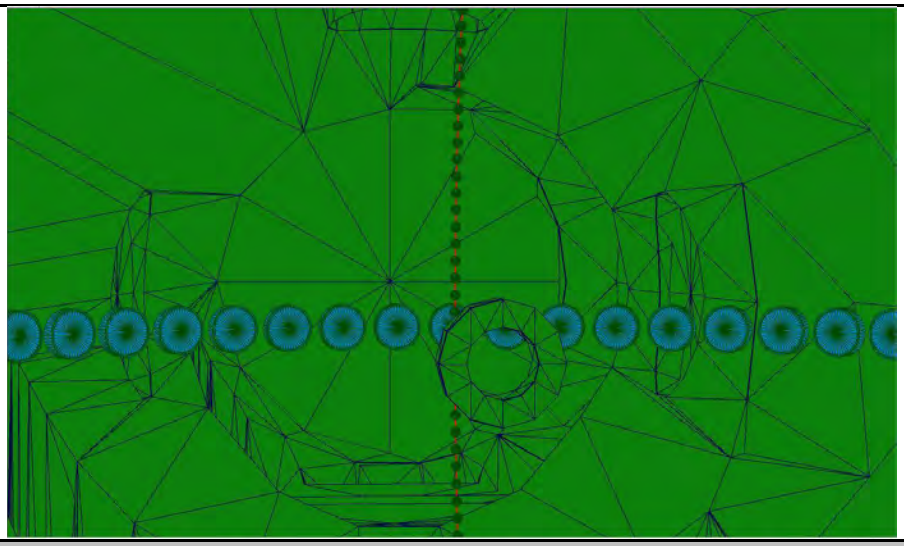

Fig.4.22. beams with SMA

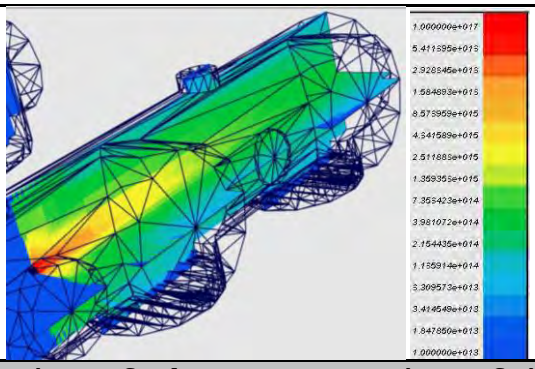

Fig.4.23. The calculation of the concentration of ions in uncorrected distribution (general view) (1/m3)

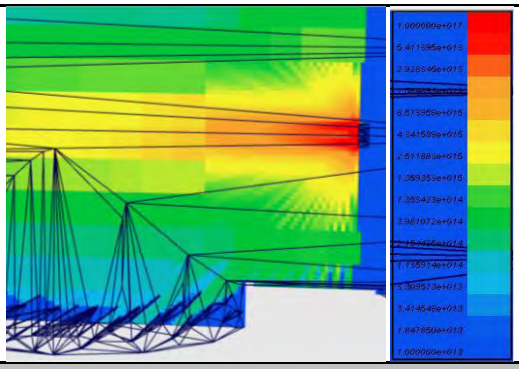

Fig.4.24. The calculation of the concentration of ions in uncorrected distribution (the accelerator) (1/m3)

The initial angular distribution of ions as we thought the two main disadvantages: firstly, it includes a rechargeable share ions, second, part of the accelerated ions interact with neutral atoms losing charge and is not fixed probe. After adjusting the data, we found another point that the probe does not record the whole coming to him talk. After integration over the area of ion current and the transfer of the value of the mass flows through the scope for the moment it became clear that the true value of the current in 3-4 times more measured.

It should be noted that so far the best way to filter the current CEX ions are measured by the RPA probes, which do not allow low-ions. Good description is given in [45]. Although we have also developed a method of computing filter CEX ions, but its effectiveness has been much worse.

But the second factor can be very effectively corrected using a computer reconstruction of the lost on the interaction of ions with neutral gas.

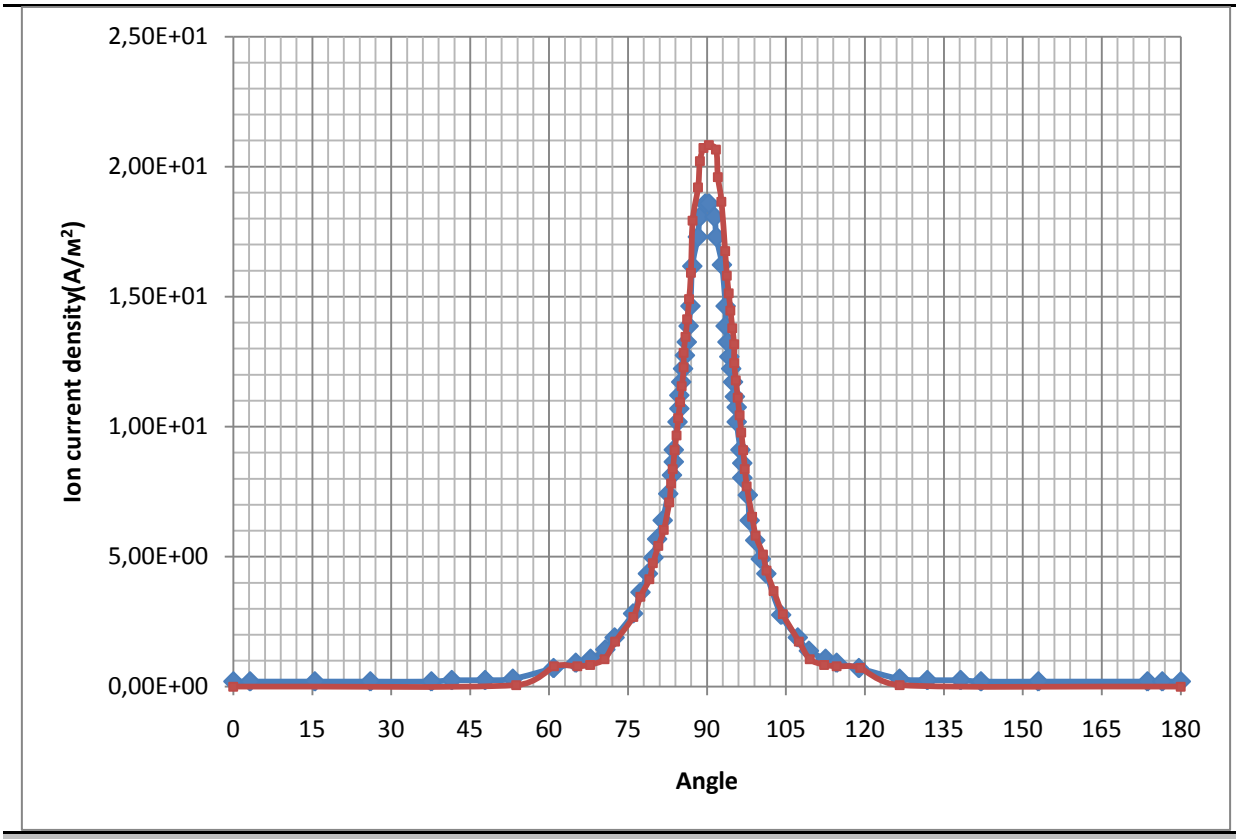

Figure 4.25. A) Uncorrected angular distribution ion current density (blue) B) Filtering RPA probes at angles greater than 30 degrees, and mathematical reconstruction of the lost ions in collisions with neutral gas (red).

After adjusting for RPA probes spread of mass shifted, so we assume that the more close to the real picture of the distribution of primary ions must be as follows:

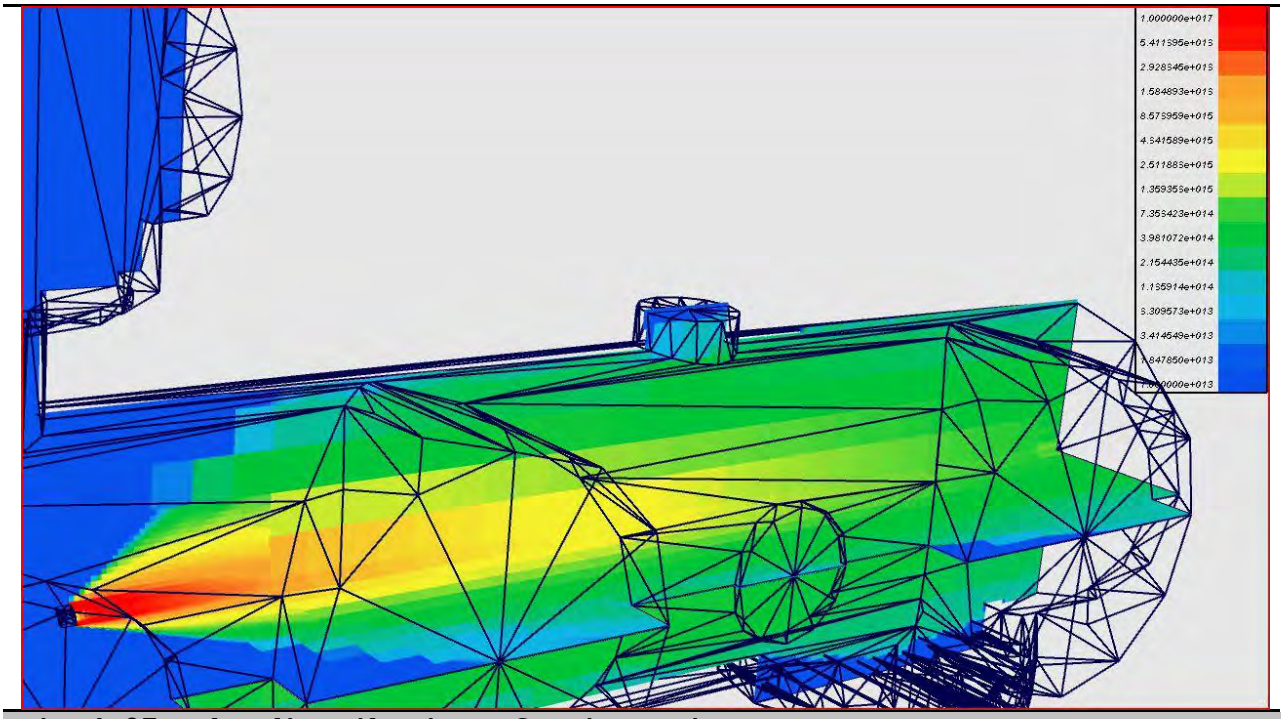

Fig.4.27. The distribution of primary ions

The fact that the corrected distribution over the case, confirmed by the calculation of the integral propulsion accelerator. Calculation of traction control is done using the teat, which is a few cm from the engine, which blocked all possible trajectory of an ion accelerator, so that all of the ions come in contact with the surface of boss, giving it some momentum. The total momentum of all simulated particles and traction motor.

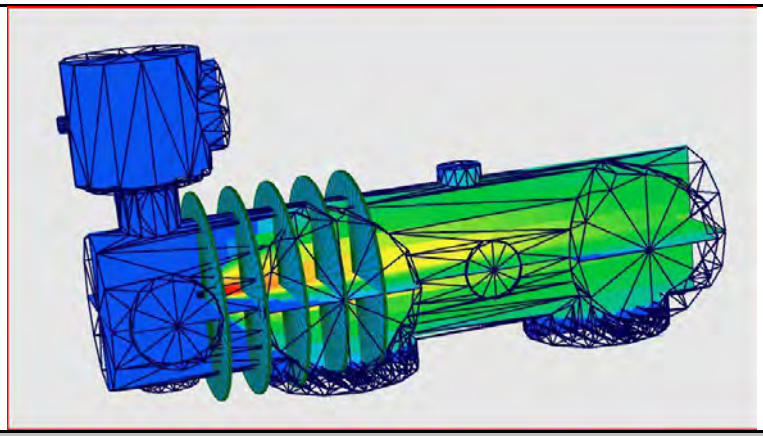

Fig.4.28. The system thrust of measuring

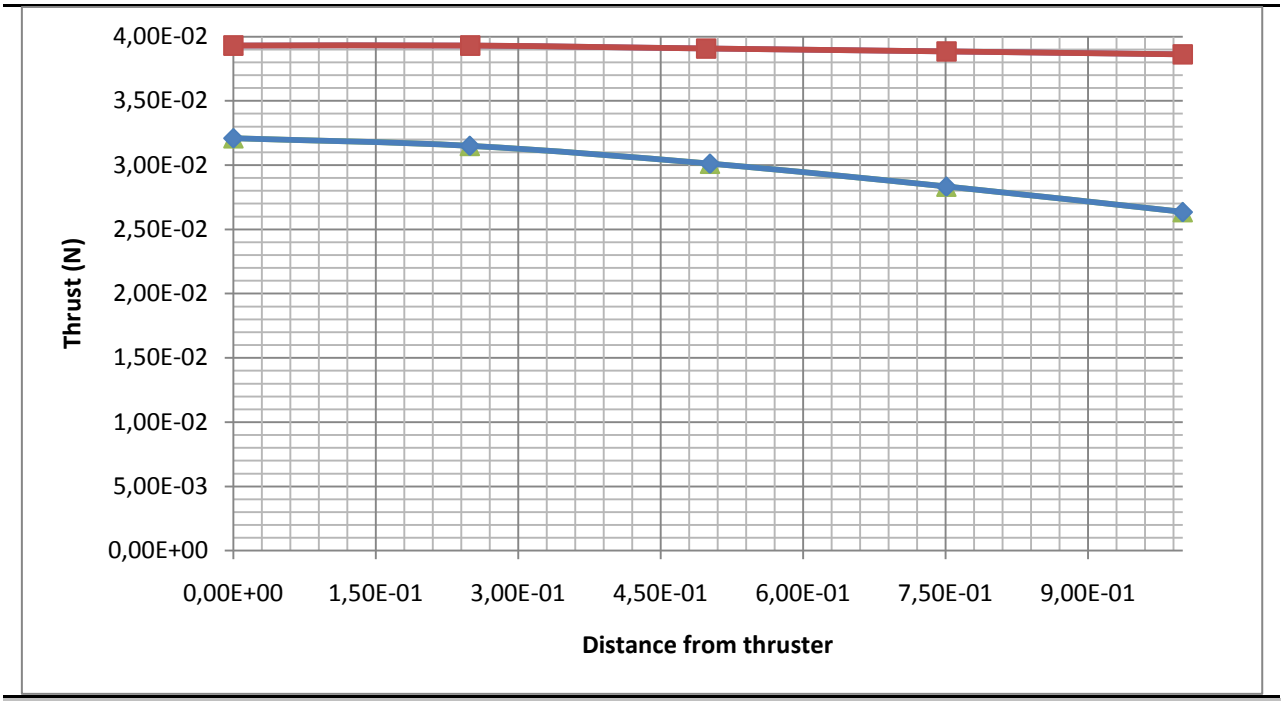

Fig.4.29. The distribution of traction on thrustmeter (100% ionization at a cost of 2.2 mg / c), on the left - uncorrected distribution right - the distribution obtained by RPA filtering in the corners more than 30 degrees, and the restoration of lost on the interaction with the neutrals in the corners is less than 30 degrees.

Experimentally measured value of traction for the SPT-70 was 40mN. For the three distributions considered. Without any adjustments, taking into account the 95% ionization of 30.5 mN. Further adjustments to the computer and the restoration of the lost, taking into account the 95% ionization of 34 mN. Since filtration RPA probes and recovery of lost in the interaction with the gas, taking into account the 95% ionization of 38 mN.

4.2.2. Stand in the center of Keldysh

For the mathematical presentation of the model we used as input data: the engine mass flow, the angular distribution of ion current, the energy distribution of ions in the jet at different angles. Use this for the engine number 2.

The algorithm is based on the method of tracking a specified number of initial particles (ions). The probability of the angle of departure modeled ion is calculated using the defined distribution of ion current density of the angle, taking into account the volume ratio. Depending on the angle of departure, given the importance of ion energy, taken with the probability of the distributions, in chapter 3. We analyze the number of trajectories of ions around 10^6-10^7.

Computational domain is divided into rectangular finite element mesh, a criterion for the breakdown was 40 in each direction. When the ions through the cell, calculated the time spent by them in the cell. Then add up all the values of the time of the ions in cells, this array is then transformed into an array of distribution of concentration of ions in the cell shown in Fig. 4.33.

To verify the model, as well as for the more usual presentation of the simulation results, proposed method of surface mathematical analysis. Its essence is that the calculated geometric model of the probe is inserted under a given angle and coordinates in the design model, then, if the particle collector respect PMA, he remembers its charge and energy. After calculating the information accumulated at the SMA energy particles hit it, and the total quantity. These data can be converted to various parameters such as pressure sensor, traction, ion current density, mass flow rate through the probe. Since the probes are installed at some distance from the engine, modeled ion beam passing through the medium of neutral atoms in a vacuum chamber is weakened, as reflected through the reduction factor.

Also, the ions formed by re-invest its share of the total current. Although it should be noted that the RPA probes practically solve the problem.

In our calculations, we used a system of probes (beam), in order to represent the result of probes on a single graph.

1. Model
2. At the indicated figure estimated model

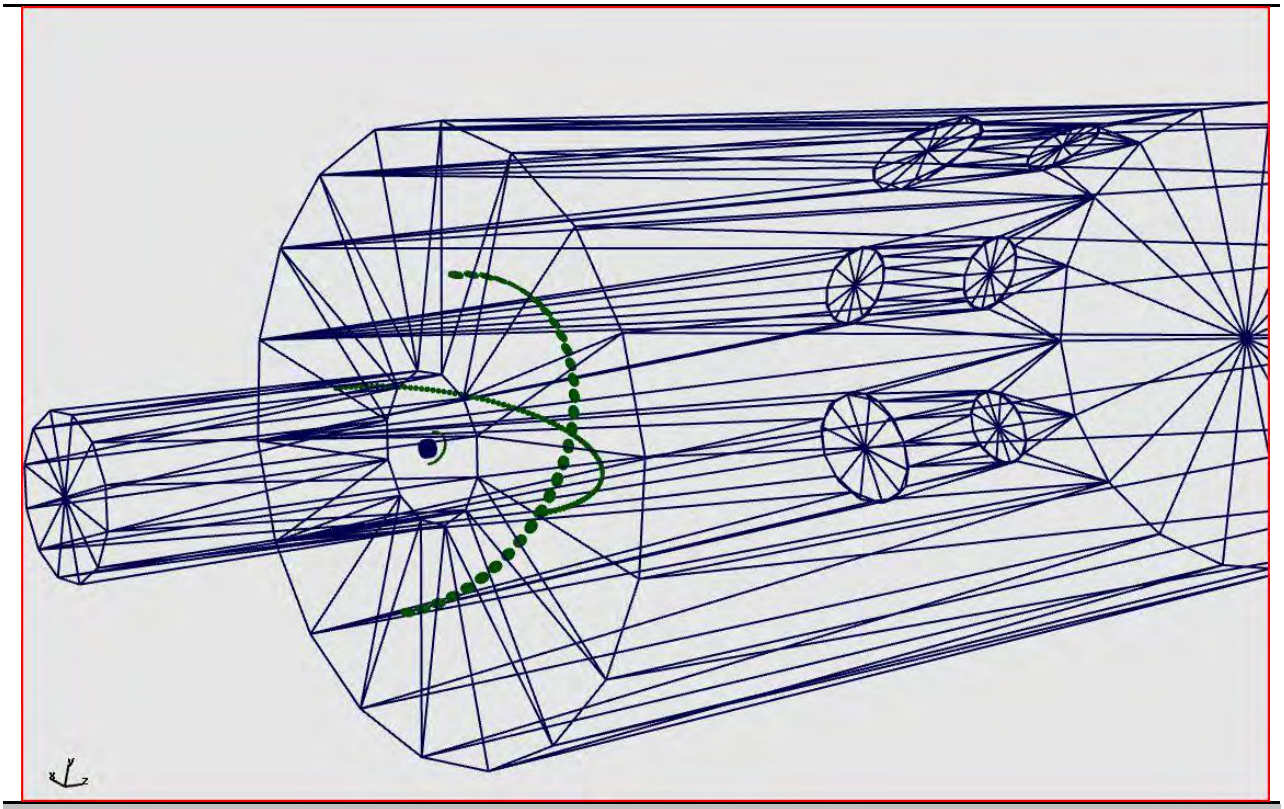

Fig.4.30. The system probes the overall appearance

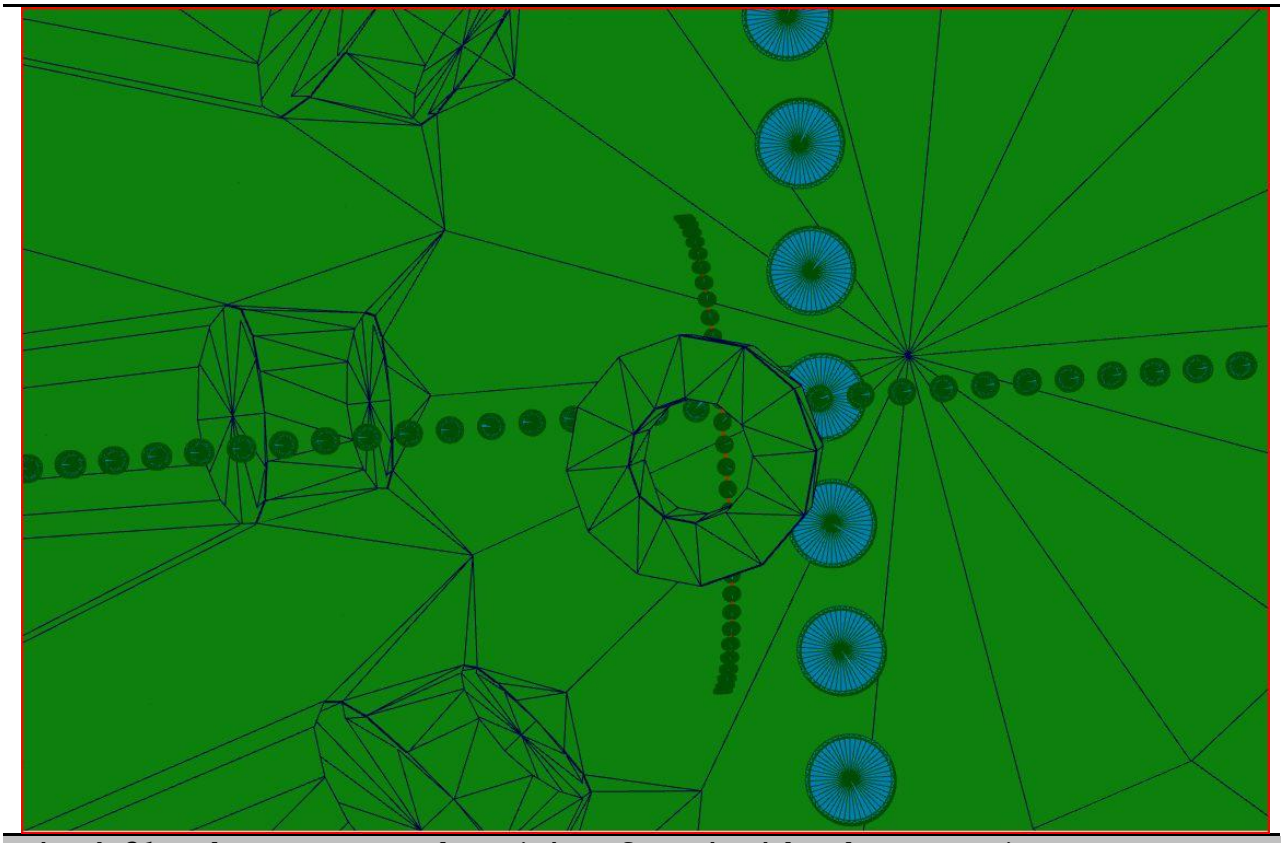

Fig.4.31. The system probes (view from inside the camera)

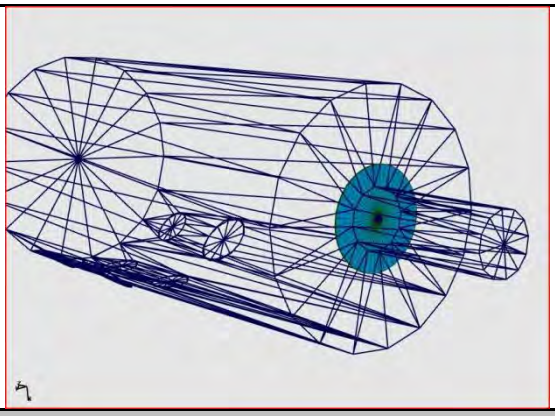

Fig.4.32. A SMA for thrust measure

In our calculations, we used several of probes: 1 - 31 probe diameter 70 mm for the lifting of the energy spectrum at a distance of 1.05 m from the motor, 2 - 91 tube diameter of 18 mm for the withdrawal of the angular distribution of current on the probes at a distance of 1 m and 31 for removal of the probe angular distribution at a distance of 0.5 m, 3 - 31 probe 2 mm in diameter for removal of the distribution at a distance of 100 mm from the engine.
The same was added to the probe-tyagomer, which was determined by using engine thrust as shown in Fig. 4.32.

2. Results

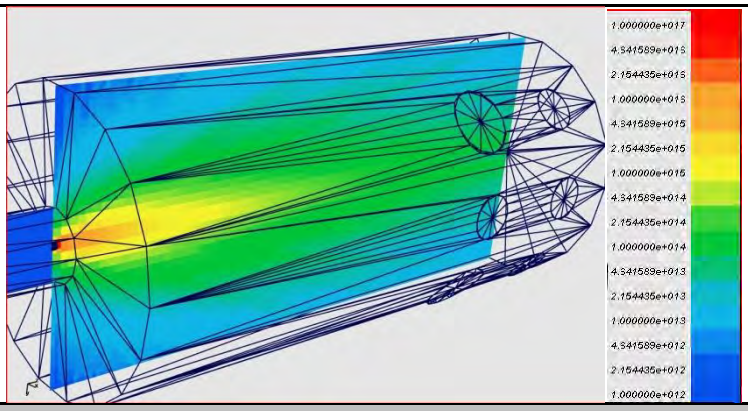

Fig.4.33. The distribution of primary ions in the volume of the chamber

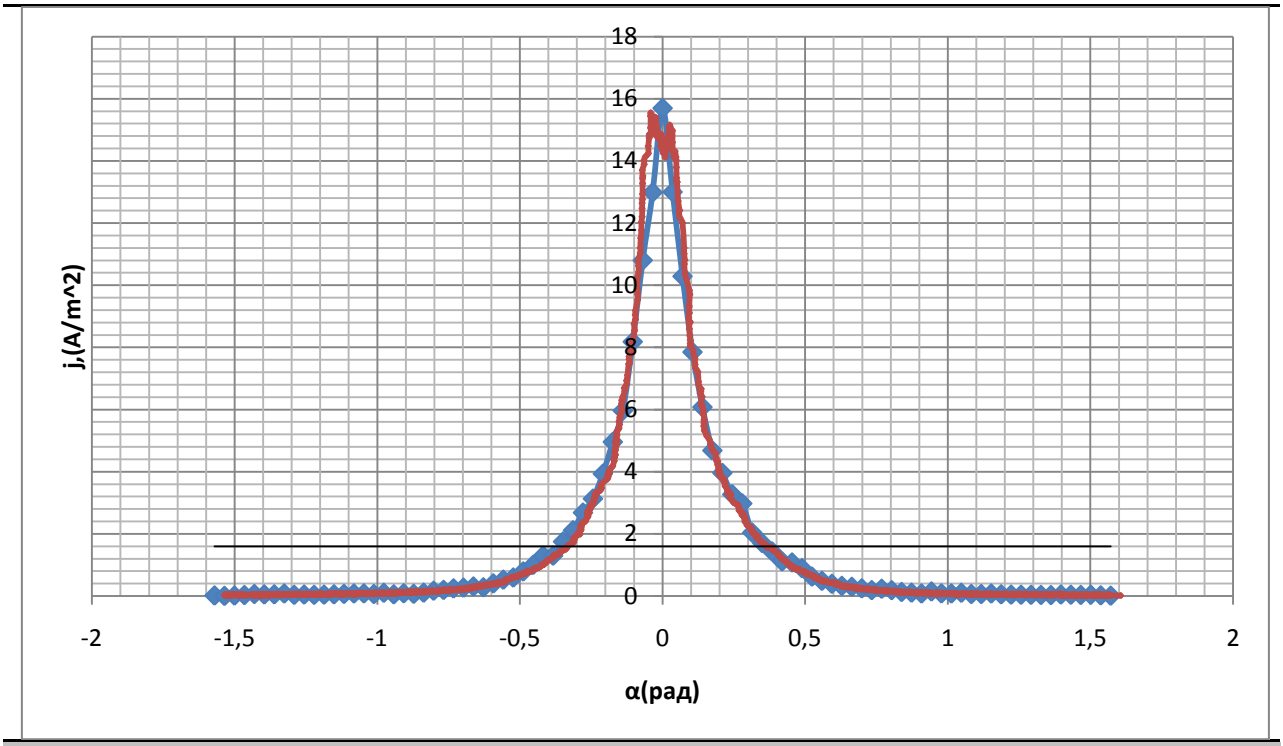

Fig.4.34. Comparison of the modeled current density obtained by the formula (3), the beam with the PMA, which consist of 91 PMA diameter 18 mm (blue curve) at a distance of 1m, with experimentally removed (red curve)

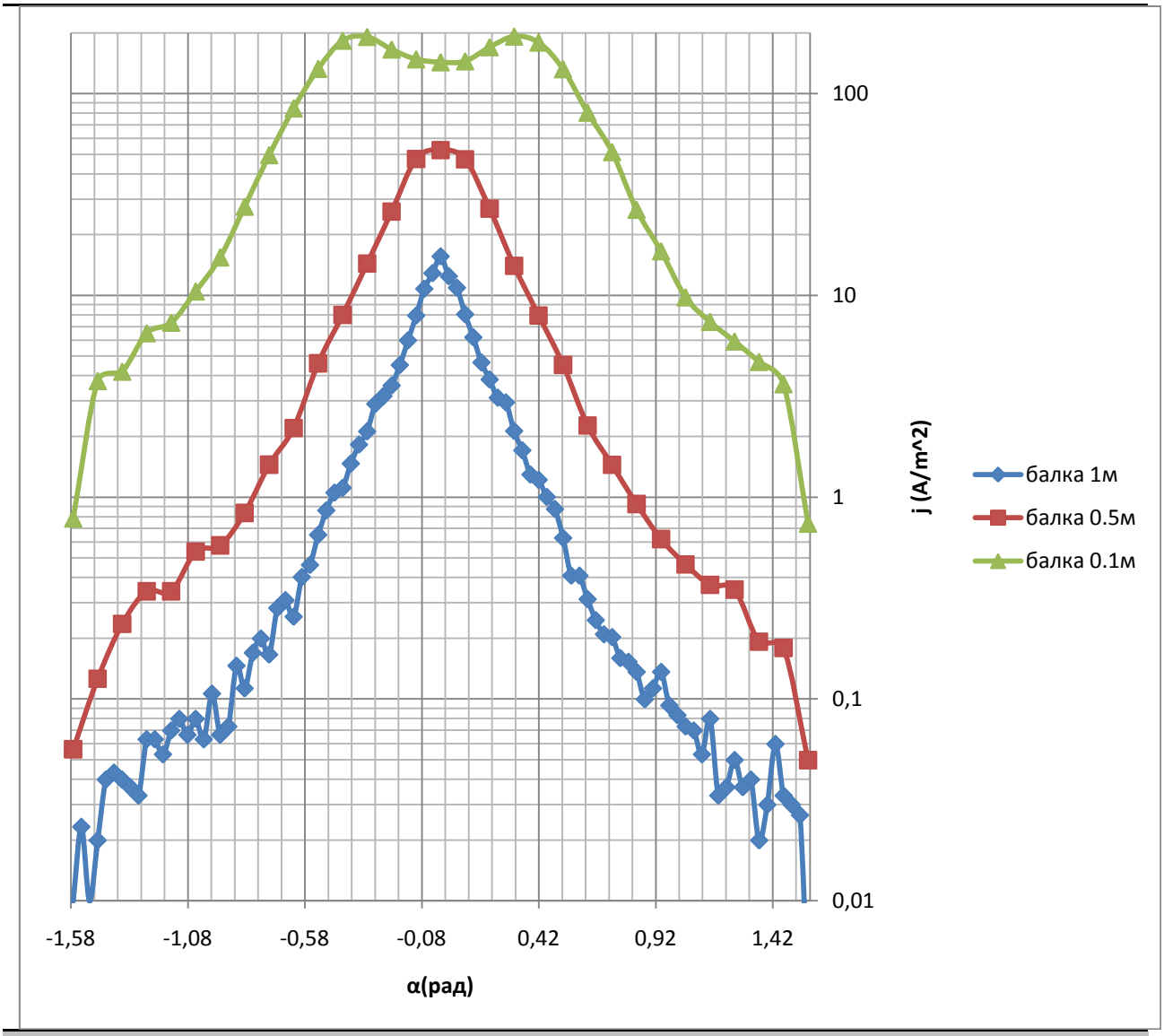

Fig.4.35. Ion current density at the beams at different distances from the engine

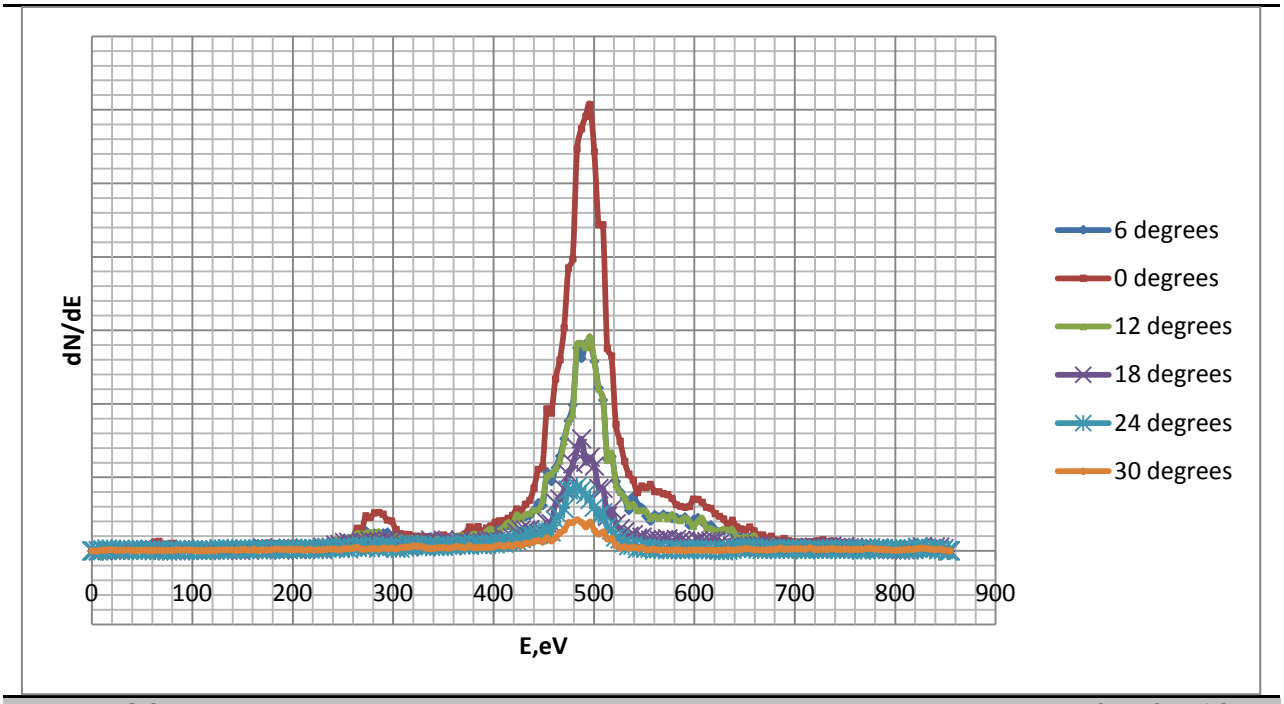

Fig.4.36. Distribution of ion energies motion for the angles 0, 6, 12, 18, 24, 30 degrees at 70 mm PMA at a distance of 1m from the engine

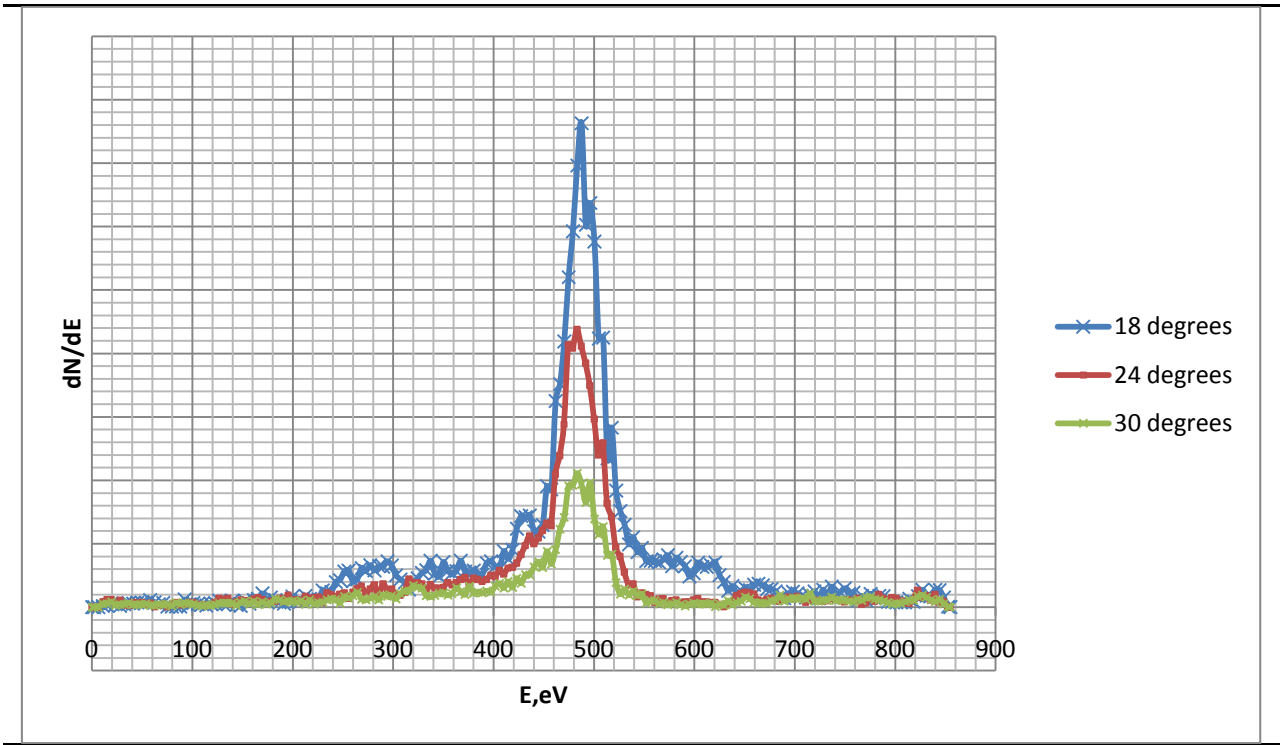

Fig.4.37. Distribution of ion energies motion for the angles 18, 24, 30 degrees at 70 mm SMA at a distance of 1m from the engine

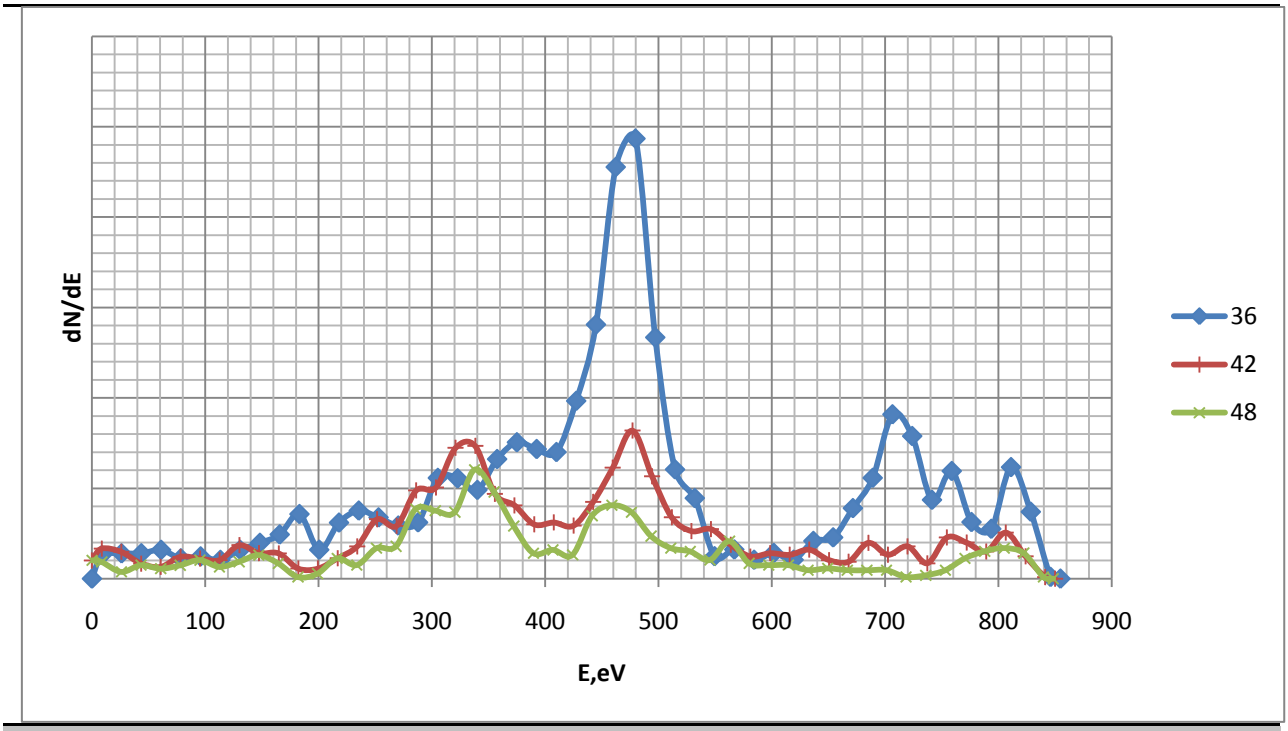

Fig.4.38. Distribution of ion energies motion for the angles 36, 42, 48 degrees at 70 mm SMA at a distance of 1m from the engine

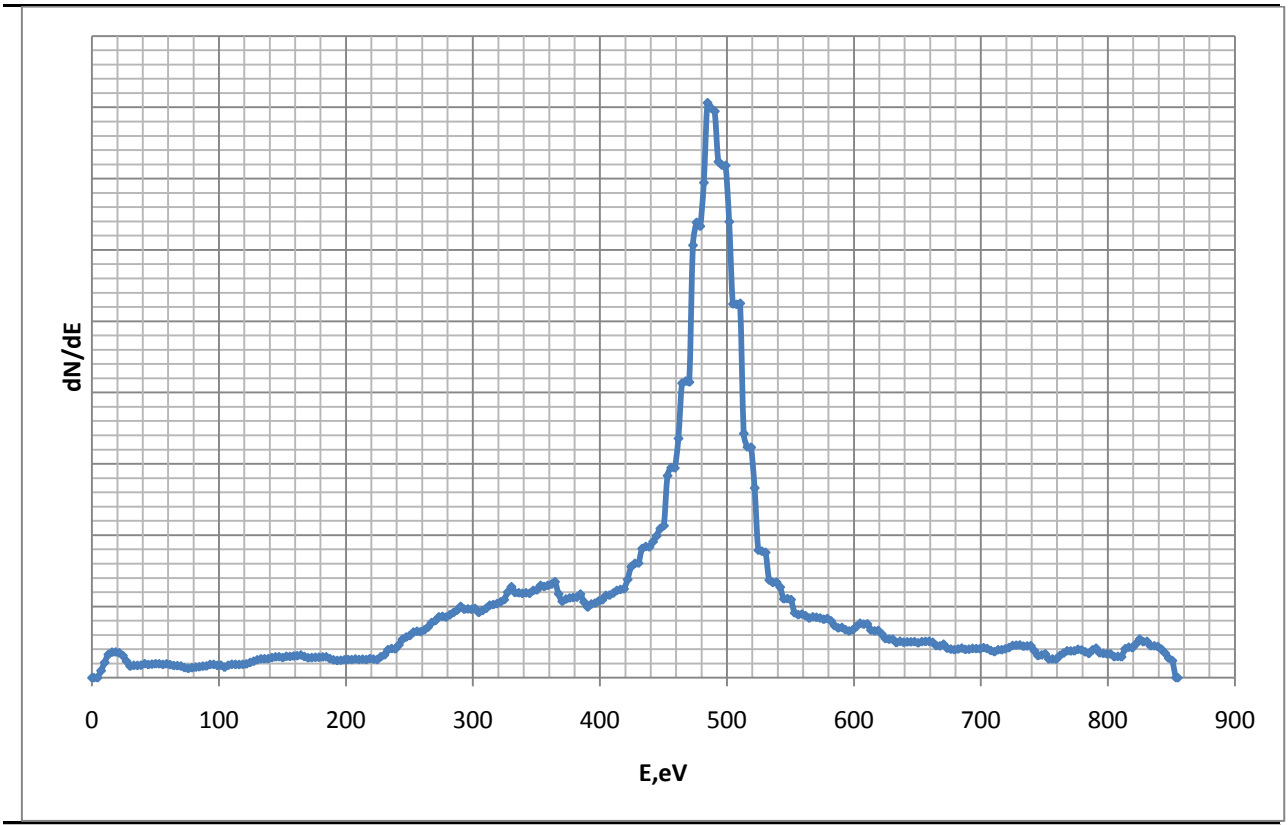

Fig.4.39. Distribution of ion energies for the total (fixed on PMA-tyagomere (Fig. 4.32.))

Integral value of thrust calculated by 3000000 ions modeled on SMA-thrustmeter equal to 81.07 mN, taking into account the 100% ionization mass consumption of 3.5 mg / sec. Experimentally measured thrust is ~ 75mN.

4.2.3. Stand 71-3-90 in KB «Torch»

3. The calculation of the concentration of primary ions

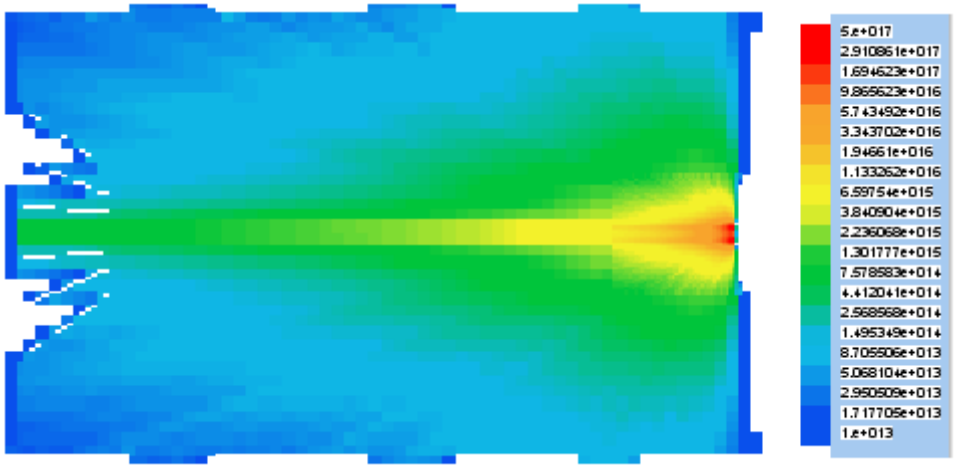

Fig.4.40. The concentration of primary ions.

To verify the algorithms, we set the camera inside the arc beam with 25 Faraday probes, the geometry of which was given in [36]. Then we celebrated collector probes, and when ingested in the collector ion, we recorded the charge and energy ions. This algorithm is very well illustrates the accuracy of our simulated field potentials, because the rechargeable ions are accelerated by these fields.

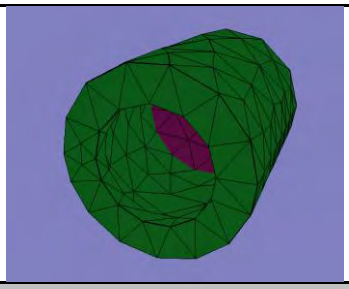

Fig. 4.41. The geometry of the probe.

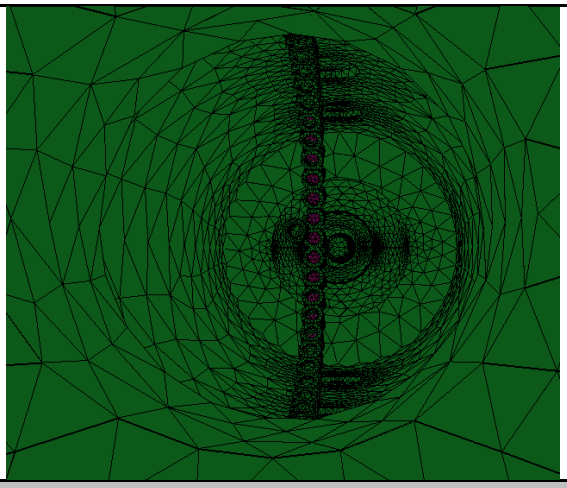

Fig. 4.42. The view from the front of the camera. (To enhance the signal probes increased 5-fold, red marked surface reservoir).

4.2.4. Comparison with the calculation of ISP

A test of comparison with the analogous calculation for the jet (package ISP [46]).

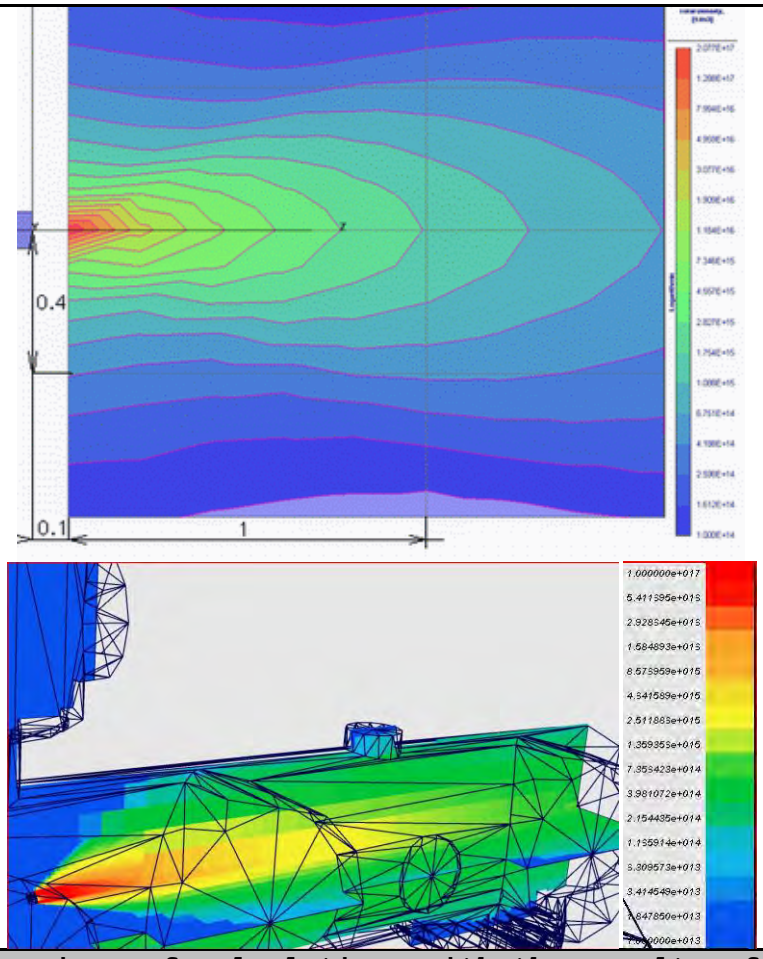

Fig. 4.43. Comparison of calculations with the results of the package ISP.

There has been a convergence of models in order of magnitude. It should be noted that the calculations were carried out for different angular distributions, with the same mass flow. In our model ions emit equal to the surface of «virtual cathode», while the ISP used the emission of ions from the point. However, the zone near the accelerator remains problematic in these studies because of the complexity of the processes occurring in it.

4.2.5. Comparison with simulations carried out by [8]

The data for the engine number 4 has been used for this comparison.

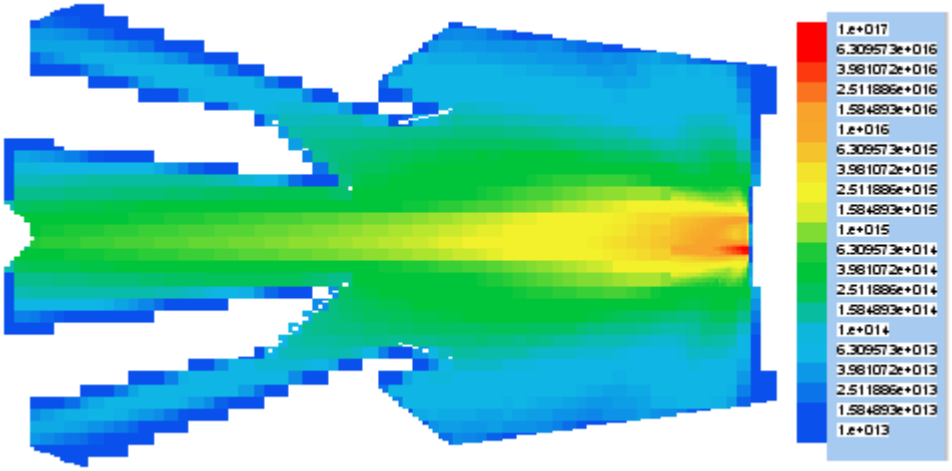

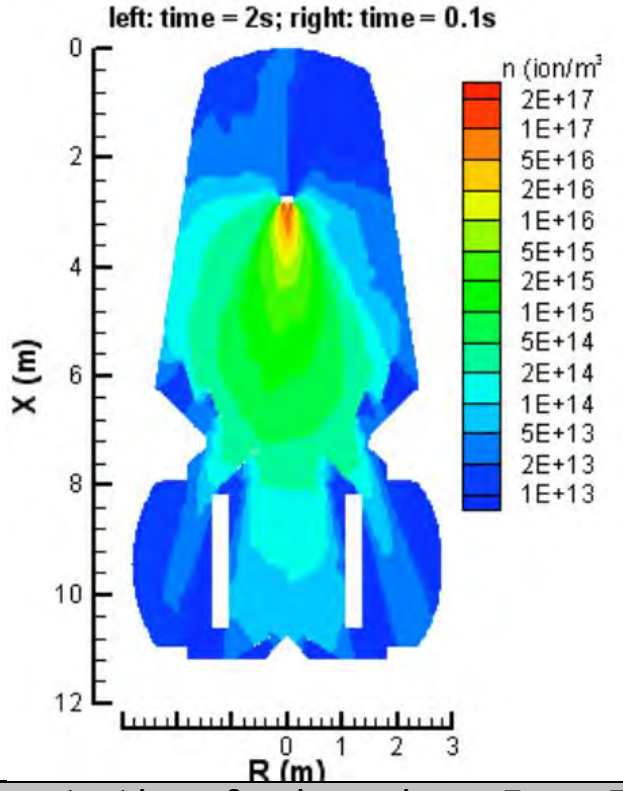

Fig. 4.44. The concentration of primary ions. Top - EpcLab, bottom - [8].

4.2.6. The calculation for the area around the accelerator

Inside the engine of the settlement has taken place, the boundary condition has a surface displacement of 25 mm from the anode. To emit a particle in the computational domain. Used engine number 1.

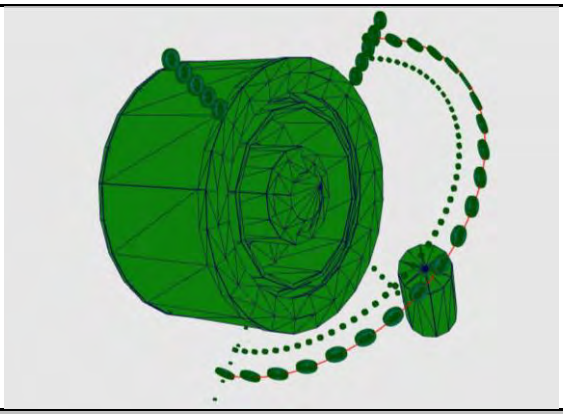

Fig. 4.45. The system probes (small - measuring the current density, large - for the measurement of energy)

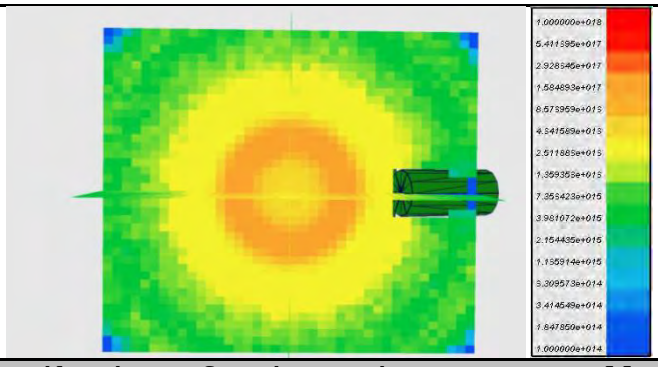

Fig.4.46. The distribution of primary ions at a small distance from the engine.

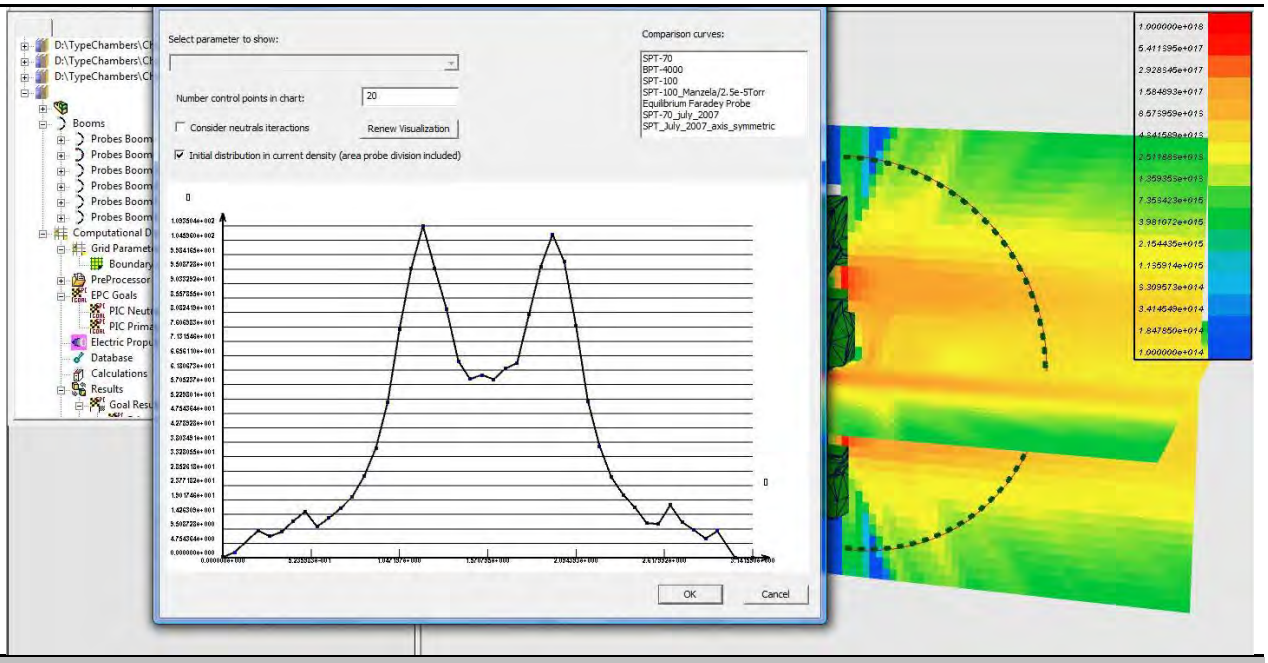

Fig.4.47. Visualization of the distribution of power in the beam of primary ions with probes

4.3. Calculation of sputtering and deposition

4.3.1. Stand MAI

4.3.1.1. Calculation ISP

When the plasma engine in a vacuum chamber, a jet of accelerated ions interact with the wall of the chamber. In doing so, the material is sprayed the walls of vacuum chamber, and a portion of the sputtered particles fly back to the engine, creating a process where the real work of the engine in space does not occur.

To solve this problem was written by the library CadExchanges.dll, capable of in order to record the points arrays of triangles describing the surface forms with the normals in appropriate

locations. These arrays are automatically exported into the ISP [46] with the corresponding construction of the tree assembly. Here is an example of import:

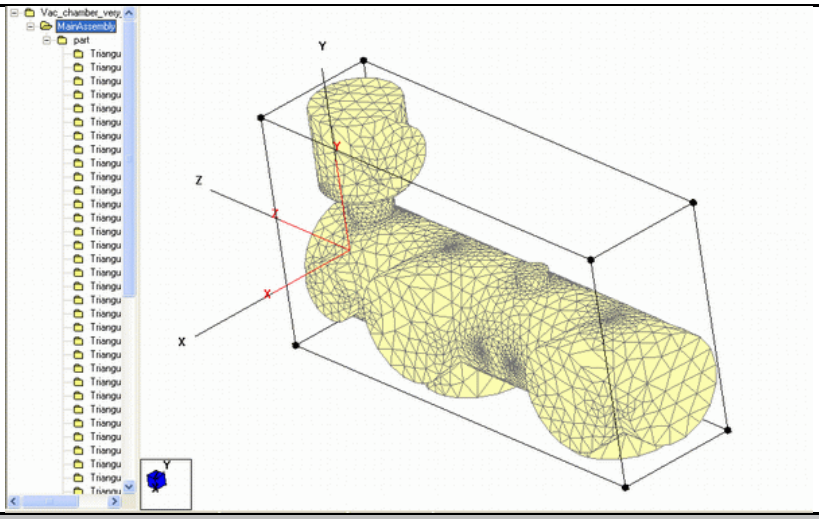

Fig. 4.48. Export triangulation in ISP

To create a triangulation and draw normals was used OpenSource product OpenCascade 5.2.

To calculate the dispersion and deposition processes must define the relevant characteristics of the wall material:

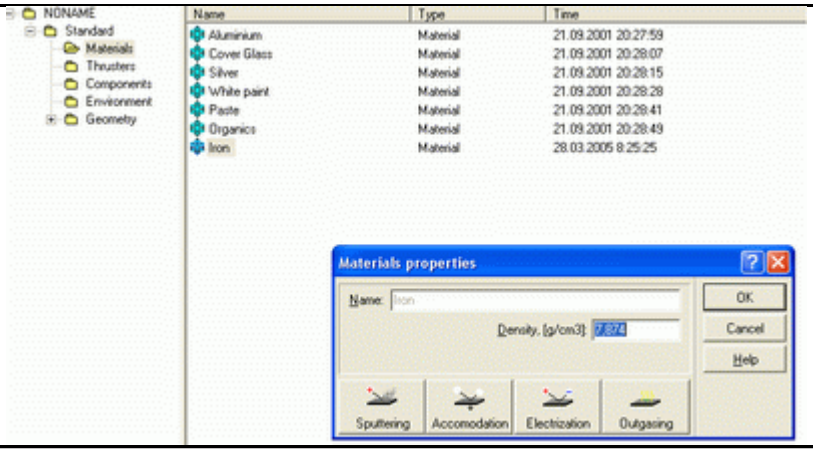

Fig. 4.49. The choice of material wall camera

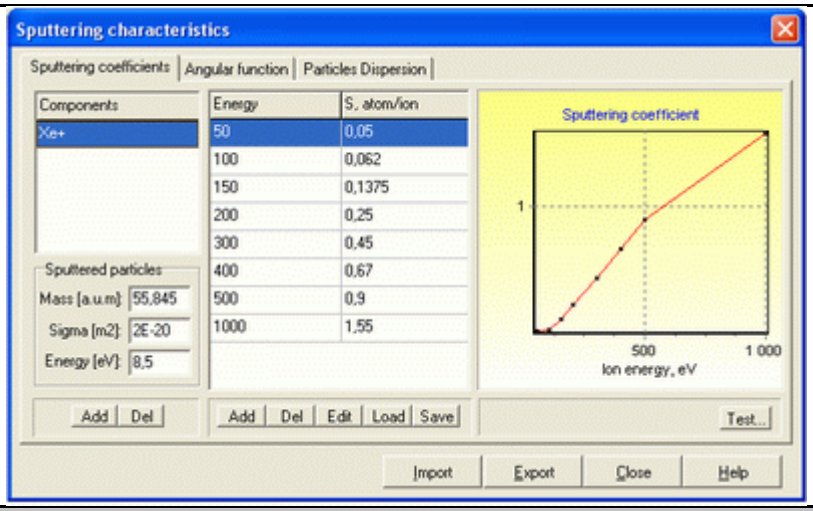

Fig. 4.50. Figure dependency rate of dissipation of energy

Fig. 4.51. Figure dependency rate of dispersal of the incidence angle

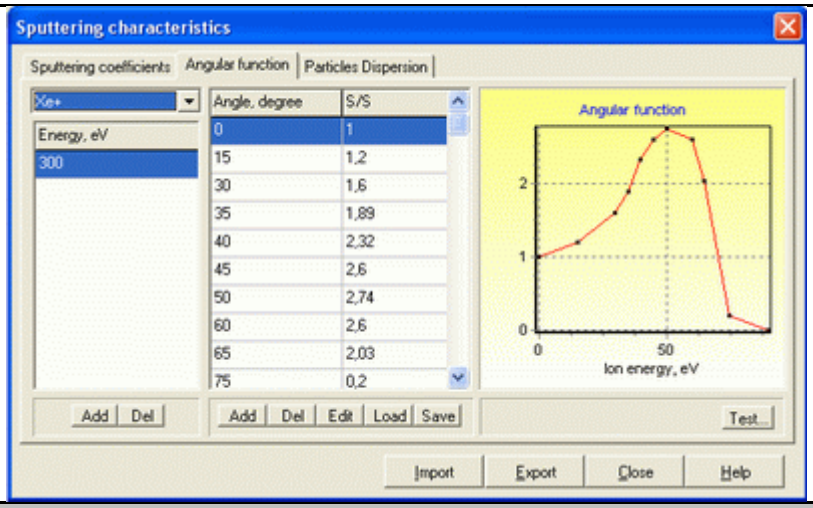

Fig. 4.52. The distribution of particles

Characteristics of the accelerator:

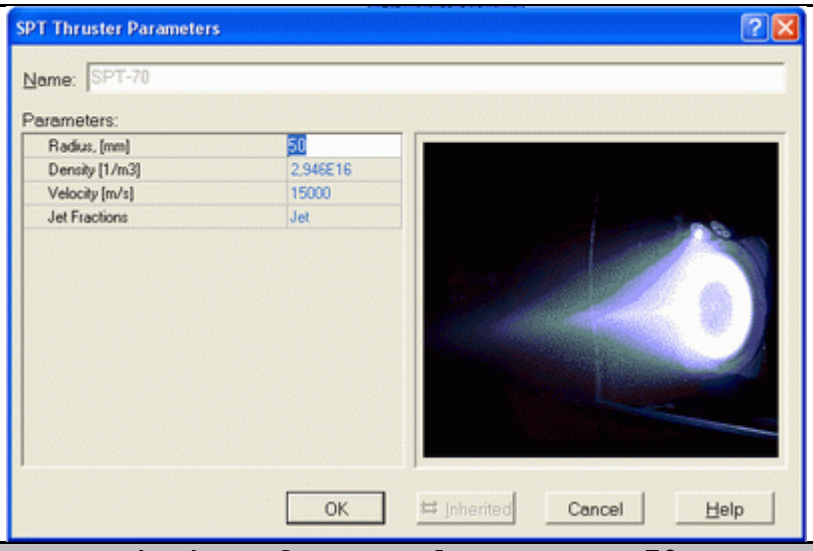

Fig. 4.53. Characteristics of an accelerator SPT-70

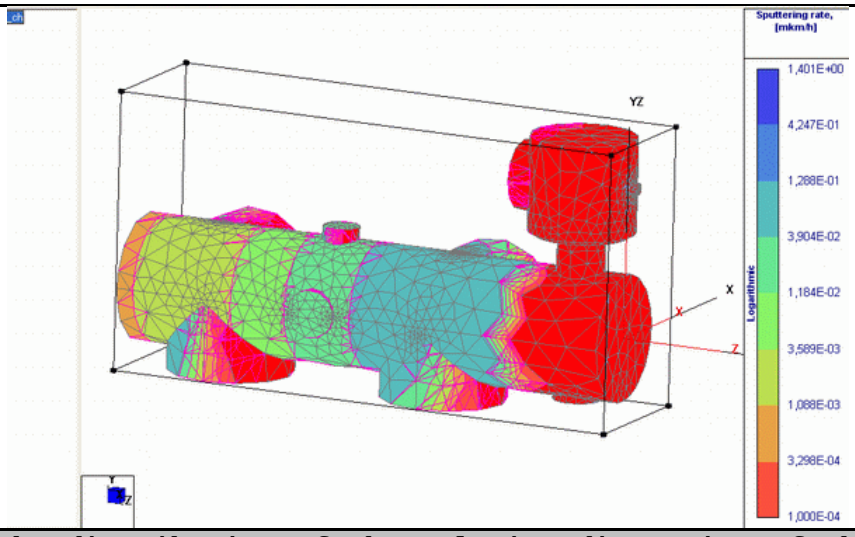

Fig. 4.54. The distribution of the velocity dispersion of the material on the sides of the chamber wall [mkm / h]

Figure 4.54 presented the picture of the sputtering chamber:

Figure 4.55 shows the visualization sprayed the walls with the vacuum chamber wall material on the camera and on the surface of the accelerator.

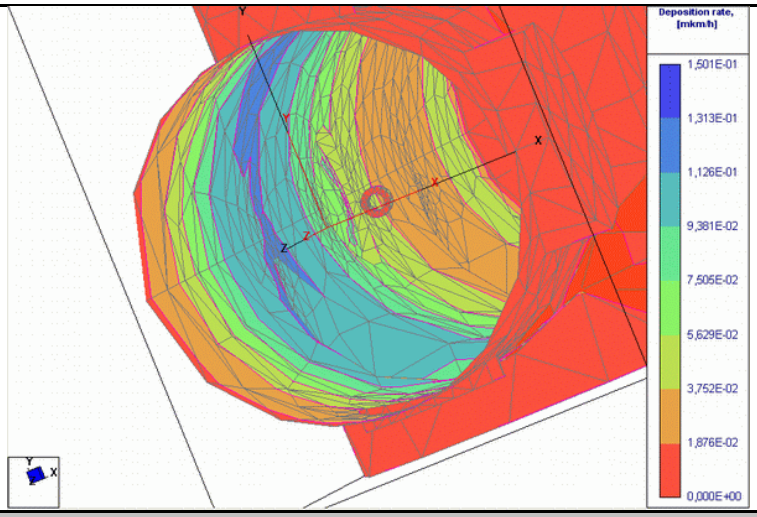

Fig. 4.55. Coating material sprayed on walls of the camera

4.3.1.2. Calculation EPCLab

This section contains the results for the sputtering engine № 1.2 and № 1.1.

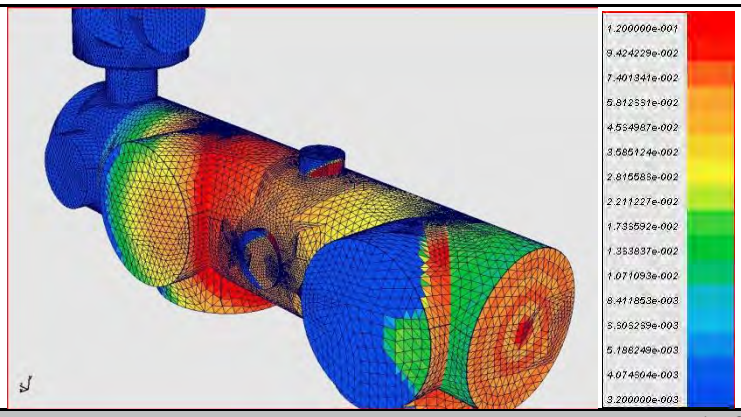

Fig. 4.56. Calculation of dispersion for the engine № 1.2 [mkm / h].

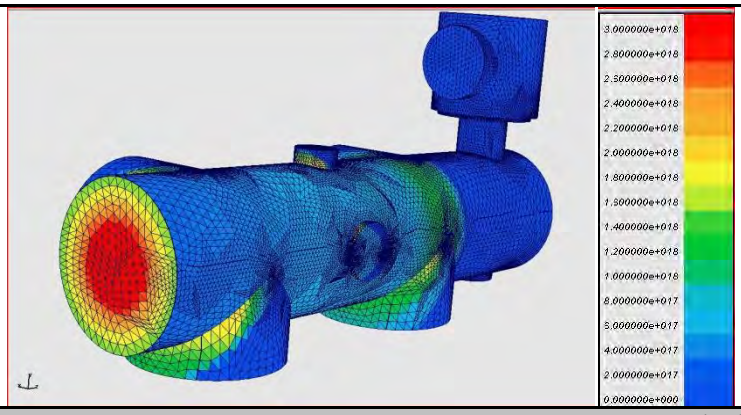

Fig. 4.57. Calculation of dispersion for the engine № 1.1 [1 / s].

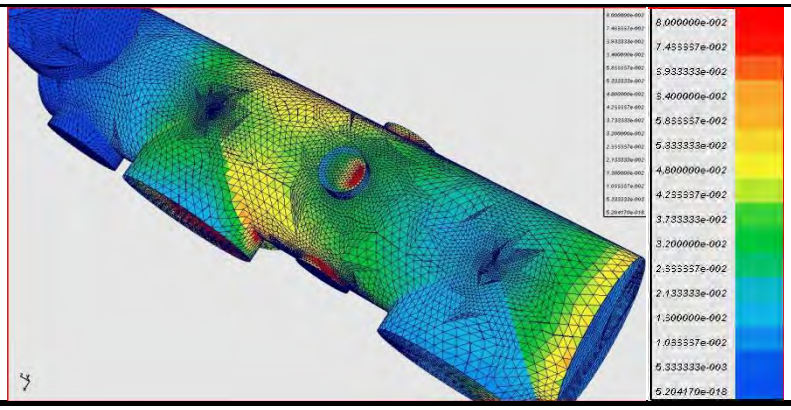

Fig. 4.58. The calculation for the engine perepyleniya № 1.2 [mkm / h].

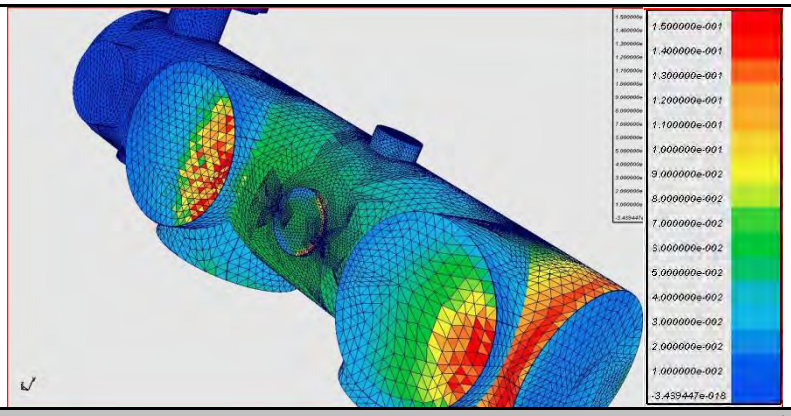

Fig. 4.59. The calculation for the engine perepyleniya № 1.1 [mkm / h].

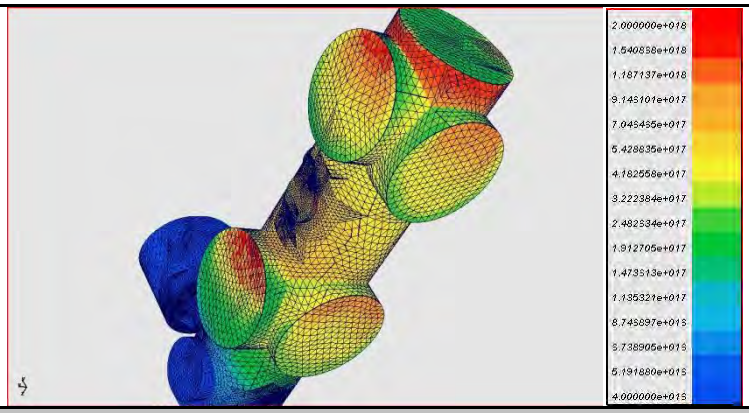

Fig. 4.60. The calculation for the engine perepyleniya № 1.1 [1 / s].

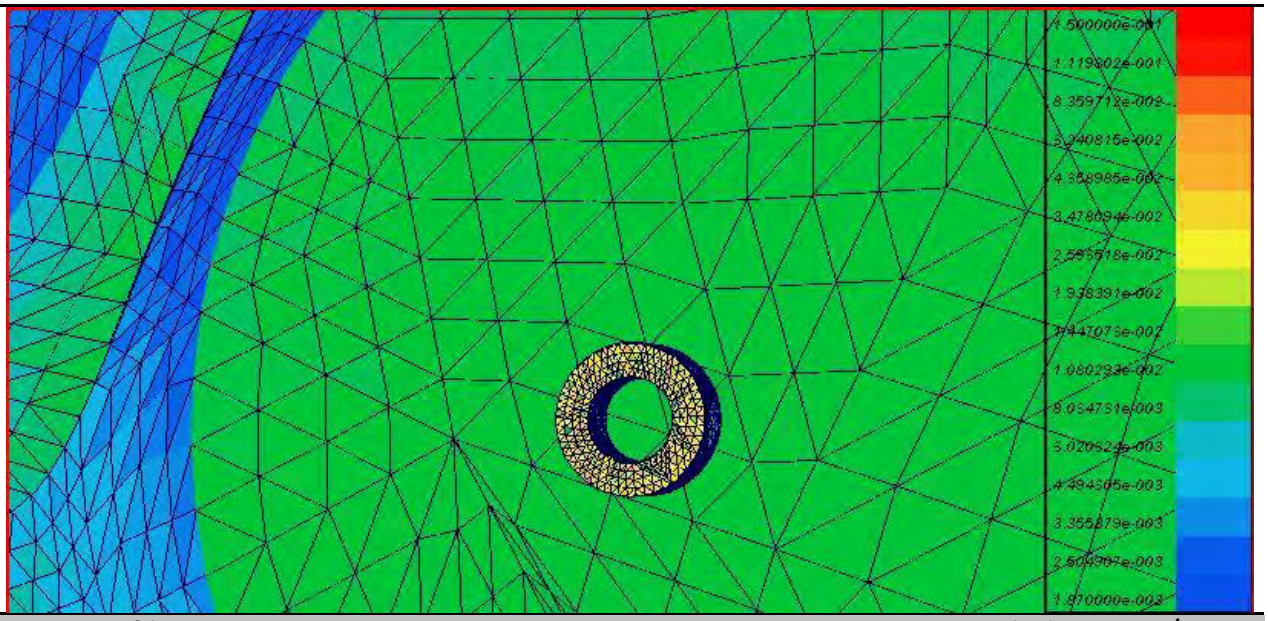

Fig. 4.61. The calculation for the engine perepyleniya № 1.1 [mkm / h].

4.3.2. Stand in the center of Keldysh

In this section we apply our model to the sputtering chamber in the center of aeronautics at engine number 2.

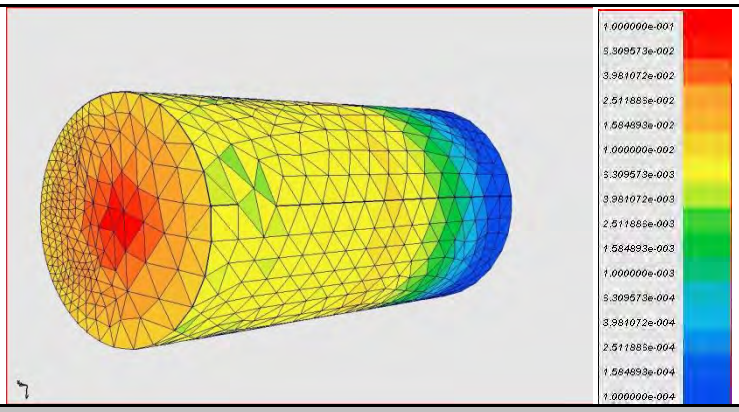

Fig. 4.62. Calculation of dispersion for the engine number 2 [mkm / h].

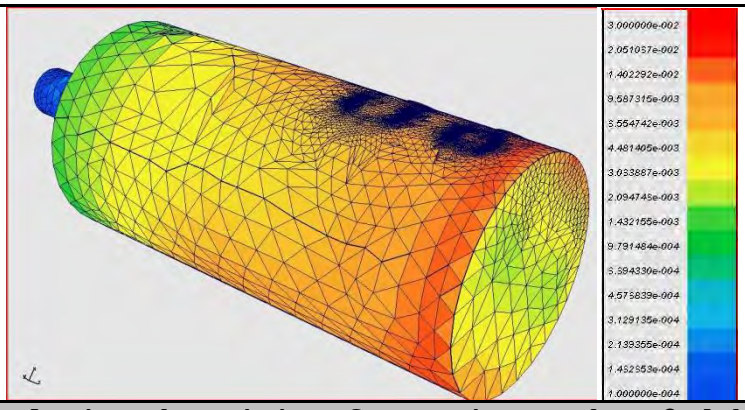

Fig. 4.63. Calculation deposition for engine number 2 [mkm / h].

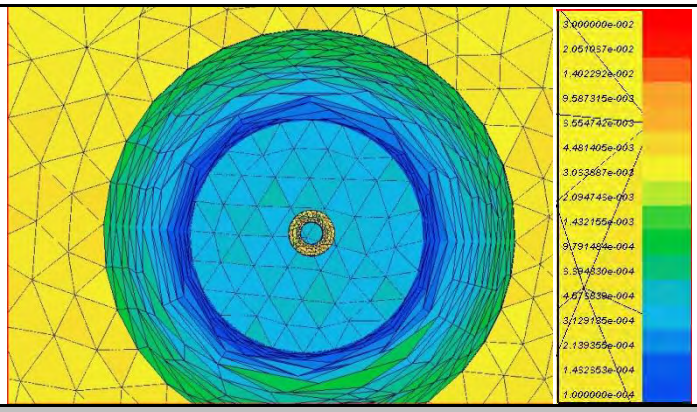

Fig. 4.64. Calculation deposition for engine number 2 [mkm / h].

4.4. Application of magnetohydrodynamic models and calculation of ions generated by the exchange of neutral gas atoms with ions off of the accelerator

4.4.1. Stand MAI

The following figure shows the beam with the probes, which was used for fixation of simulated ions.

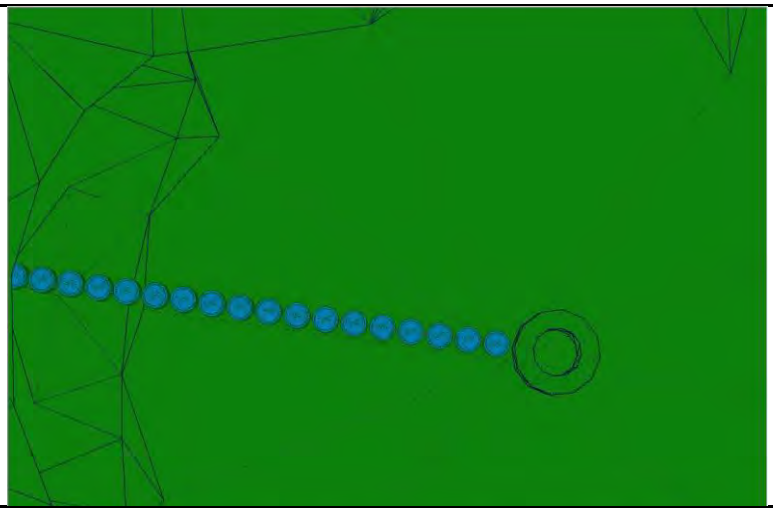

Fig.4.65. Beam with probes, which was used for fixation of simulated ions

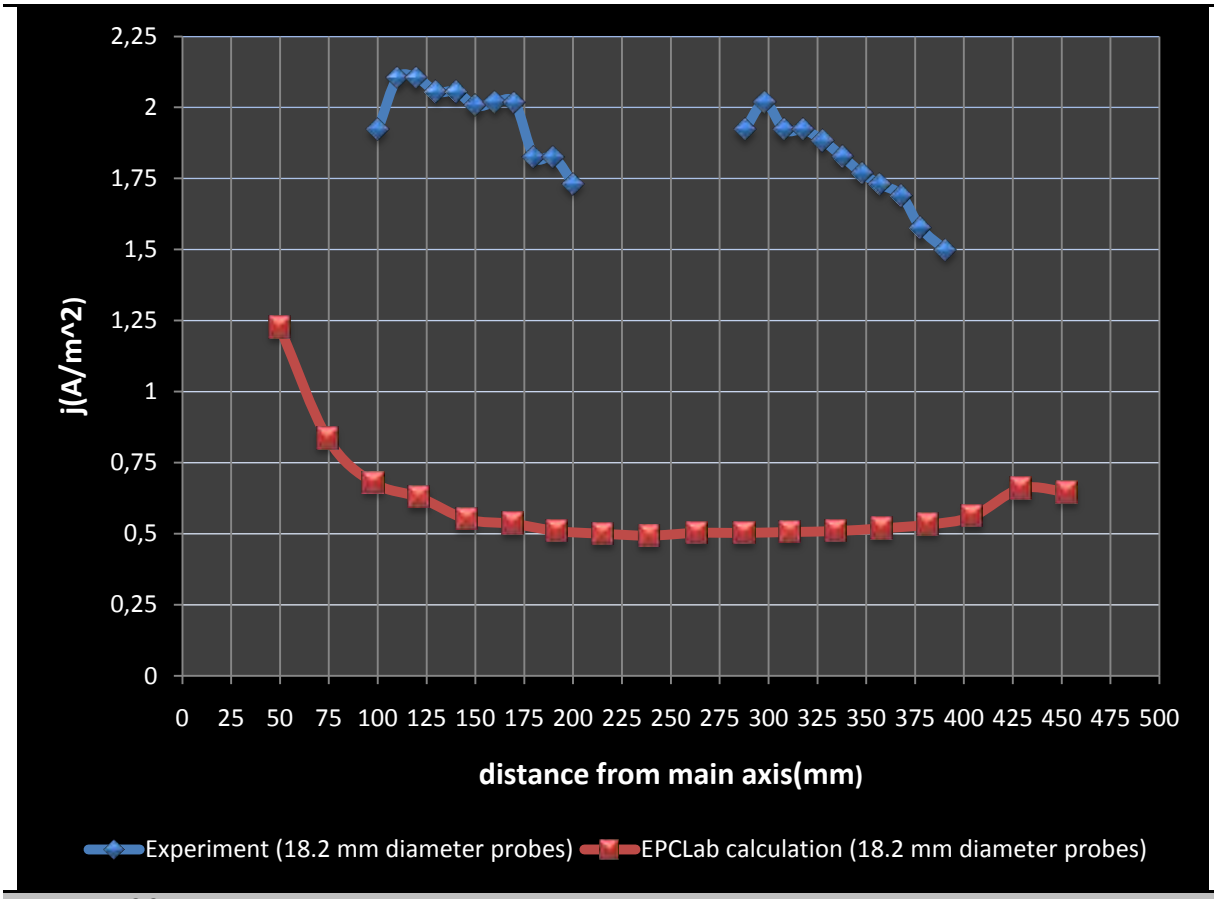

Fig.4.66. Ion current density at the beam

This comparison shows only a convergence in the order of magnitude. Also, it should be added that in the current probes in the experiment included the proportion of molecules and atoms reload a static vacuum, which we did not take into account in the calculations, so the estimates is slightly lower than the experimental.

4.4.2. Stand 71-3-90 in KB «Torch»

The calculation of the concentration of particles without rechargeable field.

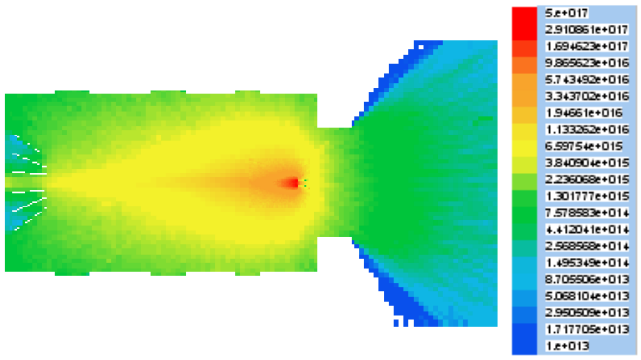

Fig. 4.67. The concentration of particles without rechargeable field.

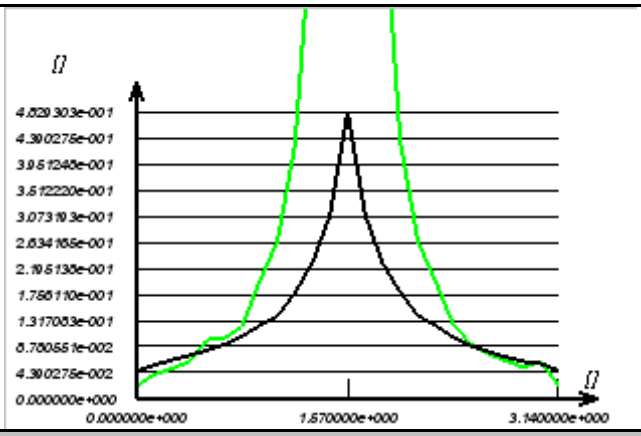

Fig. 4.68. Comparison of current primary ions emitted by probe data for the vacuum and recharge the particles in the current probe.

The total charge in a vacuum chamber reload the particles remained almost constant, but the speed, and hence the distribution of the concentration of particles is governed reload configuration of electromagnetic fields.

As can be seen from the graph at the corners more than 45 degrees most of the current account reload particles.
We did not have accurate data on the distribution of potentials in the probes, as there was no particular significance in the capacity of any point of the camera. Therefore, there can only be to consider principles.

For field potentials, we put 20 in a distance of 1 m from the engine with displacement of the axis of 0.5m. We then equated the value potential in all cells in the chamber. And then the finite difference method, iterations go on building the distribution under the concentrations of ions and neutrals.

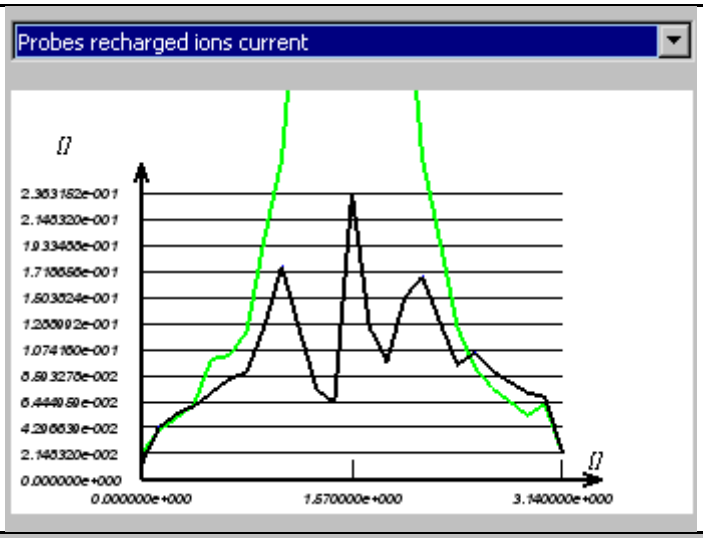

Fig. 4.69. Comparison of current rechargeable particles emitted on the probe characteristics in the simulation of light fields.

3. Adjustment of the initial distribution

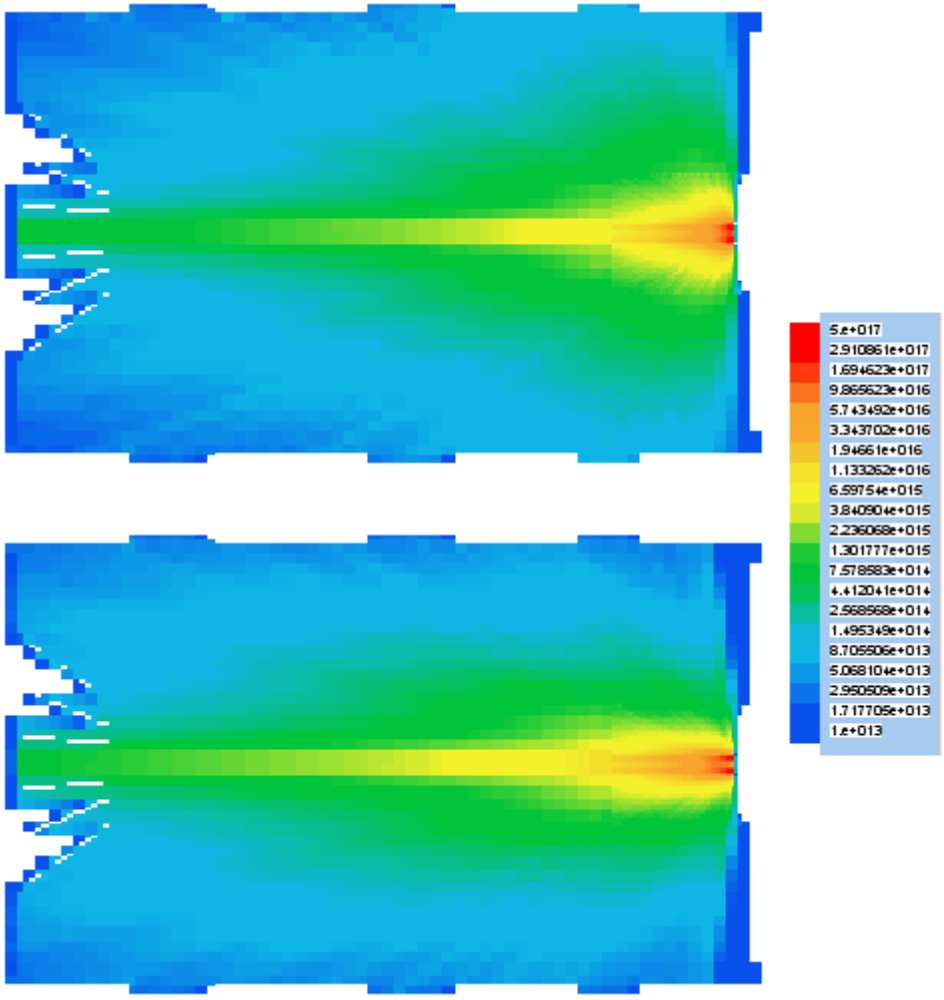

Fig. 4.70. Corrected concentration of primary ions (bottom), the concentration of ions emitted by probe characteristics [1/m3]

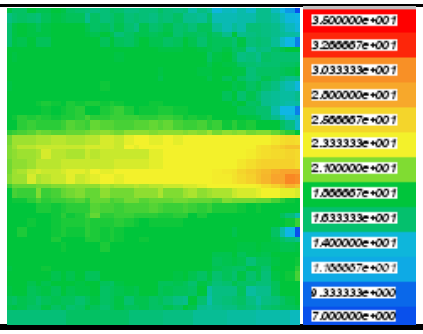

Fig. 4.71. Field potentials in the estimated area of 0.5 m from the engine [B].

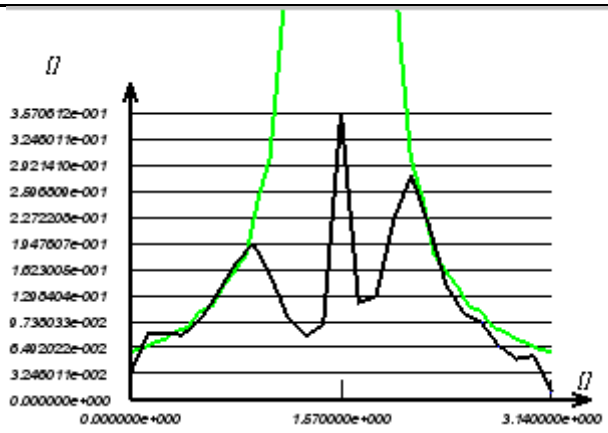

Fig. 4.72. Comparison of current rechargeable particles emitted on the probe characteristics in the simulation of light fields.

Here is an energy characteristic of the probe, with a different angle from the axis of the accelerator. Black green represents experimental data, as measured in the green calculation. On the left figure shows the energy characteristics of the adjustment, net of the overall ion recharge particles. On the right in green shows the proportion of recharge of particles in the range of energies.

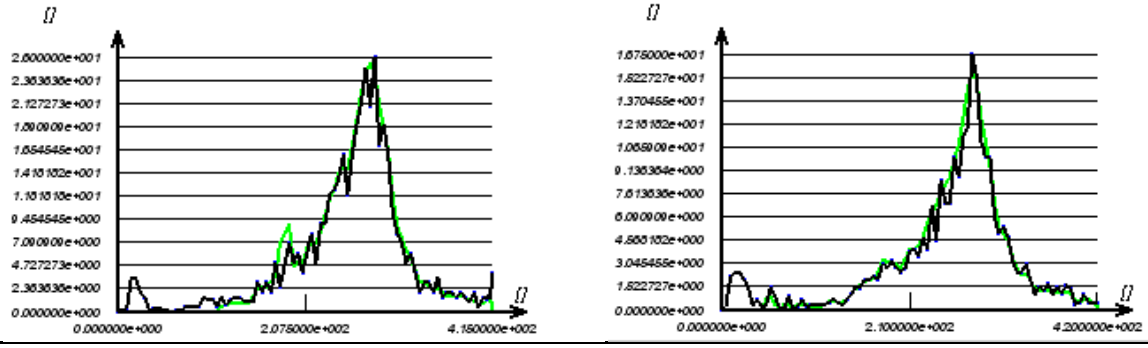

Fig. 4.73. 0, 7.5 degrees from the axis of the accelerator.

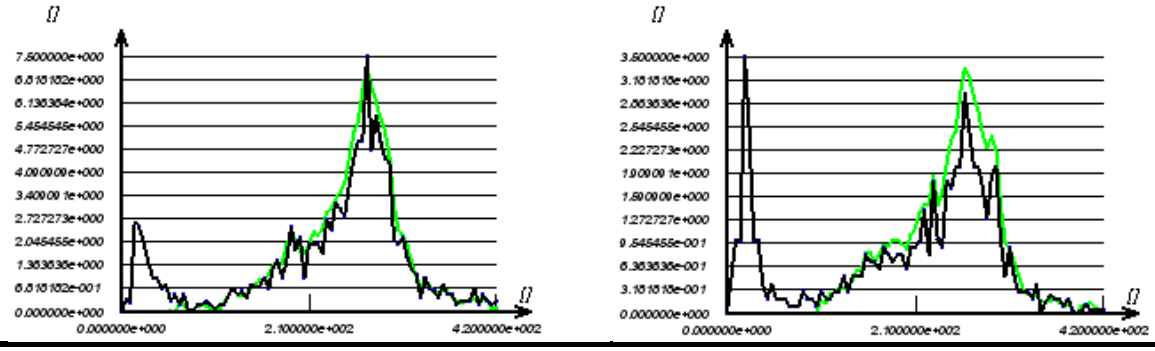

Fig. 4.74. 15 and 22.5 degrees from the axis of the accelerator.

At that power characteristics (right) do not coincide with the experimental, there are two possible reasons: 1) in our model does not take into account the possible transfer of momentum from the primary ion (section re a lot more cross-section of elastic interactions, so often there is no momentum transfer) 2) When experiment did not take into account the capacity of the cell, if one considers it, a maximum in the distribution of rechargeable particles shifted to 20-25 eV, which is much closer to our calculated distribution is shown in green on ris.89-92 (right).

4.4.3. Comparison with simulations carried out by [8]

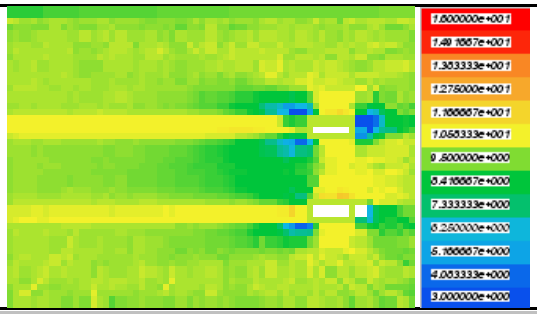

Fig. 4.75. The calculation of the distribution capacity in a vacuum chamber. [V]

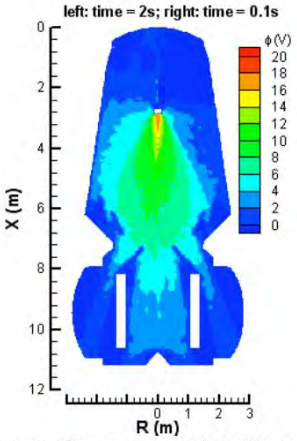

Figure 5. Plasma potential at different times.

Fig. 4.76. The calculation of the distribution capacity in a vacuum chamber made by a group of developers in [8].

In the model [8] was taken as the boundary condition that the potential at the end of the chamber is zero. We wanted to assess the drop in capacity due to the difference between the concentrations of ions in the stream. It also requires a fine mesh at the wall for the correct calculation of the fall from the building wall. For these reasons, we do not put such a boundary condition.

Figures 4.77 presents the results of calculations of the experimental data distribution capabilities. Do not pay attention to absolute values, because we are in the simulation did not know the initial capacity at any point of the camera. Important only relative values. Also keep in mind that the experimental values obtained for the accelerator BPT-200, the parameters of the jet which we in this form are not known.

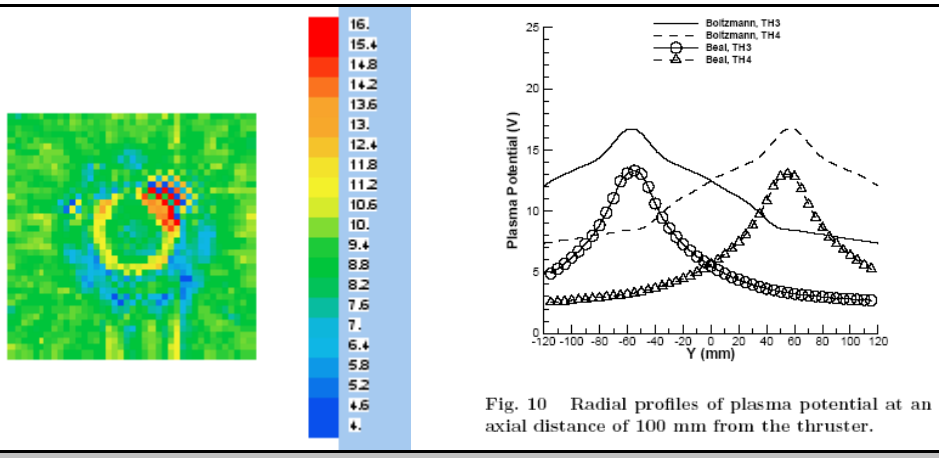

Fig. 10 Radial profiles of plasma potential at an axial distance of 100 mm from the thruster.

Fig.4.77. Comparison with the experiment capacity, cross section of 100 mm from the engine. [V].

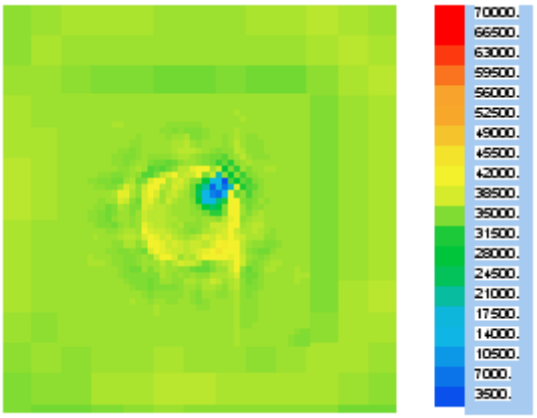

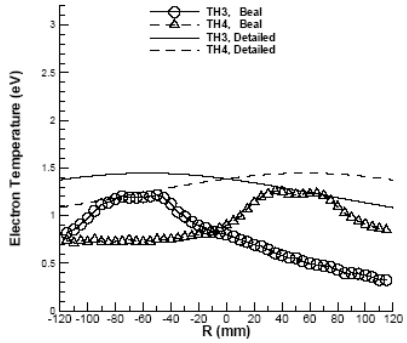

Fig. 14 Radial profiles of electron temperature at an axial distance of 150 mm from the thruster.

Fig. 4.78. The temperature of the electrons at a distance of 150 mm [K].

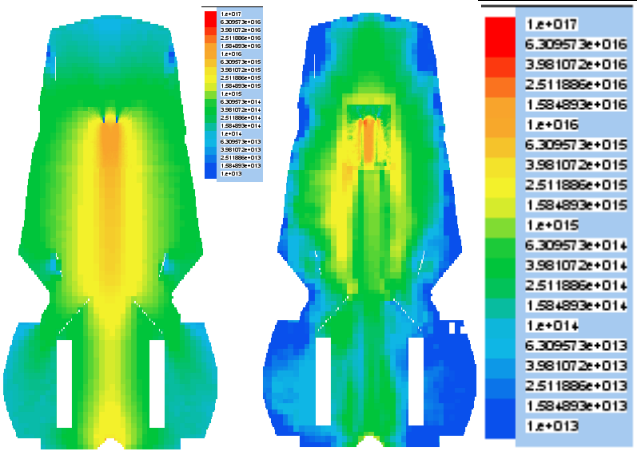

Fig. 4.79. Concentration perezaryadochnyh ions without an electric field (left) and field (right) [1/m3].

Since beam maximum potential, the ions formed as a result of overcharging, to expel the field from the beam, as shown on a large grid. However, the smallest grid we actually circular beam as shown by Figure 4.81. They are combined so that they are not visible, only at a distance of meters. Under the action of electric field, rechargeable ions will move towards the second part of the beam, but there tension to prevent them from passing through it. Perezaryadochnye ions produced as if in a trap. This we see in increasing the concentration of ions perezaryadochnyh in the middle of almost an order of magnitude, compared to their concentration in the beam. At a large grid of this phenomenon is not observed, since the entire accelerator is placed in cell 3.

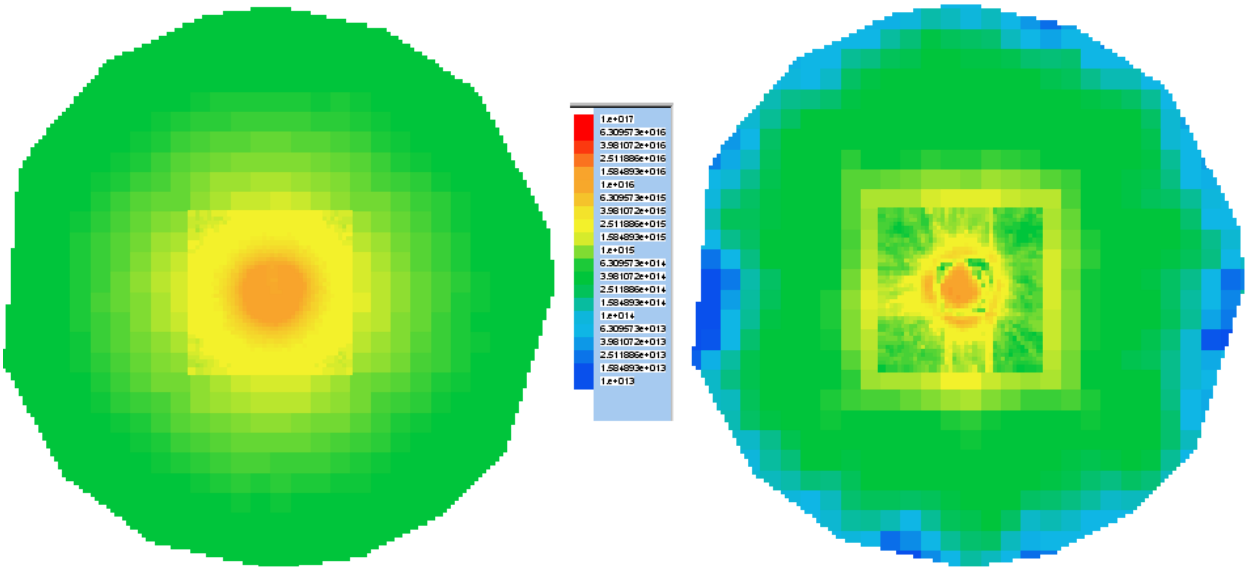

Fig. 4.80. Concentration perezaryadochnyh ions without an electric field (left) and field (right). The cross-section of 200 mm from the engine [1/m3].

In general, the number perezaryadochnyh ions, resulting in the interaction of a jet of primary ions with neutral gas in the chamber at all times in both models. However, the electric field affects the velocity of ions, directing them to the wall, and increasing it by an order of magnitude. Therefore, the concentration decreases by an order of magnitude as the time spent in the ion cell is reduced.

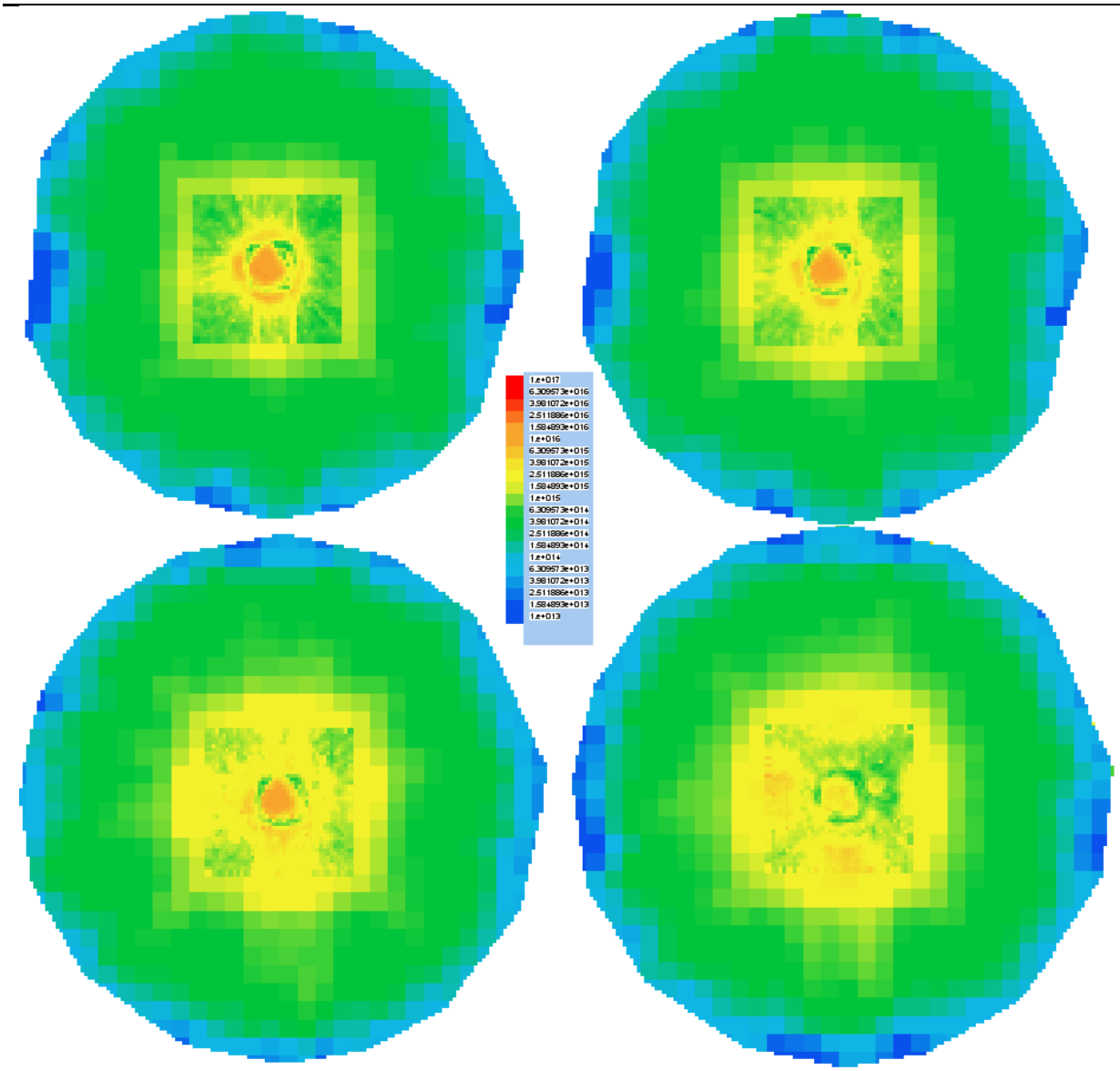

Fig. 4.81. The concentration of ion exchange [1/m3] (section (upper left side - 200 mm, right upper - 400mm, bottom left - 800 mm, bottom right - 1150 mm from the engine)).

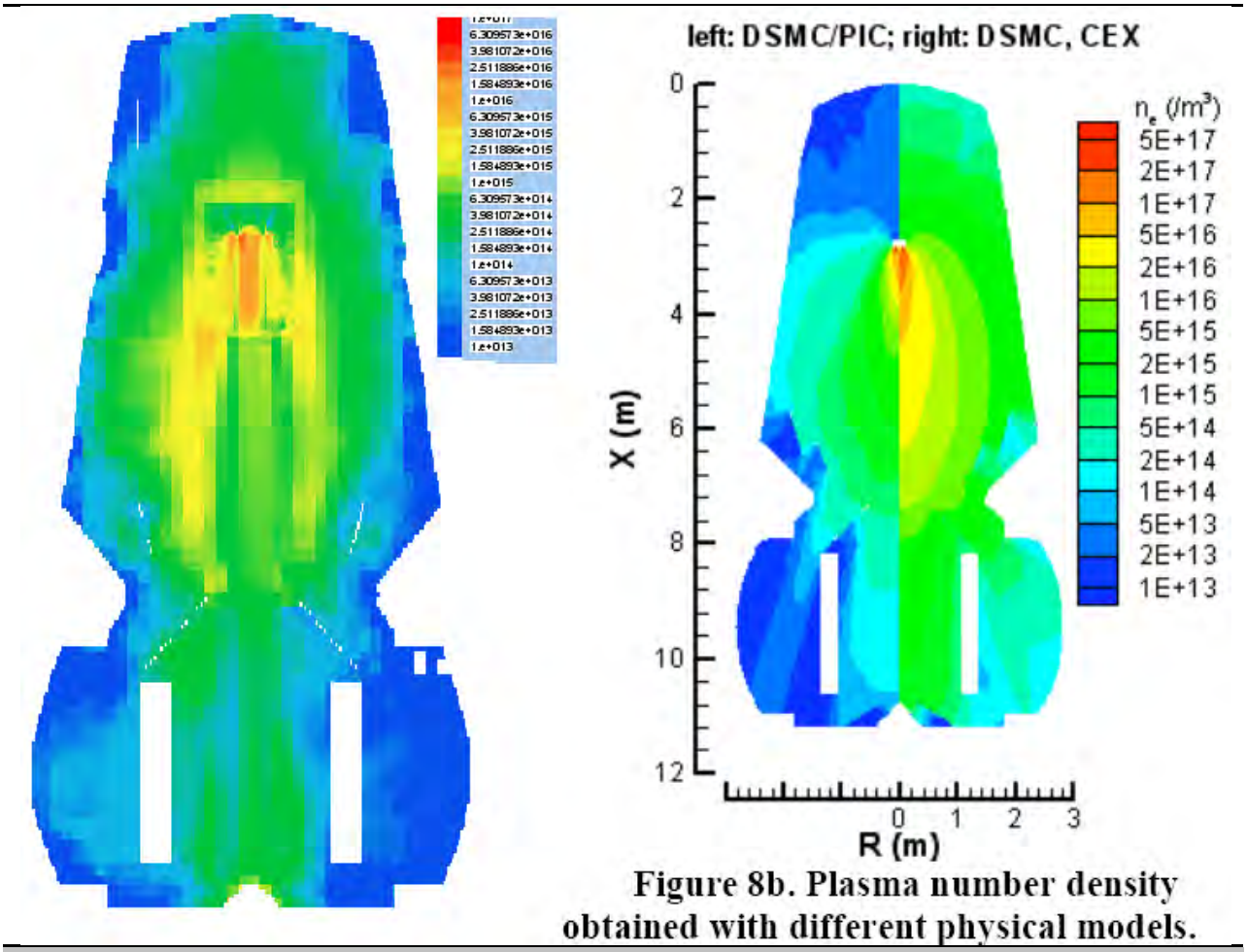

Fig. 4.82. Comparison of recharging two models (on the left - EpcLab; right – [8]).

Analysis: In general, as well as the known mass flow rate, known trajectory of the primary ions, as well as the well known section of the resonant re-Xe atom on its own, and known concentration of neutral particles. Number of ion rechargeable defined in the vacuum chamber. A distribution of their concentration, we can see at a rate equal to room temperature at fig.51.

Conclusions

1. The mathematical model and software for numerical simulation of processes: the spread of the neutral gas in a vacuum chamber, the spread of primary ions, taking into account the exchange ions on Xe, reload the spread of the particles in the vacuum chamber with a view of a field of tension, and atomization perepylenie design of vacuum chamber in the interaction with a jet engine.

2. A satisfactory verification of the product with the experiment, it should be noted that the best camera for verification of product is the camera with a cryogenic pump, where there is no oil vapors.

3. An verification program with the development of other similar research groups.

4. An algorithm for the calculation of some integral characteristics of the engine (thrust, total current), as well as various integral characteristics of local areas through the SMA.

5. A method for assessing the loss of power ion beam in the interaction with atoms of the neutral gas to the collision with the probes measure the density of ion current.

6. A method for assessing the effectiveness of the probe.

7. A detailed analysis of models for calculating the cross sections of elastic collisions of particles.

8. For the first time, an algorithm has been applied the spatial distribution of sputtered particles with the help of a spline approximation of the given measurements in two planes.

9. In the course of the work was first compiled table distribution of the velocity and direction of neutral beam particles interacting with Xe atoms of the same rarefied gas at T = 300K.

10. In the course of the work was first calculated the trajectory of an electron off from the cathode in an external magnetic field created by a motor coils.

11. A verification model of the dynamics of neutral particles in the calculation of coefficients Klauzinga.

12. A partial analysis of the electromagnetic field in a vacuum chamber with the engine running.

13. In the course of work was evaluated the influence of capacity in a vacuum chamber for the distribution of recharge of ions in the stream.

14. The analysis of selection of different models to assess the elastic interaction of particles.

15. It was shown that the concentration of rechargeable particles depends on the distribution of field potentials. Thus, in our, albeit gross calculations, due to an increase in speed reload the particle concentration decreased by an order of magnitude.

References

1. COMPARISON OF MATHEMATICAL MODEL OF A PLASMA PLUME WITH OUTCOMES OF SPACE EXPERIMENTS. A.G.Korsun, F.F.Gabdullin, E.M.Tverdokhlebova, V.I.Garkusha V.P.Khodnenko (IEPC-2003)
2. С.Асхабов , Бургасов М., Фишгойт В., и др. „Исследование струи стационарного плазменного ускорителя с замкнутым дрейфом электронов“ – Физика плазмы, 1981, т. 7, вып. 31, стр.225-230.
3. Научно технический отчет. Анализ стабильности тяги модулей М100 в процессе ресурсных испытаний и влияние загрязнения на стабильность тяги. ОКБ «Факел», 1993 г.
4. Manzella, D. H., Sankovic, J. M., “Hall Thruster Ion Beam Characterization,” AIAA-95-2927, 31st Joint Propulsion Conference, San Diego, CA, July 10-12,1995.
5. L. Artsimovich, I. Andronov, Yu. Esipchuk et al. “Development of the stationary plasma thruster (SPT) and its test onboard “Meteor” satellite” – “Kosmicheskie issledovaniya”, v. XII, #3, 1974, p.p. 451-468.
6. «The Distinction between the EP Plume Expansion in Space and in Vacuum Chamber», Anatoly G. Korsun; Ekaterina M. Tverdokhlebova; Flur F. Gabdullin, IEPC-2005
7. «A Comparison of Nude and Collimated Faraday Probes for Use with Hall Thrusters», Richard R. Hofer; Mitchell L.R. Walker; Alec D. Gallimore.IEPC-2001.
8. «Particle Simulation of Hall Thruster Plumes in the 12VVacuum Chamber.» , Iain D. Boyd1, Quanhua Sun, and Chunpei Cai, Kenneth E. Tatum. IEPC-2005.
9. Biagioni, L., *et al*., “Particle Simulation of Tailored Vacuum Pumping Configurations for Electric Propulsion Testing,” *4th International Symposium on Environmental Testing for Space Programmes*, Liege, Belgium, 2001.
10. Andrenucci M., *et al*., “PIC/DSMC Models for Hall Effect Thuster Plumes: Present Status and Ways Forward”,AIAA Paper 2002-4254, *38th AIAA/ASME/SAE/ASEE Joint Propulsion Conference*, Indianapolis IN, USA, 2002.
11. V. Kim, V. Kozlov, G. Popov “Plasma parameter distribution determination in SPT-70 plume” IEPC-2003.
12. V.K. Absalyamov et al “Measurement of plasma parameters in the stationary plasma thruster (SPT-100) plume and its effect on spacecraft components” AIAA-92-3156, 28th Joint Propulsion Conference, July 6-8, 1992, Nashville, USA.
13. «TRANSPORT-PROPERTY AND MASS SPECTRAL MEASUREMENTS IN THE PLASMA EXHAUST PLUME OF A HALL-EFFECT SPACE PROPULSION SYSTEM» Lyon Bradley King. A dissertation submitted in partial fulfillment of the requirements for the degree of Doctor of Philosophy (Aerospace Engineering) 1998
14. Beal, B. E. and Gallimore, A. D., «Energy Analysis of a Hall Thruster Cluster,» IEPC Paper 2003{35, March 2003,Toulouse, France.
15. Е.Н. Бондарев, В.Т. Дубасов, Ю.А. Рыжов и др. Аэрогидромеханика. М.: Машиностроение. 1993 г.
16. А.Ф. Александров, Л.С. Богданкевич, А.А. Рухадзе. Основы электродинамики плазмы. М. Высшая школа. 1978 г.
17. В.М. Вержбицкий. Основы численных методов. М. Высшая школа. 2002 г.
18. К. Флетчер. Вычислительные методы в динамике жидкостей. М. Мир. 1991 г., т. 1,2.
19. Р. Хокни, Дж. Иствуд. Численное моделирование методом частиц. М. Мир, 1987 г.

20. Г.В. Горелова И.А. Кацко «Теория вероятностей и математическая статистика в примерах и задачах с применением Excel», Феникс, Ростов-на-Дону 2002 г.
21. Физико-химические процессы в газовой динамике / под ред. Г.Г. Черного и С.А. Лосева. - М.: «Научный мир», 2007.
22. Ivanovskiy G.F., Petrov V.I. "Ion plasma working of materials", Moscow, Radio i svyaz, 1986 - pp 232 (in Russian).
23. Solid objects sputtering by ions bombardment: Transl. from English/ Edit. by R.Berish. - Moscow, Mir, 1984 - pp 336 (in Russian).
24. Бронштейн И.Н., Семендяев К.А. Под ред.: Гроше Г., Циглер В."Справочник по математике для инженеров и учащихся втузов." Пер. с нем. Изд.12, переработанное.1980. Твердый переплет. 976 с.
25. «Hall Thruster Plume Simulation Using a Detailed Hybrid Model» Iain D. Boyd and John T. Yim AIAA 2004–3952
26. «3-Dimensional Simulation of Plasma Dynamics in SPT» Vladimir Kim, Alexander Bishaev, Alexei Lazourenko, IEPC-01-340
27. А.А.Шагайда "Метод численного моделирования течений разреженного газа и его применение для расчета электрофизических устройств" – Автореф. дисс., М.: ИЦ им.М.В.Келдыша, 2000г.
28. А.И.Морозов, Ю.В.Есипчук, Г.Н.Тилинин и др. „Экспериментальное исследование плазменного ускорителя с замкнутым дрейфом электронов и протяженной зоной ускорения" – ЖТФ, 1972, XLII, №1, с.54-63.
29. Jeremiah J. Boerner and Iain D. Boy «Numerical Simulation of Faraday Probe Measurements in a Multi-component Non-equilibrium Plasma» IEPC-2005
30. http://hometown.aol.com/gmagnetics/download.htm (2001г).
31. http://www.fieldp.com (2001 г).
32. http://www.ansys.com/ansys/emag.htm (2001 г).
33. V.V.Abashkin, N.V.Blinov, S.V.Irishkov, O.A.Gorshkov „The Influence of Magnetic Field on Work Processes in Low Power Hall Thrusters" – IAF-99-S.4.06, 50th International Astronautical Congress, Amsterdam, the Netherlands, Oct. 1999.
34. ELCUT 5.4. User Manual. Tor Ltd. Saint-Petersburg 2006.
35. Andrenucci M. et. al. The new EP test facilities at Centrospazio and Alta. - IEPC-03-229/ Proceedings of 28 IEPC, CNES, Toulouse, France, March 17 – 21, 2003, electronic version on CD.
36. «Исследование характеристик стационарных плазменных двигателей (СПД) мощностью 1.5…6 кВт». Приданников С.Ю. Калининград, 2002 г.
37. Miller, J. S., Pullins, S. H., Levandier, D. J., Chiu, Y., and Dressler, R. A., "Xenon charge exchange cross sections for electrostatic thruster models," *Journal of Applied Physics*, Vol 91, No. 3, 2002, pp. 984-991.
38. Черный Г.Г., Лосев С.А., *Физико-химические процессы в газовой динамике* (Т.1) М. Научный мир 2007г.
39. Bird, G. A., *Molecular Gas Dynamics and the Direct Simulation of Gas Flows*, Clarendon Press, 1994.
40. A. Abrahamson, *Born-Mayer-Type Interatomic potential for Neutral Ground State Atoms with Z=2 to Z=105,* Physical Review Feb. 1968
41. Кошмаров Ю.А., Рыжов Ю.А. Прикладная динамика разреженного газа. - М: "Машиностроение", 1977.
42. Kim V., Kozlov V., Popov G., Skrylnikov A. Plasma parameter distribution determination in SPT-70 plume. – IEPC-03-107 / Proceedings of 28 IEPC, CNES, Toulouse, France, March 17 – 21, 2003, electronic version on CD.

43. Biagioni L. et. al. Basic issues in electric propulsion testing and the need for international standards. - IEPC-03-230 / Proceedings of 28 IEPC, CNES, Toulouse, France, March 17 – 21, 2003, electronic version on CD.
44. http://www.arnold.af.mil/aedc/factsheets/12v4pg/12v.pdf
45. «A Comparison of Nude and Collimated Faraday Probesfor Use with Hall Thrusters»,Richard R. Hofer Mitchell L.R. Walker Alec D. Gallimore, IEPC-2001
46. Perrin V., Metois P., Khartov S., Nadiradze A. Simulation tools for the plasma propulsion and satellite environment // 52nd International Astronautical Congress Toulouse, France, October 1-5, 2001.